

Molecular Kinetics of Metabotropic Glutamate Receptors

Thesis

**in partial fulfilment of the requirements for the degree of
“Doctor of Philosophy” (PhD)**

**submitted to the Council of the Faculty of Medicine
at the Friedrich Schiller University of Jena**

by M.Pharm & M.Sc. Organic Chemistry, Taulant Kukaj
born on 21.09.1988 in Glllogoc, Kosovo

Molekulare Kinetik der Metabotroper Glutamatrezeptoren

Dissertation

zur Erlangung des akademischen Grades

“Doctor of Philosophy” (PhD)

vorgelegt dem Rat der Medizinischen Fakultät

der Friedrich-Schiller-Universität Jena

von M.Pharm & M.Sc. Organic Chemistry Taulant Kukaj

geboren am 21.09.1988 in Glllogoc, Kosovo

Dissertation, Friedrich-Schiller-Universität Jena, [2021]

Gutachter / Reviewer:

1. Prof. Dr. Klaus Benndorf

Institut für Physiologie II – Herz-Kreislauf-Physiologie, Universitätsklinikum Jena

2. Prof. Dr. Carsten Hoffmann

Institut für Molekulare Zellbiologie, Universitätsklinikum Jena

3. Prof. Dr. Tobias Langenhan

Rudolf – Schönheimer - Institut für Biochemie, Universität Leipzig

Tag der öffentlichen Verteidigung / Date of the public disputation: **18.05.2021**

Table of Contents

Table of Contents	I
List of abbreviations.....	V
Summary	VII
Zusammenfassung.....	IX
1. Introduction	1
1.1. Glutamate Receptors	1
1.2. Metabotropic Glutamate Receptors.....	1
1.2.1. Structural features of metabotropic glutamate receptors	3
1.2.2. Dimerization of mGluRs	5
1.2.3. The role of mGluRs in the Nervous System (NS)	6
1.3. Activation of GPCRs	7
1.4. Application of FRET methods to study kinetics in GPCRs.....	8
1.4.1. Development of fluorescent proteins.....	10
1.4.2. Förster resonance energy transfer (FRET)	11
2. Objectives	13
3. Materials and Methods	14
3.1. Molecular Biology.....	14
3.2. Preparation of <i>Xenopus laevis</i> oocytes and cRNA injection	17
3.2.1. Preparation of <i>Xenopus laevis</i> oocytes	17
3.2.2. Preparation of micropipettes for cRNA injection.....	17
3.3. Chemicals and Solutions	17
3.4. Confocal patch-clamp fluorometry experiments in outside-out membrane patches 18	
3.4.1. Preparation of pipettes for outside-out patches	18
3.4.2. FRET experiments in membrane patches	19
3.5. Analysis of FRET data	21
Fitting of activation and deactivation kinetics	22
4. Results.....	23
4.1. Expression of mGluR sensors in <i>Xenopus laevis</i> oocytes	23
4.2. Optimization and characterization of measuring conditions for mGluR1 FRET sensors expressed in <i>Xenopus laevis</i> oocytes	24

Crosstalk and direct excitation	24
4.3. The functionality of the mGluR sensors	26
4.4. Glutamate effect in mGluR1 FRET sensors.....	28
mGluR sensors are functional	28
4.5. Kinetics	32
4.5.1. Activation and deactivation kinetics in the mGluR ₁ E-sensor	32
4.5.2. A-sensor.....	37
4.6. Functional interaction of the subunits of all members in metabotropic glutamate receptors	38
4.6.1. Dimer assembly studied by FRET efficiency.....	39
4.6.2. Kinetics in homodimers.....	40
4.6.3. Kinetics of heterodimers.....	45
5. Discussion	53
5.1. Fast solution exchange system in combination with cPCF	54
5.2. Characterization of mGluR1 FRET sensors in <i>Xenopus laevis</i> oocytes	54
5.2.1. mGluR1 FRET sensors assemble as dimers in the cell membrane	55
5.2.2. mGluR1 FRET sensors are functional.....	55
5.2.3. mGluR1 activates and deactivates nearly in a stepwise manner	57
5.3. Activation and deactivation kinetics of all other members of the human mGluR family	60
5.3.1. Kinetics within homodimeric mGluRs	61
5.3.2. Kinetics in heterodimeric mGluRs	61
6. Conclusions.....	67
7. References.....	69
Declaration	XI
Acknowledgments.....	XIII
Curriculum Vitae and Publication List.....	XIV

Table of Contents	I
List of abbreviations.....	V
Summary	VII
Zusammenfassung.....	IX
1. Introduction	1
1.1. Glutamate Receptors	1
1.2. Metabotropic Glutamate Receptors.....	1
1.2.1. Structural features of metabotropic glutamate receptors	3
1.2.2. Dimerization of mGluRs	5
1.2.3. The role of mGluRs in the Nervous System (NS)	6
1.3. Activation of GPCRs	7
1.4. Application of FRET methods to study kinetics in GPCRs.....	8
1.4.1. Development of fluorescent proteins.....	10
1.4.2. Förster resonance energy transfer (FRET)	11
2. Objectives	13
3. Materials and Methods	14
3.1. Molecular Biology.....	14
3.2. Preparation of <i>Xenopus laevis</i> oocytes and cRNA injection	17
3.2.1. Preparation of <i>Xenopus laevis</i> oocytes	17
3.2.2. Preparation of micropipettes for cRNA injection.....	17
3.3. Chemicals and Solutions	17
3.4. Confocal patch-clamp fluorometry experiments in outside-out membrane patches	18
3.4.1. Preparation of pipettes for outside-out patches	18
3.4.2. FRET experiments in membrane patches	19
3.5. Analysis of FRET data	21
Fitting of activation and deactivation kinetics	22
4. Results.....	23
4.1. Expression of mGluR sensors in <i>Xenopus laevis</i> oocytes	23
4.2. Optimization and characterization of measuring conditions for mGluR1 FRET	
sensors expressed in <i>Xenopus laevis</i> oocytes	24
Crosstalk and direct excitation	24
4.3. The functionality of the mGluR sensors	26

4.4. Glutamate effect in mGluR1 FRET sensors.....	28
mGluR sensors are functional	28
4.5. Kinetics	32
4.5.1. Activation and deactivation kinetics in the mGluR ₁ E-sensor	32
4.5.1.1. Further characterization of mGluR1 E-sensor.....	35
4.5.1.2. The effect of one binding site in the kinetics of mGluR1 E-sensor	36
4.5.2. A-sensor.....	37
4.6. Functional interaction of the subunits of all members in metabotropic glutamate receptors.....	38
4.6.1. Dimer assembly studied by FRET efficiency.....	39
4.6.2. Kinetics in homodimers.....	40
4.6.2.1. Group I mGluRs	40
4.6.2.2. Group II mGluRs	42
4.6.2.3. Group III mGluRs.....	44
4.6.3. Kinetics of heterodimers.....	45
4.6.3.1. Heterodimerization within the same groups.....	45
Group I	45
4.6.3.2. Heterodimerization between groups.....	47
5. Discussion	53
5.1. Fast solution exchange system in combination with cPCF	54
5.2. Characterization of mGluR1 FRET sensors in <i>Xenopus laevis</i> oocytes	54
5.2.1. mGluR1 FRET sensors assemble as dimers in the cell membrane	55
5.2.2. mGluR1 FRET sensors are functional.....	55
5.2.3. mGluR1 activates and deactivates nearly in a stepwise manner	57
5.3. Activation and deactivation kinetics of all other members of the human mGluR family.....	60
5.3.1. Kinetics within homodimeric mGluRs	61
5.3.2. Kinetics in heterodimeric mGluRs	61
5.3.2.1. Heterodimeric mGluRs within the same group	61
5.3.2.2. Heterodimeric mGluRs between different groups.....	64
6. Conclusions.....	67
7. References.....	69

Declaration	XI
Acknowledgments	XIII
Curriculum Vitae and Publication List	XIV

List of abbreviations

τ_{off}	Deactivation kinetics
τ_{on}	Activation kinetics
(S)-3, 5-DHPG	(S)-3, 5-Dihydroxyphenylglycine
Ca^{2+}	Calcium
CaCl_2	Calcium chloride
cAMP	Cyclic adenosine monophosphate
CFP	Cyan fluorescent protein
CNS	Central nervous system
cPCF	Confocal patch-clamp fluorometry
CRD	Cysteine rich domain
cRNA	Complementary ribonucleic acid
D_A	Donor signal in the presence of acceptor
DAG	Diacylglycerol
DMSO	Dimethyl sulfoxide
EC_{50}	Half maximal effective concentration
EGTA	ethylene glycol-bis(β -aminoethyl ether)-N,N,N',N'-tetraacetic acid
ER	Endoplasmatic reticulum
ERG	Electroretinogram
fc	Crosstalk factor
FLIM	Fluorescence lifetime imaging
FRET	Förster resonance energy transfer
FRET _{xc}	FRET corrected from crosstalk of donor signal
GABA _B	Gamma-aminobutyric acid receptor B
GDP	Guanosine diphosphate
GTP	Guanosine triphosphate
GPCR	G protein-coupled receptors
HEPES	N-2-hydroxyethylpiperazine-N-ethanesulfonic acid
IP3	Inositol trisphosphate

KCl	Potassium chloride
LBD	Ligand binding domain
LRET	Luminescence resonance energy transfer
LSM	Laser scanning microscope
LTD	Long term depression
mGluR	Metabotropic glutamate receptors
MgSO ₄	Magnesium sulfate
mM	Millimolar
mRNA	Messenger ribonucleic acid
ms	Millisecond
MΩ	Megaohm
NaCl	Sodium chloride
NaHCO ₃	Sodium bicarbonate
ng	Nanogram
nl	Nanoliter
nm	Nanometer
NMDA	N-methyl-D-aspartate
NMR	Nuclear Magnetic Resonance
PCF	Patch-clamp fluorometry
PCR	Polymerase chain reaction
PKC	Protein kinase C
PLC	Phospholipase C
ROI	Region of interest
s	Second
TMD	Transmembrane domain
YFP	Yellow fluorescent protein
μs	Microsecond

Summary

Metabotropic glutamate receptors (mGluRs) belong to class C G-protein-coupled receptors (GPCRs). They get activated by glutamate and are involved in many functions in the brain, including synaptic plasticity, memory and learning. mGluRs are characterized by a large extracellular domain which is composed of the ligand-binding domain (LBD), followed by a cysteine rich-domain (CRD) that ends up at the transmembrane domains (TDM). The orthosteric binding site for glutamate is located in a cleft between the two lobes of the LBD.

After glutamate binding, the two subunits of the mGluR dimer first move towards one another (intermolecular rearrangement) and then intramolecular rearrangements follow.

mGluRs are organized either as homodimers or heterodimers. Eight members belonging to mGluRs are classified in three groups: group I (mGluR1 and mGluR5), group II (mGluR2 and mGluR3), and group III (mGluR4, mGluR6, mGluR7 and mGluR8). Upon activation, group I mGluRs trigger a $G_{\alpha q}$ protein pathway. They are expressed at postsynaptic sites of neurons. In contrast, group II and III mGluRs activate $G_{\alpha i/o}$ protein pathway. Group III expresses at the presynaptic sites of neurons, whereas group II can be found either at pre- or postsynaptic sites.

Activation kinetics of ligand-activated GPCRs has been reported to be in the range of 10-80 ms, with mGluR1 being the fastest receptor measured so far. However, the available kinetic values for mGluR1 were limited by the method that was used in the respective studies. On the other hand, activation kinetics of rhodopsin, a light-activated GPCR, is in the range of 1 ms, measured with optical methods. These methods, however, cannot be applied to ligand-activated GPCRs. Therefore, we used the advantage of confocal patch-clamp fluorometry (cPCF) combined with fast concentration jumps and a high-resolution laser scanning microscope (LSM) to analyze the real activation kinetics of mGluR1 in outside-out membrane patches expressing mGluR1 FRET sensors.

We used two FRET sensors to study the kinetics of intermolecular and intramolecular rearrangements in the transmembrane domains of mGluR1 during activation. The intermolecular FRET sensor, so-called E-sensor with either CFP or YFP fused in each monomer at the second intracellular loop 2, was used to monitor the intermolecular conformational changes. To measure the intramolecular conformational changes, we used the intramolecular sensor, so-called A-sensor, with CFP fused to the C-terminal part and YFP fused at the intracellular loop 2. The “quality control system” of GABAB_B receptor was used to control the subunit composition of mGluR1 dimers in the E-sensor.

Our data show fast intermolecular activation kinetics of ~ 1 ms, which is about ten times faster than data published previously and our value is not limited by our technique, as indicated by the fact that for concentrations above 1mM, the activation speed became independent of the concentration. The kinetics within a receptor subunit (A-sensor) was around 20 times slower for both activation and deactivation kinetics. The observed deactivation kinetics was determined to be in the time range of tens of ms for the E-sensor, and hundreds of ms for the A-sensor.

The fast kinetics requires two functional binding sites because introducing the so-called YADA mutation to disrupt glutamate binding in one of the binding sites slows down activation kinetics in inter-subunit sensor about six times.

For long, metabotropic glutamate receptors (mGluRs) were considered to constitute homodimers; however, recently, some functional heterodimers were reported for mGluR2/3, mGluR2/4 and mGluR2/7.

We applied a similar approach as above, by generating intermolecular FRET sensors for all members, mGluR1 to mGluR8, and systematically analyzed dimerization and kinetics for all 36 homo- and heterodimeric forms. Five out of eight possible homodimeric receptors and 11 out of 28 heterodimeric receptors developed dynamic FRET responses with specific time courses. In heterodimeric combinations of mGluR1/2, mGluR1/3, mGluR1/5 and mGluR2/3, the activation and deactivation kinetics are dominated by the slower subunit compared to the respective homodimers. A specific effect was observed for mGluR7, not inducing a dynamic response as homodimer. When combined with mGluR2 and mGluR3, forming mGluR2/7 and mGluR3/7, respectively, mGluR7 turned out to be a strong accelerator in the activation kinetics compared to respective mGluR2 and mGluR3 homodimers.

In conclusion, functional heterodimers were identified for subunits within each group and between subunits of group I and II as well as of group II and III, but not between group I and III, i.e. heterodimerization between groups needs at least one subunit from group II.

Zusammenfassung

Metabotrope Glutamatrezeptoren (mGluRs) sind G-Protein-gekoppelten Rezeptoren (GPCRs) der Klasse C. Sie werden durch Glutamat aktiviert und sind an vielen Funktionen im Gehirn, wie beispielsweise synaptischer Plastizität, Gedächtnis und Lernen beteiligt. mGluRs bestehen aus einer großen extrazellulären Domäne, die sich aus einer Ligandenbindungsdomäne (LBD), einer Cystein-reichen Domäne (CRD), und einer darauffolgenden Transmembrandomäne (TDM) zusammensetzt. Die orthosterische Bindungsstelle für Glutamat befindet sich zwischen den zwei Flügeln der Ligandenbindungsdomäne, die sich nach Ligandenbindung aufeinander zu bewegen; ähnlich dem Schließen einer Venusfliegenfalle.

Nach Bindung von Glutamat bewegen sich als erstes die beiden Untereinheiten des mGluR Dimers aufeinander zu (intermolekulare Umlagerung) und anschließend folgen intramolekulare Umlagerungen.

Die acht Mitglieder der mGluR-Familie werden in drei Gruppen eingeteilt: Gruppe I (mGluR1 und mGluR5), Gruppe II (mGluR2 und mGluR3) und Gruppe III (mGluR4, mGluR6, mGluR7 und mGluR8). Gruppe I mGluRs aktivieren den G_{α_q} -Signalweg und werden auf der postsynaptischen Seite von Neuronen exprimiert. Die Gruppen II und III aktivieren den $G_{\alpha_i/o}$ -Signalweg. Gruppe III mGluRs exprimieren an den präsynaptischen Seite von Neuronen, während Gruppe II mGluRs sowohl an der prä- als auch postsynaptische Seite lokalisiert sind. mGluRs sind konstitutive Dimere, wobei sowohl funktionelle Homodimere, als auch Heterodimere (mGluR2/3, mGluR2/4 und mGluR2/7) beobachtet wurden.

Für ligandenaktivierte GPCRs sind Aktivierungskinetiken im Bereich von 10 bis 80 Millisekunden (ms) berichtet worden, wobei mGluR1 der bisher schnellste gemessene Rezeptor ist. Die bisherigen kinetischen Werte für mGluR1 wurden jedoch durch die in den Studien verwendete Methodik limitiert. Allerdings wurden bereits schnellere Kinetiken für GPCRs beschrieben. Die Aktivierungskinetik des lichtaktivierten GPCR Rhodopsin wurde mit optischen Methoden im Bereich von 1 ms gemessen. Die dabei verwendeten Methoden können jedoch nicht für ligandenaktivierte GPCRs angewendet werden. Diese Limitierung umgehen wir in der vorliegenden Arbeit mit der konfokalen Patch-Clamp-Fluorometrie (cPCF). Dabei werden mGluR1-FRET-Sensoren in outside-out Patches schnellen Ligand-Konzentrationsprüngen ausgesetzt und mit einem hochauflösenden Laser-Scanning-

Mikroskop (LSM) vermessen, um die tatsächliche Aktivierungskinetik von mGluR1 zu analysieren.

Wir verwendeten zwei FRET-Sensoren, um die Kinetik von sowohl intermolekularer als auch intramolekularer Umlagerungen in den Transmembrandomänen von mGluR1 während der Aktivierung zu untersuchen. Der FRET-Sensor, der die intermolekulare Umlagerungen detektiert, enthält in jedem Monomer entweder CFP oder YFP in der zweiten intrazellulären Schleife II und wird „E-Sensor“ genannt. Um die intramolekularen Konformationsänderungen zu messen, verwendeten wir den intramolekularen A-Sensor, wobei CFP im C-terminalen Teil und YFP in der intrazellulären Schleife II fusioniert waren. Ein "Qualitätskontrollsystem" von GABA_B wurde verwendet, um die Zusammensetzung der Untereinheiten von mGluR1-Dimeren im E-Sensor zu kontrollieren.

Unsere Daten zeigen eine schnelle intermolekulare Aktivierungskinetik von etwa einer ms, die etwa zehnfach schneller ist, als die zuvor veröffentlichten Daten und nicht durch unsere Technik beschränkt wird dafür Konzentrationen über 1 mM die Aktivierungsgeschwindigkeit unabhängig von der Konzentration ist. Die Kinetik innerhalb einer Rezeptoruntereinheit war sowohl für die Aktivierungs- als auch für die Deaktivierungskinetik etwa 20-mal langsamer. Es wurde festgestellt, dass die beobachtete Deaktivierungskinetik im Zeitbereich von zehn ms für den E-Sensor und Hunderten ms für den A-Sensor liegt.

Die schnelle Kinetik erfordert zwei funktionelle Bindungsstellen. Wenn man die Glutamatbindung an einer Bindungsstelle durch die Einführung der YADA-Mutation stört, wird die Aktivierungskinetik zwischen zwei Untereinheiten etwa sechsmal verlangsamt.

Wir haben dann einen ähnlichen Versuchsansatz für alle Mitglieder der mGluR-Familie, mGluR1 bis mGluR8 verwendet und sowohl die Dimerisierung als auch die Kinetik für alle 36 möglichen homo- und heterodimeren Rezeptoren analysiert. Fünf von acht möglichen homodimeren Rezeptoren und 11 von 28 möglichen heterodimeren Rezeptoren zeigten dynamische FRET-Antworten mit spezifischen Zeitverläufen. In den Heteromeren mGluR1/2, mGluR1/3, mGluR1/5 und mGluR2/3 wird die Aktivierungs- und Deaktivierungskinetik von der langsameren Untereinheit im Vergleich zu den jeweiligen Homodimeren dominiert. Bei mGluR7 konnte keine dynamische Reaktion in der homodimeren Form mit gesättigter Konzentration festgestellt werden. In Kombination mit mGluR2 und mGluR3 als Heterodimer mGluR2/7 und mGluR3/7 zeigte sich allerdings eine starke Beschleunigung in der Aktivierungskinetik im Vergleich zu den jeweiligen Homodimeren 2 und 3.

Zusammenfassend wurden funktionelle Heterodimere für Untereinheiten innerhalb jeder mGluR-Gruppe identifiziert. Kombinationen aus Untereinheiten der Gruppen I und II sowie der Gruppen II und III, jedoch nicht zwischen Gruppe I und III zeigten funktionelle Antworten auf Sprünge von Glutamat. Es lässt sich schlussfolgern, dass die Heterodimerisierung zwischen verschiedenen Gruppen mindestens eine Untereinheit aus Gruppe II benötigt.

1. Introduction

1.1. Glutamate Receptors

Glutamate (Glu) is an essential excitatory neurotransmitter in the central nervous system (CNS). It is involved in synaptic transmission by activating a group of ion channels and receptors. Ion channels activated by glutamate are called ionotropic glutamate receptors (iGluR), and in this group are included: N-methyl-D-aspartate (NMDA) receptors, α -amino-3-hydroxy-5-methyl-4-isoxazole propionic acid (AMPA) receptors and kainite receptors. Glutamate receptors not generating an ionic conductance by themselves are called metabotropic glutamate receptors (mGluRs) (Blackshaw et al. 2011) (Fig. 1).

The ionotropic glutamate receptors (iGluRs) are involved in fast excitatory responses in synapses, whereas metabotropic glutamate receptors induce slower metabolic responses by activating a cascade of intracellular pathways mediated by G-proteins.

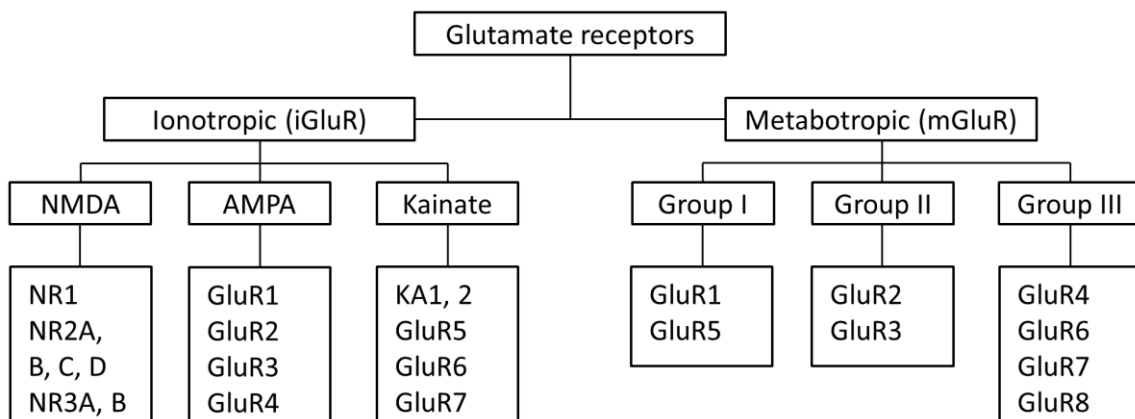


Figure 1: Classification of Glutamate Receptors

1.2. Metabotropic Glutamate Receptors

mGluRs play a regulatory role on neuronal excitability in the central nervous system (CNS), synaptic transmission, long term depression (LTD) and long term potentiation (LTP). This effect is realized by regulating several classes of ion channels, including voltage-dependent potassium channels, voltage-dependent Ca^{2+} channels, non-selective cation channels, and ligand-gated ion-channels (Saugstad et al. 1995).

mGluRs comprise eight isoforms. They can be classified into three groups based on sequence similarity, the second messenger pathways they initiate and pharmacology (Nakanishi 1994,

Pin and Duvoisin 1995, Conn and Pin 1997). Numbering from 1 to 8 is related to the timeline their cDNA has been cloned (Nakanishi 1994, Pin and Duvoisin 1995).

mGluR1 and mGluR5 belong to group I, mGluR2 and mGluR3 to group II, and mGluR4, mGluR6, mGluR7 and mGluR8 to group III (Pin and Duvoisin 1995). An evolutionary phylogenetic tree of metabotropic glutamate receptors is shown in Fig. 2.

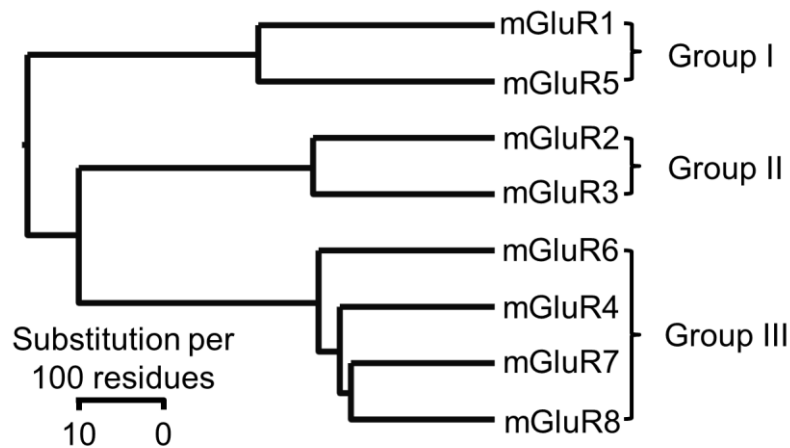


Figure 2: Phylogenetic tree of the eight human mGluRs

Sequence identity within members of the same group is about 70 %, whereas about 30 % between different groups (Pin and Duvoisin 1995). Different groups appear to express in different regions in the synapse, and even trigger different messenger pathways upon ligand binding (Bhattacharyya 2016).

Group I mGluRs are mainly expressed at postsynaptic sites, group II mGluRs are represented at both pre and postsynaptic sites, whereas group III mGluRs are mostly represented at presynaptic sites (Bhattacharyya 2016, Kim et al. 2008).

Upon activation, members of group I mGluRs (mGluR1 and mGluR5) couple to the G_{α_q} -protein pathway, activating Phospholipase C (PLC), generating diacylglycerol (DAG) and inositol 1,4,5-triphosphate (IP_3). IP_3 activates inositol triphosphate (IP_3) receptors in the endoplasmic reticulum (ER), triggering Ca^{2+} release into the cytosol. High levels of Ca^{2+} concentrations in the cytosol, together with diacylglycerol (DAG) contribute to protein kinase C (PKC) activation. An outcome of this signaling pathway is an increase in postsynaptic excitability involving several ion channels and receptors: Ca^{2+} channels, small current (SK) K^+ channels, N-Methyl-D-Aspartate (NMDA) receptors (Conn and Pin 1997, Kim et al. 2008, Bhattacharyya 2016).

Members of Group II and Group III mGluRs are functionally antagonistic to group I mGluRs. Upon activation they couple to the $G_{\alpha i/o}$ -protein, leading to the inhibition of adenylate cyclase. This leads to an inhibition of the cAMP formation and of various Ca^{2+} channels, but to an activation of K^+ channels (Schoepp 2001, Pin and Acher 2002, Niswender and Conn 2010).

1.2.1. Structural features of metabotropic glutamate receptors

The structure of mGluRs contains three central regions (Fig. 3): the extracellular-region (including the LBD and the CRD), the transmembrane domain (TMD), containing seven transmembrane helices penetrating the cell membrane, and the cytoplasmic domain (C-terminal domain) (Kunishima et al. 2000).

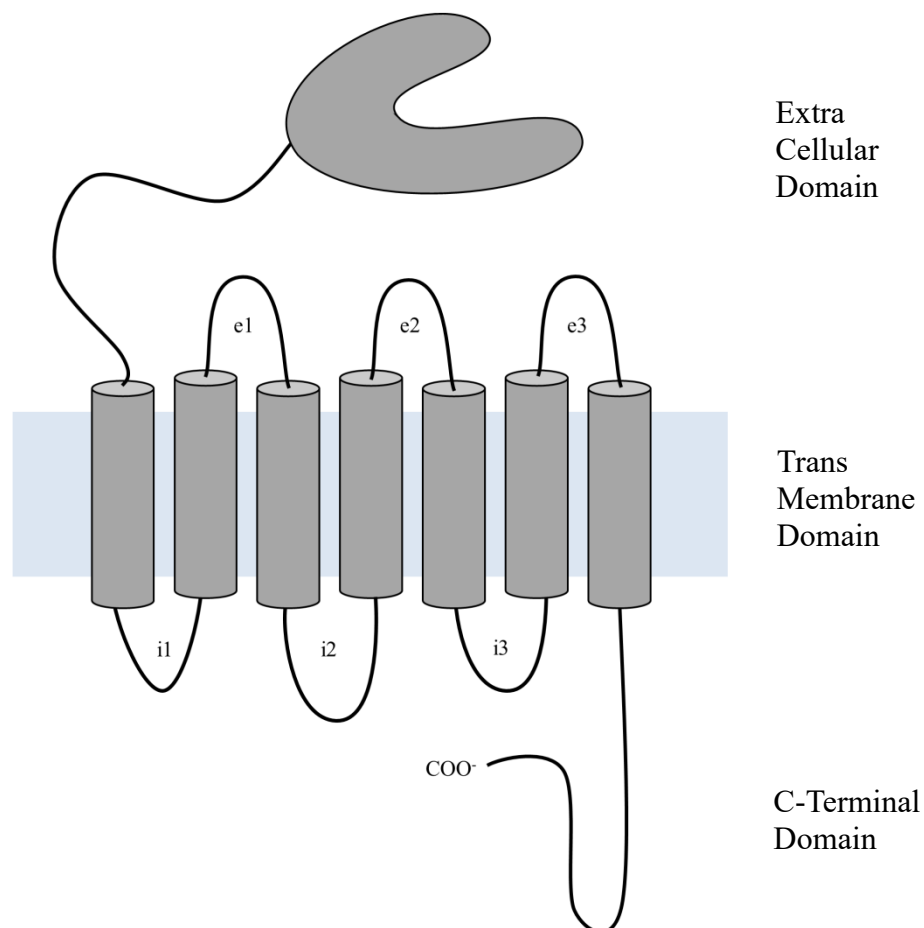


Figure 3: Structure of an archetypical mGluR subunit. Large extracellular domain composed of the LBD and a long CRD. Seven transmembrane helices, connected by three intracellular and three extracellular loops form the TMD. The C-terminal domain is located in the cytoplasm.

Extracellular domain

The extracellular domain is a massive structure composed of two lobes forming a similar shape like a Venus flytrap (Muto et al. 2007). A cleft between the lobes is responsible for binding the native ligand, glutamate. The binding site is also termed 'orthosteric binding site'. Based on the mutational analysis in mGluR1, Tyr74 is identified as the most critical position that forms a hydrogen bond with glutamate (Kunishima et al. 2000, Tsuchiya et al. 2002).

The LBD of each subunit can exist in three conformational states: open-open (inactive) conformation that is fixed by antagonists, open-closed, and closed-closed (active) that is promoted by agonists that bind to one or both binding sites (Niswender and Conn 2010).

The LBD is followed by a long cysteine-rich domain, organized in three β -sheets, each composed of two anti-parallel β -strands (Muto et al. 2007). The CRD contains nine cysteine residues which are very well conserved in the whole family of class C GPCRs except for the GABA_B receptor. Eight of these cysteines create disulfide bridges within the CRD to make the entire domain a compact structure. The 9th cysteine residue creates a disulfide bridge with extracellular loop 2 (Cys 234) and is found to be responsible for transmitting the signal from the LBD to the TMD. Mutation of this cysteine (Cys 234) prevents receptor activation after applying glutamate, even though glutamate binds to the orthosteric binding site (Rondard et al. 2006).

The TMD

The TMD is formed by seven α -helices integrated on the cell membrane; each helix is linked to the next by loops, three extracellular and three intracellular loops. The intracellular loop 2 plays a role in regulating the binding of the receptor with G-proteins, and also kinases, including G-protein coupled kinase 2 (Niswender and Conn 2010), whereas extracellular loop 2 creates a disulfide bridge with the CRD as mentioned above and helps to transmit the signal on the transmembrane domain. Besides the orthosteric binding site, located in the extracellular domain, the TMD contains an additional allosteric binding site that can be targeted by positive or negative allosteric modulators (Feng et al. 2015).

C-terminal domain

The C-terminal domain is located on the intracellular side of the cell. It plays a role in modulating the coupling of the G-protein with the activated receptor, and also plays a role in dimerization (Niswender and Conn 2010). The C-terminus is a very heterogeneous domain. Different splice variants of mGluR1 appear to have different C-terminal lengths and composition. mGluR1a have a long C-terminus with 318 amino acids, another splice variant mGluR1b lacks 292 amino acids at the end, mGluR1d has a C-terminus with 26 amino acids, and mGluR1e does not have a C-terminal tail at all. These differences presumably play a role in coupling with different proteins in the cytosol to regulate receptor neurotransmission (Hlavackova et al 2017).

1.2.2. Dimerization of mGluRs

Dimerization of mGluRs is required for their function (El Moustaine et al. 2012). mGluRs are constitutive dimers, the LBDs of each monomer dimerize by a “disulfide bridge” between the rear sides. The covalent bond is formed between Cys140 of each monomer in mGluR1 (Kunishima et al. 2000) and it is formed already in the ER (Robbins et al. 1999). A similar bond is also reported for mGluR5 (Romano et al. 1996). First, it was believed that mGluRs are constitutive homodimers, but later, it has been proven that these receptors also form functional heterodimers. A recent study suggests that homo- and heterodimerization is realized by interactions at the hydrophobic interface in the upper lobe of LBDs with some modest contribution from an intersubunit disulfide bridge and TMD interactions (Levitz et al. 2016).

At the level of TMDs, FRET studies suggest that the transmembrane helix 5 plays a critical role in receptor-receptor interface formation (Yanagawa et al. 2011). Six molecules of cholesterol found in the crystal structure of transmembrane domains in mGluR1, near the dimer interface, might also play a role in dimerization and activation (Wu et al. 2014).

One of the most extensive studies in heterodimerization of mGluRs was done using time-resolved FRET (Doumazane et al. 2011). These authors labelled all mGluRs except mGluR6 with the SNAP and CLIP technology and tagged them with organic dyes. They identified 11 out of 21 possible combinations to form heterodimers. Furthermore, they concluded that heterodimerization is likely to happen between members of each group, and between members of group II and III, but not between members of group I and II or I and III. The first

heterodimer that was characterized pharmacologically was mGluR2/4, a dimer between-group II and III mGluRs (Kammermeier 2012). Researchers in this study co-expressed both receptors in a setting that promotes heterodimerization in isolated sympathetic neurons that naturally does not express mGluRs. Selective agonists for mGluR2 or mGluR4 applied separately did not activate the receptors, whereas when both selective agonists were used in combination, the receptor was fully active. Heterodimerization within group II was described for mGluR2/3 using a single-molecule approach (Levitz et al. 2016) and later work from the same group (Lee et al. 2020) showed that heterodimerization between mGluR2 and mGluR3 is preferable compared to respective homodimers. Another functional heterodimer was detected using an LRET-based approach by creating biosensors and targeting a surface system for heterodimers only (Moreno Delgado et al. 2017), mGluR2/4 heterodimer is detected in native cells. Furthermore, another heterodimer between group II and III was reported recently between mGluR2/7 (Habrian et al. 2019). In this combination, mGluR2 brings the EC_{50} value for mGluR7 not only into the physiological range (for mGluRs in μ M concentrations) but also improves efficiency about sevenfold compared to the mGluR2 homodimer. Still, a lot of work needs to be done to study other mGluR heterodimers, and the role of respective subunits.

1.2.3. The role of mGluRs in the Nervous System (NS)

Metabotropic glutamate receptors are widely spread in the brain. Members of group I (mGluR1 and mGluR5) are preferably found in the hippocampus. They are believed to play a crucial role in synaptic plasticity (Hlavackova et al. 2017). Moreover, mGluR1 alpha was detected using antibodies in cerebellum and hippocampus (Baude et al. 1993). In the cerebellum, mGluR1 alpha is linked to modulating motor activity. In mice deficient of mGluR1, a severe motor deficit was seen. Also, another effect was difficulty in learning, linking the involvement of mGluR1 in long term depression (LTD) in the cerebellum (Conquet et al. 1994). Activation of mGluR1 induces calcium in Purkinje cells, an effect which is responsible and required for LTD induction (Aiba et al. 1994). mGluR1 and mGluR5 are also present during prenatal development, and there is evidence that they play a role in the development of the cortex (Aiba et al. 1994, Miyata et al. 2000). mGluR1 is also expressed in the thalamus (Lourenço Neto et al. 2000). Except in the CNS, group I mGluRs are also found in peripheral nociceptors (Bhave et al. 2001, Walker et al. 2001).

Members of group II (mGluR2 & mGluR3) are also present in neurons, mainly in neurons responsible for sensing and conducting pain (Jia et al. 1999, Carlton et al. 2011). Agonists of Group II mGluRs can be potential drugs on treating schizophrenia because they share similar

biochemical and pharmacological pathways like the antipsychotic drug clozapine (Swanson Schoepp 2002).

Group III mGluRs (mGluR4, mGluR6, mGluR7 and mGluR8) have a more diverse location and function. mGluR4 is expressed in the cerebellum, and it inhibits forskolin-stimulated cyclic AMP accumulation (Tanabe et al. 1992). A similar pathway also activates mGluR7 which is present mainly in the retinal inner nuclear layer where ON-bipolar cells are distributed (Okamoto et al. 1994).

mGluR6, a $G_{i/o}$ -coupled receptor, expresses on ON-bipolar cells in the retina, in knockout mice lacking mGluR6, electroretinogram (ERG) recordings on superior colliculus shows that mGluR6 deficiency abolishes ON responses in optical transmission but does not affect OFF responses. Hence, the function of mGluR6 in the bipolar cells is essential for synaptic transmission (Masu et al. 1995, Vardi et al. 2000). The mGluR8 gene was found to be highly expressed on the olfactory bulb and mammillary body, and it is also present in retinal cells and in the cortex at a lower level, mGluR8 also appears in different brain regions during the development (Duvoisin et al. 1995). Location of mGluR8 and pharmacology in mitral/tufted cells tells that this receptor can be presynaptically located, and plays a positive role in modulating glutamate release by these cells in their axon terminals in entorhinal cortex (Duvoisin et al. 1995).

1.3. Activation of GPCRs

A G-protein coupled receptor is activated when ligand bonds to the orthosteric binding site, or, in case of rhodopsin, when light activates the 'the fixed' 11-cis retinal.

Many studies have shown that activation of GPCRs upon ligand binding is associated with a conformational change in the transmembrane helices III, V and VI (Farrens et al. 1996, Sheikh et al. 1996, Sheikh et al. 1999, Wieland et al. 1996, Ward et al. 2002). These conformational changes facilitate the interaction with the G proteins, triggering the downstream signaling cascade inside the cell, resulting in the control of ion channels or secondary messengers. Inside the cell, signaling cascades can be studied by dynamic changes of FRET signals (Lohse et al. 2008).

G-protein coupled receptors have an intermediate activation speed, slower compared to ion channels, for example, nicotine acetylcholine receptors, which activate very fast and transmit

the signal within milliseconds, and faster than tyrosine kinase or guanylyl cyclase receptors which activate and send their signal in minutes to hours (Lohse et al. 2014).

Rhodopsin is one exception within the GPCR family, it is activated by light, and the process that transforms rhodopsin (inactive state) to metarhodopsin II (active state) happens with a time constant of about 1 ms. This process includes several intermediate states which can be identified by spectroscopic methods (Arshavsky et al. 2002). Rhodopsin is easily accessible because it is present in rod segments in high amounts and it is also easy to isolate and handle for experimental procedures. Therefore, for long time, rhodopsin served as a model to describe characteristics of the whole family of GPCRs (Ernst et al. 2000, Heck et al. 2000).

First attempts to study kinetics on ligand-activated GPCRs were made in β_2 -adrenergic receptors which were purified and reconstituted into lipid vesicles. Several cysteines were introduced in sensitive areas of the receptor and were labelled with environmental sensitive fluorophores. Changes in conformation were associated with changes in fluorescence because of the movement of the fluorophore in different environments (Gether et al. 1995). These changes in fluorescence as a result of conformational changes within the receptor were in the range of minutes, which does not match functional responses in intact cells. Using the same methods, similar slow responses in fluorescence were reported in leukotriene B4 reconstituted purified receptors (Damian et al. 2008). However, this slow activation can be attributed to the experimental conditions. An explanation might be that receptors are removed from their native system cell membrane, and other essential elements are missing, like cholesterol which is seen to be present in crystal structures. Herein, a more recent fluorescence-based strategy to study receptors is applied. FRET-based biosensors were developed by fusing or attaching fluorophores in sensitive regions of the receptors, and any change in fluorescence as a result for conformational changes within the receptor could be visualized and quantified in native cells (Marcaggi et al. 2009, Hlavackova et al. 2012) or even membrane patches (Grushevskiy et al. 2019).

1.4. Application of FRET methods to study kinetics in GPCRs

Methods that are based on resonance energy transfer are widely used also in the GPCR community. Resonance energy transfer can be either fluorescence resonance energy transfer (FRET) or bioluminescence resonance energy transfer (BRET). In BRET measurements a fluorescent enzyme (*Renilla luciferase*) serves as a donor molecule; usually, it is coupled with GFP or variants of it. In FRET measurements, acceptor and donor molecules can be different

fluorescent proteins, as for example CFP or YFP. More recently, also more stable and brighter low molecular dyes were used (Marullo and Bouvier 2007). For FRET measurements the donor chromophore should be fluorescent, whereas it should be bioluminescent for BRET measurements. The acceptor chromophore can be fluorescent, but it is not strictly necessary for both methods (Marullo and Bouvier 2007).

Fluorescent proteins for FRET and BRET measurements can be genetically expressed and fused into the target protein that is being studied. The fusion of both donor and acceptor molecules to a target protein allows to measure events happening within the protein, including conformational changes during activation or deactivation, and fusing these chromophores in two different proteins enables to observe their interactions.

During activation the transmembrane helices 5 and 6 are essential and change their position. The loop that connects these transmembrane helices (intracellular loop 3) was used already before as a place to fuse chromophores (Ward et al. 2002), and the other preferred position was the C-terminal domain. Placing fluorophores in these positions preserved the ability of receptors to couple with G-proteins and remain functional (Farrens et al. 1996, Ward et al. 2002).

FRET constructs containing donor and acceptor in intracellular loop 3 and the C-terminal domain showed a decrease in the FRET signal during activation, indicating an increase in distance between intracellular loop 3 and C-terminal domain. This strategy was applied for α_{2A} -adrenergic receptors and PTHRs (parathyroid receptors) where CFP was fused to the intracellular loop 3 and YFP in the C-terminal domain. Activation kinetics of ~ 40 ms for α_{2A} -adrenergic and ~ 1 s for PTHR were recorded (Villardaga et al. 2003). Another strategy was used by Hoffmann and colleagues (Hoffmann et al. 2005), who fused CFP in the C-terminal domain and instead of YFP they introduced a tetra-cysteine domain in the intracellular loop 3 which could be labelled with the fluorescein arsenical hairpin binder (FlAsH). This strategy was applied to study the activation kinetics of the human adenosine A_{2A} receptor and the α_{2A} -adrenergic receptor. The observed kinetics for both constructs were about 66-88 ms. Another example is placing Cerulean (Cer) in the C-terminal and YFP in the intracellular loop 3 of the β_1 -adrenergic receptor, where the activation kinetics were in the range of 60 ms (Rochais et al. 2007). In all examples mentioned above, modified FRET sensors retained their biological functions as non-modified receptors (Villardaga et al. 2003, Hoffmann et al. 2005, Rochais et al. 2007).

Exceptional slow activation kinetic (80 seconds) was observed noticed for the bradykinin B₂ receptor (Chachisvilis et al. 2006).

The FRET approach was also applied to dimeric GPCRs. The process of activation in metabotropic glutamate receptor 1 was shown to involve a rearrangement between two monomers by moving towards each other (Tateyama et al. 2004). This process was studied by placing CFP in intracellular loop 2 of one monomer and YFP in the same position in the other monomer. Later on, this process was observed by another group using a superfusion system. The authors identified a first component of intermolecular movement of 35 ms and a slower rearrangement component in each monomer in the range of 50 ms (Hlavackova et al. 2012). Another study using a similar approach in mGluR1 showed different kinetics for the intermolecular rearrangement, slightly faster than 10 ms. However, this value was technically limited, suggesting that the real activation kinetics of mGluR1 is more rapid (Marcaggi et al. 2009). The same group did not notice any conformational change within monomers.

The studies above showed that activation of ligand-activated GPCRs is slower compared to rhodopsin (Arshavsky et al. 2002). It remains unclear if rhodopsin behaves differently compared to other GPCRs by activating fast, or if the kinetics observed so far for other GPCRs was limited by the techniques that were used to study them.

1.4.1. Development of fluorescent proteins

Humans were always excited from living organisms that can emit light and there are a variety of species which can do so (Matz et al. 2002). One of the organisms which produce light is *Aequorea victoria*. This organism is a jellyfish and lives on the west coast of North America in the Pacific Ocean. The first characterization of the green fluorescence in *Aequorea* was performed in 1995 (Davenport and Nicol 1995). Osamu Shimomura first isolated and purified the molecule that is responsible for the fluorescence in the *Aequorea* jellyfish in 1962. He named it aequorin. Aequorin emits intense blue light in the presence of Ca²⁺ (Shimomura et al. 1962). Five years after Shimomura's discovery, aequorin was applied first in a biological system (Ridgway and Ashley 1967). The authors injected aequorin into the muscle of a barnacle (*Cirripedia*) and they observed Ca²⁺ signals.

While purifying aequorin from *Aequorea victoria*, another fluorescent protein was discovered and purified besides aequorin. This protein emits light in the green range and is excited from

the light emitted from aequorin (Morise et al. 1974). This new fluorescent molecule was named 'green protein' by Shimomura. Later on, it took the name 'green fluorescent protein'.

The first scientist who cloned cDNA of green fluorescent protein (GFP) was Douglas Prasher. He also proposed to use it as a trace molecule in a living organism (Prasher et al. 1992, Chalfie et al. 1994). Unfortunately, Douglass Prasher had to leave science because of lack of funding, and his name is missing sadly between the scientists who won the Nobel Prize in Chemistry in 2008 for discovering and developing of the green fluorescence protein GFP.

The discovery of GFP provided the scientific community in the fields of medicine, cell biology and physiology a great tool to label specific proteins and study their behavior without the need for exogenous labelling by using dyes or fluorescent antibodies. Using advanced fluorescent microscopes, proteins carrying GFP can be localized and studied much better than before. Movements of specific proteins inside the cell, roles of proteins in signaling processes, interactions with other proteins and conformational changes within those proteins can be made visible.

Many scientists used the enormous potential of GFP. The need to have more proteins which fluoresce with different excitation and emission spectra was strong. After many efforts, the results came by the mid-1980s, from the work of Roger Tsien. He developed different variants of GFP with different excitation and emission spectra, also with better and more stable fluorophores. Variants of GFP that he developed are a better version of GFP with a higher signal, named enhanced green fluorescent protein (EGFP), a variant which fluoresces in the cyan region, cyan fluorescent protein (CFP) and a variant which fluoresces in the yellow region, named yellow fluorescent protein (YFP). CFP and YFP are now widely used as a FRET pair. Tsien also developed other versions, the blue and violet fluorescent protein, BFP and Sapphire, respectively (Tsien 1998).

These developments made it possible to use different fluorescent proteins at the same time and investigate more than one event inside a living cell.

1.4.2. Förster resonance energy transfer (FRET)

Förster (fluorescence) resonance energy transfer (FRET) is the name of a physical effect for the radiation-less transfer of energy between two molecules (chromophores) (Förster 1948). For FRET to happen, some specific requirements must be accomplished (Vogel et al. 2006):

1. Spectral overlap: a donor fluorophore excited with an incident light on its absorption spectrum emits the energy after a brief time (nanoseconds). The emission spectrum of the fluorophore is always right-shifted to longer wavelength which is associated with a reduced energy. If an acceptor fluorophore is present in the distance less than 10 nm and its excitation spectrum corresponds with that of the emission spectrum of the donor fluorophore, an amount of energy is transferred radiation-less to it.
2. Donor and acceptor FRET pairs should be in close vicinity to each other (1-10 nm). It is shown that FRET efficiency, E_{FRET} , between the dipoles of donor and acceptor molecules depends on the 6th power of the distance amongst them:

$$E_{\text{FRET}} = R_0^6 / (R_0^6 + r^6)$$

R_0 is the Förster radius at which half of the energy from the donor is transferred to the acceptor and r distance between the donor and acceptor.

The Förster radius relies on the fluorescence quantum yield of the donor and acceptor, the refractive index of the environment (η), the dipole orientation of each fluorophore (κ^2) and the spectral overlap integral of the donor-acceptor pair (J).

$$R_0^6 = 9(\ln 10) \kappa^2 \phi_D J / 128 \pi^5 \eta^4 \tau N_A$$

3. The positions of dipoles for donor emission and acceptor excitation should not be oriented perpendicular.

FRET can be measured in different ways: monitoring changes in either donor or acceptor fluorescence as an event occur, measuring changes in both donor and acceptor signals at the same time, monitoring changes in fluorescence as a result of changes in the orientation of fluorophores (Vogel et al. 2006).

Nowadays, FRET is extensively used in biophysical experiments to study protein-protein interactions or different structural rearrangements within the proteins. Significant steps in making this technique so successful in biology are the development of different variants of the mentioned different variants of GFP (Tsien et al. 1998), and improved instruments for measuring it.

2. Objectives

The most studied GPCR is rhodopsin. It is present in the visual system and is activated by light. Due to its photochemical properties, it can be easily investigated by spectroscopic methods, which helped to reveal that the switch from rhodopsin to meta-rhodopsin II (active form) is established in about 1 ms after light induction (Arshavsky et al. 2002). However, this strategy cannot be applied to study other GPCRs since they do not possess such photochemical properties. Several different ways using fluorescent based sensors were used to study the kinetics of ligand-activated GPCRs (Villardaga et al. 2003). The fastest kinetics of a ligand-activated GPCR, described so far, were those of the metabotropic glutamate receptor 1 (mGluR1). Its activation kinetics of about 10 ms were specified by FRET based sensors and super-fusion of the ligand on the living cells. However, this published value is at the resolution limit of the technique the authors used (Marcaggi et al. 2009). Therefore, the question remains open if the ligand-activated GPCRs activate with the same speed like rhodopsin, or rhodopsin remains a unique example.

The objectives of the experiments in this work were:

- Adjust a fast solution exchange system for the application of glutamate or other solutions in excised outside-out membrane patches expressing mGluR FRET sensors. The speed of the solution exchange up to 200 μ s is reported in the literature. We aim to achieve the speed of 1 ms or faster in order to be able to measure kinetics in the range of the activation kinetics of rhodopsin.
- Determine if the activation speeds of metabotropic glutamate receptor 1 (mGluR1) is similar to the activation speed of rhodopsin.
- Investigate the contribution of the ligand binding sites in the activation and deactivation kinetics of mGluR1 using mutagenesis in only one subunit.
- After characterizing the kinetics of mGluR1, the same strategy was to be used to generate FRET sensors for all members of mGluRs and to analyze and compare kinetics of activation and deactivation for the 8 homodimers of the mGluR family.
- Test the ability for each mGluR subunit to form heterodimers by kinetic signals in all 26 possible combinations. The aggregation of heterodimers was studied by acceptor photobleaching while functionality by activation and deactivation kinetics induced by glutamate.

3. Materials and Methods

3.1. Molecular Biology

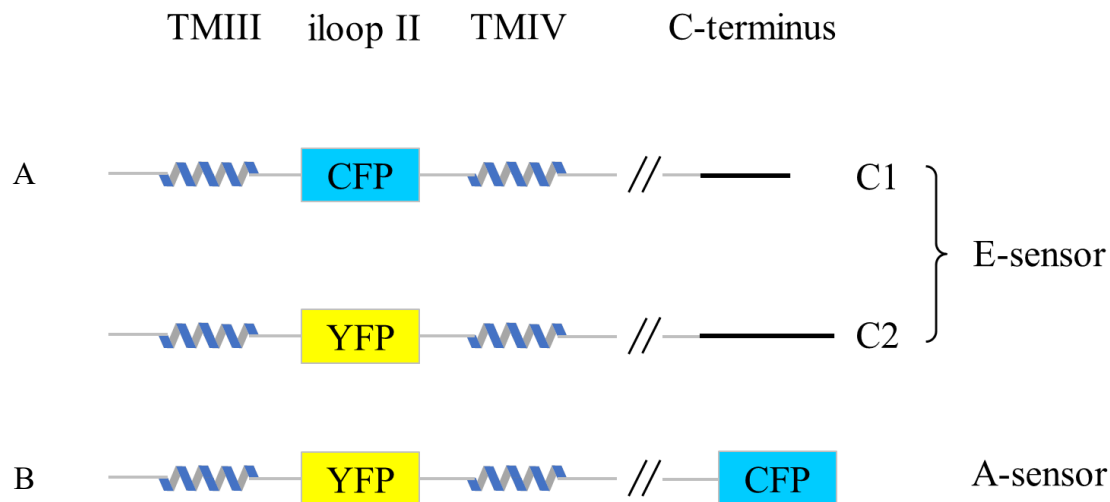
To analyze and investigate intermolecular versus intramolecular activation and deactivation kinetics of mGluR1, we used rat mGluR1 (accession number NM_001114330.1). FRET sensors for studying intermolecular rearrangements within the mGluR1 were cloned by placing CFP or YFP into intracellular loop 2 of each monomer. For monitoring intramolecular rearrangements, YFP was placed in the intracellular loop 2 and CFP in the C-terminus within each monomer as reported in (Hlavackova et al. 2012). Afterwards, those sensors were re-cloned into a pGEM-HE-new vector (Liman et al. 1992) for expression in *Xenopus* oocytes. The constructs were kindly provided to us by Dr. Ulrike Zabel (University of Würzburg).

Constructs were named as follows: D36 (mGluR1-CFP-C1) and D56 (mGluR1-YFP-C2) for the intermolecular E-sensor, and mycD63 for the intramolecular A-sensor.

D36 and D56 were used as templates later on to generate mGluR1 Y226A, mGluR1 D308A, and mGluR1 Y226A/D308A by site-directed mutagenesis performed by Dr. Tina Schwabe (Physiology II) using overlap extension PCR with the aim to investigate the contribution of individual binding sites in the kinetics of mGluR1.

For *in-vitro* cRNA production, these constructs were linearized, and cRNA was created using the mMACHINE T7 kit (Thermo Fischer) by Karin Schoknecht (Physiology II).

We extended our study to investigate activation and deactivation kinetics in the eight homodimeric metabotropic glutamate receptors mGluR1 to mGluR8. Furthermore, we investigated the ability of these mGluRs to form heterodimers. We used for this part of the study human type mGluRs. Eight members of metabotropic Glutamate Receptors: mGluR1 (accession number XM_017010783.1), mGluR2 (accession number NM_000839), mGluR3 (accession number NM_000840), mGluR4 (accession number NM_000841), mGluR5 (accession number NM_001143831.2), mGluR6 (accession number NM_00843), mGluR7 (accession number NM_000843) and mGluR8 (accession number NM_000845), were used to generate intermolecular FRET sensors analogue to the ones described (Hlavackova et al. 2012). Sensors were prepared by Prof. Dr. Thomas Zimmer and Dr Christian Sattler. In total 16 constructs were generated, two for each mGluR, see Scheme 1a.



Scheme 1: Schematic representation of constructs: A. Two different constructs were generated for each mGluR. CFP or YFP were included in intracellular loop 2, and C-terminal domain from the GABA_B “quality control system” (C1 or C2). **B.** Scheme of A-sensor (generated only for mGluR1). YFP is included in intracellular loop 2 and CFP in the C-terminus.

Either CFP or YFP was fused in intracellular loop 2, always five amino acids after the end of transmembrane helix 3. In the C-terminus, 19 amino acids after transmembrane helix 7, the GABA_B “quality control system” was introduced, either the last 87 C-terminal amino acids from GABA_{B1} (C1) or the last 181 c-terminal amino acids of GABA_{B2} (C2). C1 was introduced in the mGluR monomer containing CFP, whereas C2 was introduced in mGluR monomers containing YFP, in this way only dimers containing different C-terminal tails in length (C1:C2) or C2:C2, reach the cell membrane (Hlavackova et al. 2012, Kniazeff et al. 2004), prohibiting in this way C1:C1 dimers to leave the ER. The C-terminal part of GABA_{B1} (one of the GABA_B subunits) possesses an ER retention signal. Transportation of a functional dimeric form of GABA_B is possible only when the ER retention signal from GABA_{B1} interacts with the C-terminal part present in the GABA_{B2} (the second subunit of GABA_B). Therefore, the GABA_B “quality control system” will determine which subunits leave the ER and express in the cytoplasmic membrane.

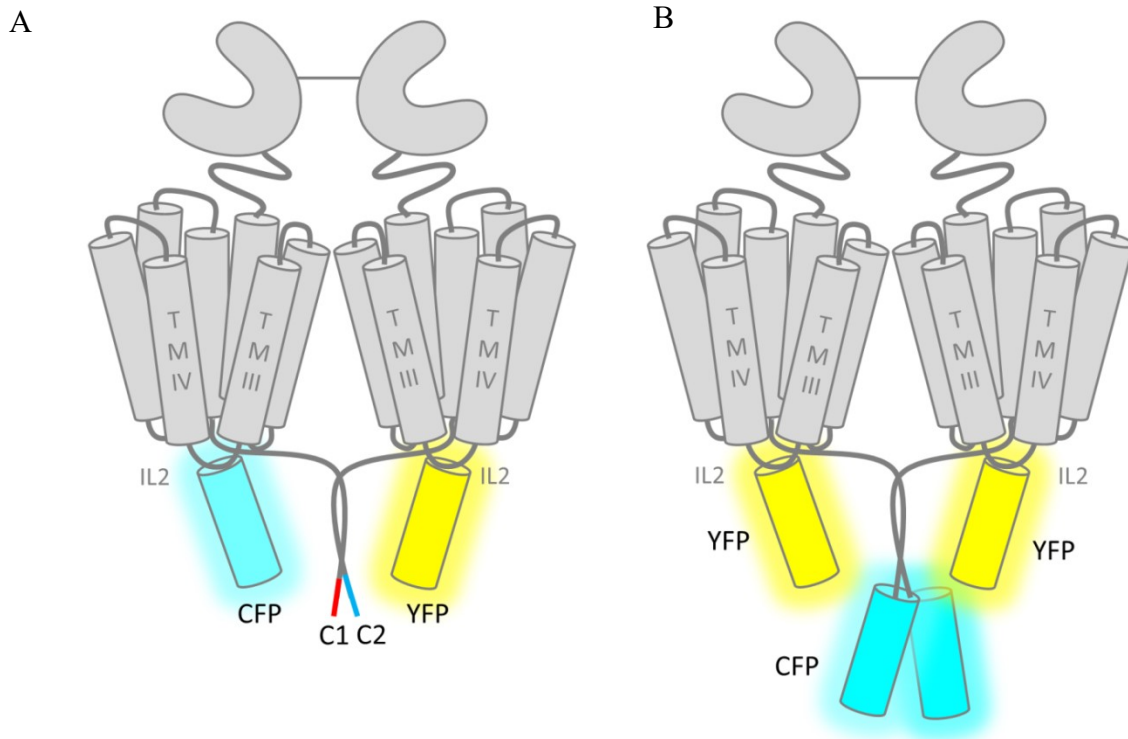


Figure 4: Schematic view of the mGluR FRET sensors: **A.** E-sensor, reporting intermolecular movement. The E-sensor is composed of two subunits, containing either CFP or YFP in the intracellular loop 2, C1 and C2 belong to the “GABA_B quality control system” that assures that only heterodimers reach the cell surface. **B.** A-sensor reporting intramolecular conformational changes within the mGluR1. The A sensor contains two mGluR1 protomers, each labelled with a YFP in the second intracellular loop and a CFP at the C-terminus. The A-sensor was used only for determining kinetics of mGluR1, not for other mGluRs.

3.2. Preparation of *Xenopus laevis* oocytes and cRNA injection

3.2.1. Preparation of *Xenopus laevis* oocytes

As expression system for mGluR FRET sensors, we used oocytes from *Xenopus laevis*, a South African adult frog. Oocytes were extracted from frogs by standard surgical procedures. Frogs were anaesthetized with 0.3 % tricaine (Pharmaq, Fordingbridge, UK). Only stage V-VI oocytes (Dumont 1972) were collected. The oocytes were incubated for 105 minutes with collagenase (3 mg/ml, Roche, Grenzach-Wyhlen, Germany) in OR2 solution at room temperature and afterwards manually dissected. The animal experiment procedure was authorized by the ethical committee of the Friedrich Schiller University of Jena.

3.2.2. Preparation of micropipettes for cRNA injection

Micropipettes for injection were prepared from capillary borosilicate glass tubing with 2.0 mm outer diameter and 1.6 mm inner diameter. Pipettes were pulled by Flaming/Brown type micropipette puller (Model P-97, Sutter Instruments CO, Novato (Ca), USA). Micropipettes were always prepared freshly to prevent contamination. Using those micropipettes an amount of 80-120 nl of 20-40 ng cRNA was injected into isolated oocytes, usually at the day of extraction from the frogs or at the next day. Oocytes were also obtained from Ecocyte Bioscience (Castrop-Rauxel, Germany).

Injected oocytes were transferred into 24 well plates in Barth medium and incubated at 18 °C. 4-6 days after injection, expression was optimal for performing the experiments. In some cases, oocytes were used up to 10-12 days after cRNA injection. Before starting experiments, the vitelline membrane was removed manually using forceps to enable the formation of membrane patches.

3.3. Chemicals and Solutions

L-glutamic acid, a native ligand for metabotropic glutamate receptors was obtained from Sigma (Sigma, St. Louise, USA). Other ligands, L-quisqualic acid, a synthetic agonist for group I metabotropic glutamate receptors (mGluR1 and mGluR5), and (S)-3,5-DHPG, a selective agonist for a group I metabotropic glutamate receptors were also obtained from Biotrend (Biotrend, Cologne, Germany). L-glutamic acid solutions were prepared freshly on the day of measurements. L-quisqualic acid and (S)-3,5-DHPG were diluted using DMSO to create a stock solution (50 mM) and from that different concentrations were prepared.

Other solutions used in the experiments:

- KCl solution (bath medium): 150 mM KCl, 10 mM HEPES, 1 mM EGTA, pH 7.4.
- Barth medium: 84 mM NaCl, 1 mM KCl, 2.4 mM NaHCO₃, 0.82 mM MgSO₄, 0.41 mM CaCl₂, 0.33 mM Ca(NO₃)₂, 7.5 mM TRIS, Cefuroxim, Penicillin/Streptomycin, pH=7.4.
- OR2 solution: 82.5 mM NaCl, 2 mM KCl, 1 mM MgCl₂, 5 mM HEPES, pH=7.5.

3.4. Confocal patch-clamp fluorometry experiments in outside-out membrane patches

3.4.1. Preparation of pipettes for outside-out patches

To generate outside-out membrane patches from *Xenopus laevis* oocytes we used micropipettes from two types of capillary glasses, borosilicate and quartz. Borosilicate capillary glasses were prepared from tubing an outer diameter 2 mm and inner diameter 1 mm by pulling with a Flaming/Brown micropipette puller (Model P-97, Sutter Instruments, Novato (CA), USA). Quartz pipettes were prepared from tubing with an outer diameter of 1.0 mm and an inner diameter of 0.7 mm (Vitrocom, New Jersey, USA) using laser puller (Model P-2000, Sutter Instruments Co., CA, USA). The pipettes were filled with bath solution filtered through a 0.2 µM non-pyrogenic filters (Sartorius stedim, Göttingen, Germany). The pipette resistance was 1.0-1.9 MΩ. Since the outcome was similar with both glasses, for most experiments, we used quartz micropipettes because it took less time to prepare them and handling is easier.

For the application of solutions on the outside-out membrane patch, a double-barreled theta glass pipettes were used. Those pipettes were prepared from double-barreled theta capillary glasses (Hilgenberg GmbH, Malsfield, Germany) using a P-97 Flaming/Brown type micropipette puller (Sutter Instruments, Novato, USA). Connection of double-barreled pipette with syringes that contain solutions was made with polyethylene tubes (Adtech Polymer Engineering LTD, Stroud, Glos, England). These tubes have an inner diameter of 0.3 mm, and an outer diameter of 0.76 mm. They were inserted in both barrels at the rear end and were sealed by Pattex power-mix glue (Henkel AG&Co.KG&A, Düsseldorf, Germany). Solutions

were supplied by a gravity-fed flow system with manual valves. Typical dimensions of the opening of the theta barrel were $\sim 100 \mu\text{m}$, and a typical flow speed was 130 mm/s.

3.4.2. FRET experiments in membrane patches

A standard patch-clamp technique was used to generate outside-out membrane patches from *Xenopus laevis* oocytes expressing mGluR FRET sensors.

Experiments were done at room temperature, using an Axopatch 200B amplifier (Axon instruments). Electrophysiology and jumps of the piezo actuator were controlled by the ISO3-Hard- and Software (MFK Niedernhausen).

The patch pipettes containing an outside-out membrane patch were carefully positioned in front of the outlet of the double-barreled (diameter of $100 \mu\text{m}$) theta glass at a distance of 10-15 μm using an MM33 manual micromanipulator. Initially, the patch pipette was positioned in front of the outlet from where the wash solution was flowing.

Jumping of the theta glass from one position to another was electronically controlled, allowing to step from wash solution to the solution containing glutamate or other agonists (L-glutamic acid and 3, 5-DHPG). This piezo actuator was purchased from Physik Instrumente, Karlsruhe, Germany and the electronic control was performed by an in house build electronics.

The speed of the solution flowing through the theta glass was about 130 mm/s, whereas the time courses of solution exchange at the patch were measured to be in the range of $220 \pm 30 \mu\text{s}$ ($n=3$), as measured with the laser scanning microscope (LSM710, Carl-Zeiss, Germany) by following the fluorescence of a $1 \mu\text{M}$ DY647 solution in the line scan mode.

Fluorescence images from an outside-out membrane patch were recorded through a 40x/1.2 C-Apochromat water immersion objective with a laser scanning confocal microscope (LSM710, Carl-Zeiss, Germany). An argon laser was used to excite CFP and YFP with the 458 or 514 nm lines. The detection channel was set to 459-508 or 517-581 nm, respectively. For fast time series, either small images (16x8 pixel) with a time resolution of 2.4 ms or line scans with a time resolution of 160 μs were acquired at 458 nm excitation. Non-confocal transmission images were obtained by recording the excitation light without any additional filter. The electrophysiology setup triggered both the microscope and the piezo device.

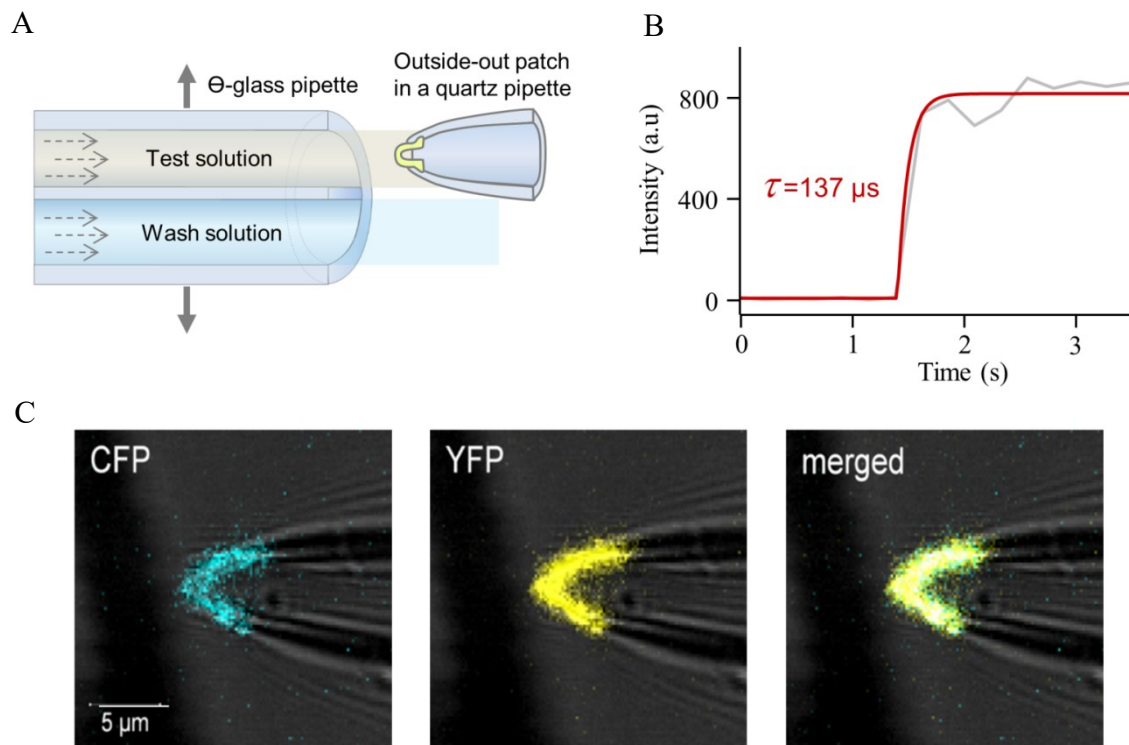


Figure 5: Solution exchange system. **A.** Scheme of the patch pipette containing an outside-out membrane patch expressing mGluR1 E-sensor positioned in front of a double-barreled theta-glass pipette. The theta glass pipette was fixed on a piezo actuator which moves it from one position to the other. **B.** Speed of solution exchange system in piezo-controlled concentration jump. Solution exchange was measured optically close to an empty outside-out patch with the fluorescent dye DY-647 in solution. The time course was fitted by an exponential function (red curve) yielding for this particular time constant of 137 μ s. The mean time constant was $220 \pm 60 \mu$ s. **C.** Confocal image of an outside-out membrane patch from *Xenopus* oocyte expressing the mGluR1 FRET E sensor. The left image shows the CFP channel excited at 458 nm, the middle image is the YFP channel excited at 514 nm, and the right image represents a merged signal. Transmission images are overlaid.

3.5. Analysis of FRET data

Regions of interest were selected manually from the images where patches were situated, and the extracted time series were analyzed with an in-house routine written by Dr. Ralf Schmauder in Igor Pro 6.34 (Wavemetrics).

Crosstalk correction

Crosstalk of CFP emission in the FRET channel was calculated by expressing mGluR1 constructs bearing only CFP, and measuring the signal in the same setting as for all measurements. Crosstalk of CFP emission in the FRET channel was quantified for each experimental setting. Removing this artefact from the FRET signal was done by:

$$\text{FRET}_{xc} = \text{FRET} - D_A * f_c \quad (1)$$

FRET_{xc} – FRET corrected from crosstalk; FRET – FRET signal; D_A – donor (CFP) signal in presence of acceptor (YFP); f_c – crosstalk factor, typically 34 %.

Photobleaching correction

Signals from both channels were corrected for photobleaching as follows: for each measurement condition, independent measurements without concentration jumps were analyzed and fitted by exponentials. Donor signals were fitted with a single exponential ($k=1$; typical $\tau_{\text{bleach}1}=0.66$ s), FRET signals were fitted with the sum of two exponentials with one time constant fixed on the donor value ($k=2$; typical $\tau_{\text{bleach}2}=2.86$ s) according to the equation:

$$\text{Signal}(t) = \text{offset} + \sum_{i=1}^k A_i \times \exp(-t/\tau_{\text{bleach}i}) \quad (2)$$

In concentration jump measurements, traces were masked from 50 ms before to 850 ms after the ligand application. The remaining traces for the donor and crosstalk-corrected FRET signal were fitted mono or bi-exponentially, respectively, with the time constant fixed to determine the bleaching amplitudes in the individual experiments. The fitted bleaching decay was subtracted from the data before further calculations according to:

$$\text{Signal}_{\text{cor}}(t) = \text{Signal} - \sum_{i=1}^k A_i \times \exp(-t/\tau_{\text{bleach}i}) \quad (3)$$

All bleaching correction was manually verified and rejected if needed. Changes in bleaching dynamics due to ligand-altered FRET efficiency were assumed to be negligible.

Fitting of activation and deactivation kinetics

For determining the activation time constant, τ_{on} , the time courses of activation of the individual experiments, evoked by stepping from zero to 1 mM glutamate, were normalized and fitted with an exponential function according to:

$$\text{FRET}_{\text{cor}}(t) = 1 - \exp(-t/\tau_{on}) \quad (4)$$

To minimize in the fits of fast time courses effects of time jitter, generated, e.g. by variable flow speed, pipette position or LSM-trigger jitter, the time point at which the signal starts, t_0 , was included as a fit parameter and the fits were performed with the modified equation:

$$\text{FRET}_{\text{cor}}(t) = \begin{cases} 0 & t < t_0 \\ 1 - \exp(-(t-t_0)/\tau_{on}) & t \geq t_0 \end{cases} \quad (5)$$

To avoid blurring of the kinetics, signals were referred to t_0 before averaging.

To determine the deactivation time constant, τ_{off} , the normalized time courses, obtained when jumping from 1 mM glutamate to zero, were fitted with:

$$\text{FRET}_{\text{cor}}(t) = \exp(-t/\tau_{off}) \quad (6)$$

In analogy to the activation time courses, the time jitter was minimized in fits of fast time courses effects by including the time point of the signal start, t_0 , using the equation:

$$\text{FRET}_{\text{cor}}(t) = \begin{cases} 0 & t < t_0 \\ \exp(-(t-t_0)/\tau_{off}) & t \geq t_0 \end{cases} \quad (7)$$

4. Results

4.1. Expression of mGluR sensors in *Xenopus laevis* oocytes

Xenopus laevis oocytes are optimal cells for expressing receptors or ion channels because of the high rate of expression. The fluorescent signal usually limits fast fluorescence measurements; thus, bright fluorophores and high expression are required. The oocyte expression system was selected to ensure the latter. mRNA prepared in vitro was injected manually in the cells, and after 4-5 days incubation at 18 °C, cells were used. Fig. 6 shows typical expression levels and spectra for individual constructs.

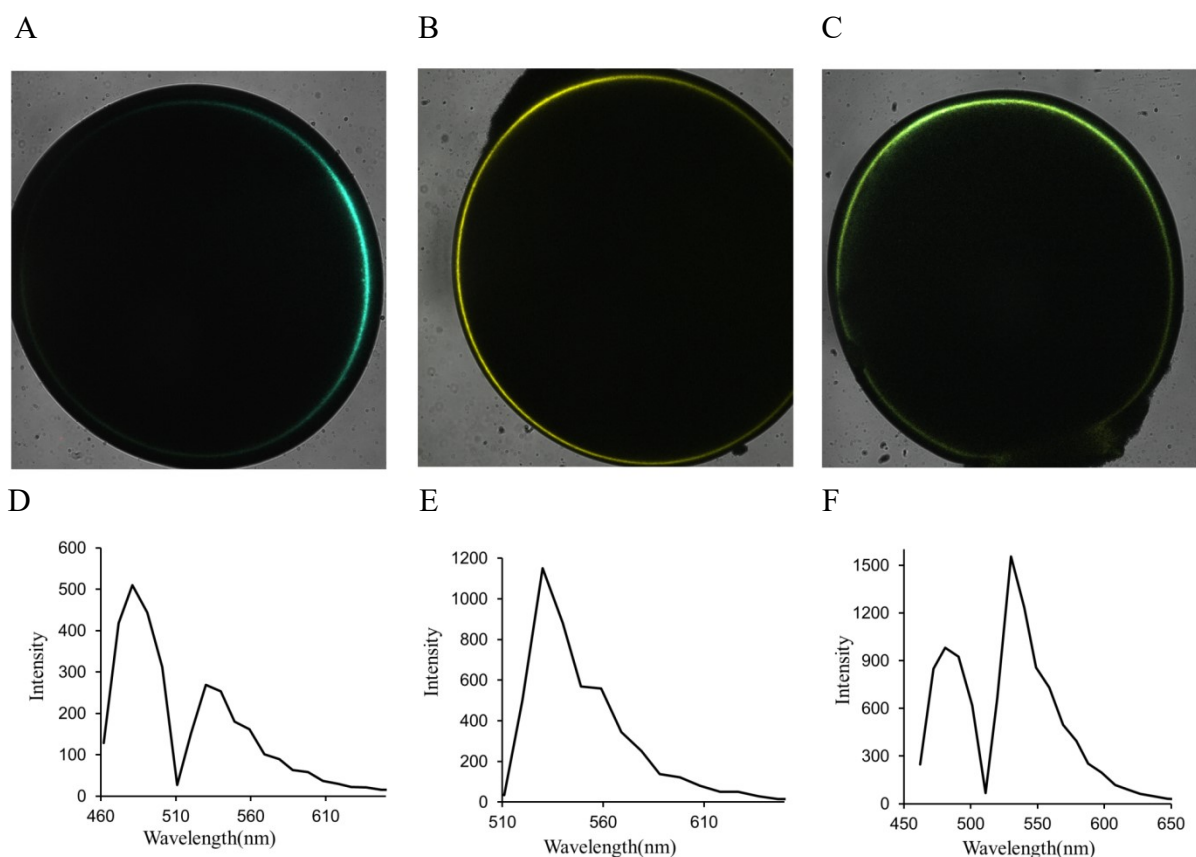


Figure 6: Expression of mGluR1 FRET sensors in *Xenopus laevis* oocytes. **A.** The image shows a cell expressing mGluR1-CFP-C1, illuminated with light of 488/514 nm. **B.** Cell expressing mGluR1-YFP-C2, illuminated with light of 488/514 nm, and **C** image of a cell expressing mGluR1-CFP-C1 and mGluR1-YFP-C2 (E-sensor), combined and measured at the same conditions (488/514 nm, channel representing YFP signal directly excited light of 514 nm was switched off, the signal comes from CFP and the FRET channel). **D.** Spectra from a region of interest in the cell expressing mGluR1-CFP-C1, **E** mGluR1-YFP-C2, and **F** E-sensor.

4.2. Optimization and characterization of measuring conditions for mGluR1 FRET sensors expressed in *Xenopus laevis* oocytes

Crosstalk and direct excitation

Both absorption and emission spectra of CFP and YFP are overlapping significantly. Thus, both direct excitation of the acceptor at donor excitation as well as crosstalk of donor fluorescence into the acceptor detector channel can occur and needs to be corrected for. The correction factors depend on the excitation light wavelength and intensity as well as on the detector spectral range and sensitivity and needs to be characterized for each setting. In our system, the detection channel for the CFP signal was set to 459-508 nm and that, for the YFP (FRET) signal to 517-581 nm. Except for the FRET signal detected in the FRET detection channel, also some signals of CFP appear as crosstalk. This crosstalk is subtracted from the whole signal detected into the FRET channel to yield a pure FRET signal.

To calculate the amount of the CFP signal leaking in the FRET detection channel, we expressed the construct mGluR1-CFP-C1, bearing only CFP, in *Xenopus laevis* oocytes and measured its signal (Fig. 7A). After calculations, we determined that approximately 34 % of the CFP signal is detected in the YFP channel (Fig. 7B). Direct excitation coming from the YFP signal excited by the 458 nm laser was negligible under our experimental conditions.

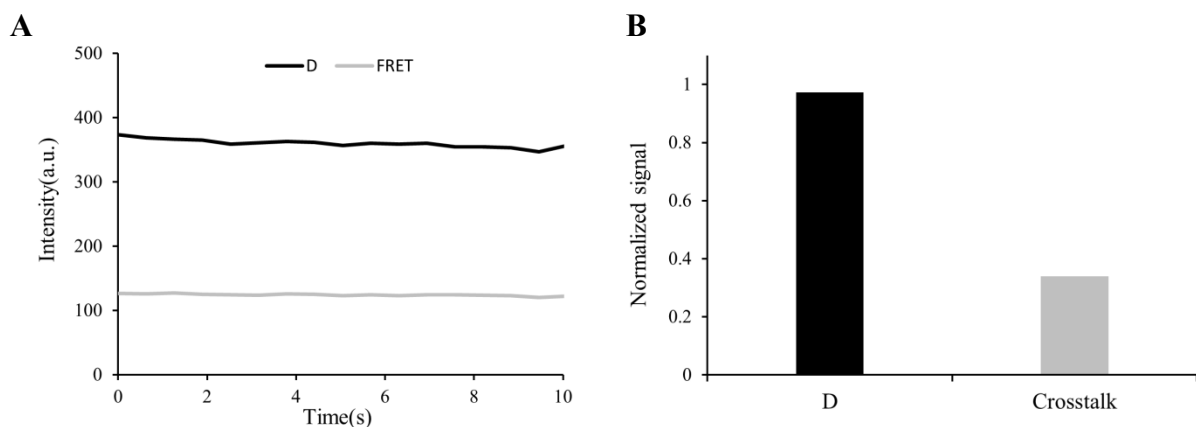


Figure 7: Crosstalk of the CFP signal into FRET signal. A. The figure shows a representative trace from a cell expressing mGluR1-CFP-C1. B. Calculated crosstalk of the CFP signal into the FRET detection channel, yielding 34 %.

4.2.1.2 Control for spectra variations upon photobleaching

Upon photobleaching it was shown that YFP can be converted in some species that emit light in the CFP emission range (Valentin et al. 2005). Following an intense discussion (Verrier and Söling 2006) it appears that the extent of the effect depends on the particular measuring conditions. To exclude this phenomenon in our experimental conditions, we did a control when we injected mGluR1-YFP-C2 constructs bearing YFP, afterwards YFP was bleached completely using full laser power at 514 nm (Fig. 8).

We did not notice any signal change in the CFP emission range after bleaching YFP, confirming that under our conditions the YFP up-conversion into a CFP-like species can be ignored.

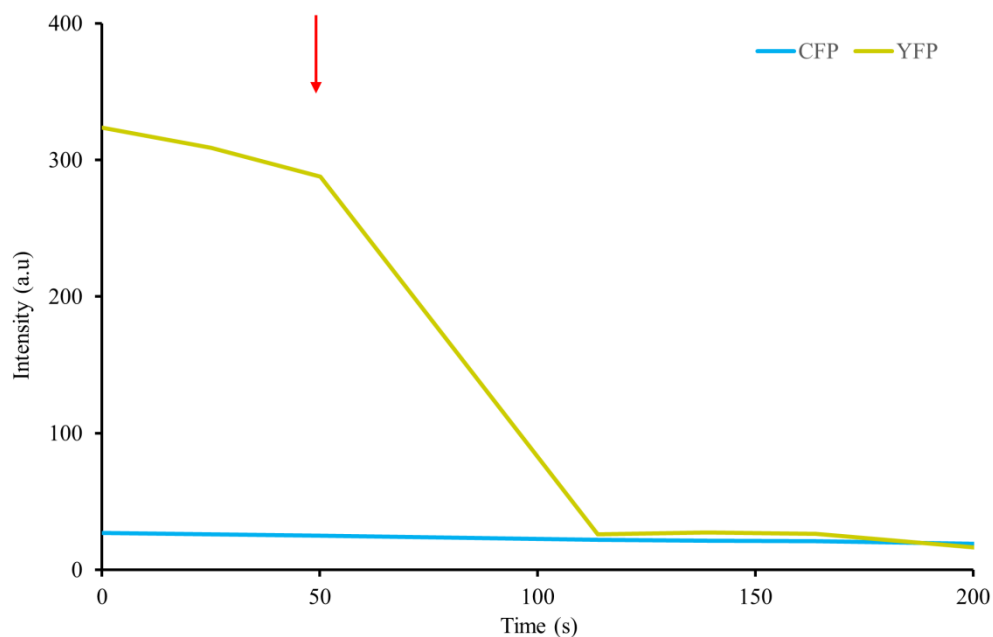


Figure 8: YFP (acceptor) photobleaching experiment. Cells expressing mGluR1-YFP-C2 were bleached at 514 nm with the argon laser (100 % laser power) indicated by the red arrow. The YFP signal (yellow) drops down, whereas the signal recorded in the CFP detection channel (cyan) stays stable, and is thus independent of what is happening with YFP.

4.3. The functionality of the mGluR sensors

4.3.1 mGluR dimerization

Metabotropic glutamate receptors are dimers, and they can exist as homodimers or heterodimers. mGluR FRET E-sensors are designed in a way that each dimer containing CFP will also contain a subunit carrying YFP (CFP in one monomer and YFP in the other one), based on the C-terminal “quality control system” from the GABA_B receptor (Margeta-Mitrovic et al. 2000, Pagano et al. 2001, Couve et al. 1998).

To test the expression of donor/acceptor dimers, the amount of FRET and our calculations to obtain the basal (or resting) FRET efficiency for our FRET sensors, we performed acceptor photobleaching experiments (Fig. 9). Intermolecular and intramolecular sensors were expressed separately in *Xenopus laevis* oocytes. Acceptor (YFP) was bleached at 514 nm laser power, and at the same time, the signal coming from the donor (CFP) is monitored. In our system, the donor (CFP) signal is quenched (with FRET being the quenching mechanism) when the acceptor (YFP) is entirely bleached. Here we assume that YFP photobleaching also abolished YFP absorption and thus FRET.

From this experiment, we calculate the FRET efficiency for both sensors according to:

$$\text{FRET}_{\text{eff}} = 1 - F_{\text{DA}}/F_{\text{D}} \quad (8)$$

FRET_{eff} – FRET efficiency, F_{DA} – signal of donor in presence of acceptor, F_{D} – signal of donor after acceptor photo bleaching.

For the intermolecular E-sensor, the FRET efficiency was: $23 \pm 2 \%$ ($n=3$) whereas for the intramolecular A-sensor was $27 \pm 2 \%$ ($n=7$). This result confirms the dimerization in the E-sensor and also the presence of the sensors in the cell membranes. No distance estimation was calculated for the FRET efficiencies as the dipole moments of CFP/YFP are fixed within the protein and the inserted protein was assumed as fixed relative to the receptor. Thus the assumption of $\kappa^2 = 2/3$ is not reasonable.

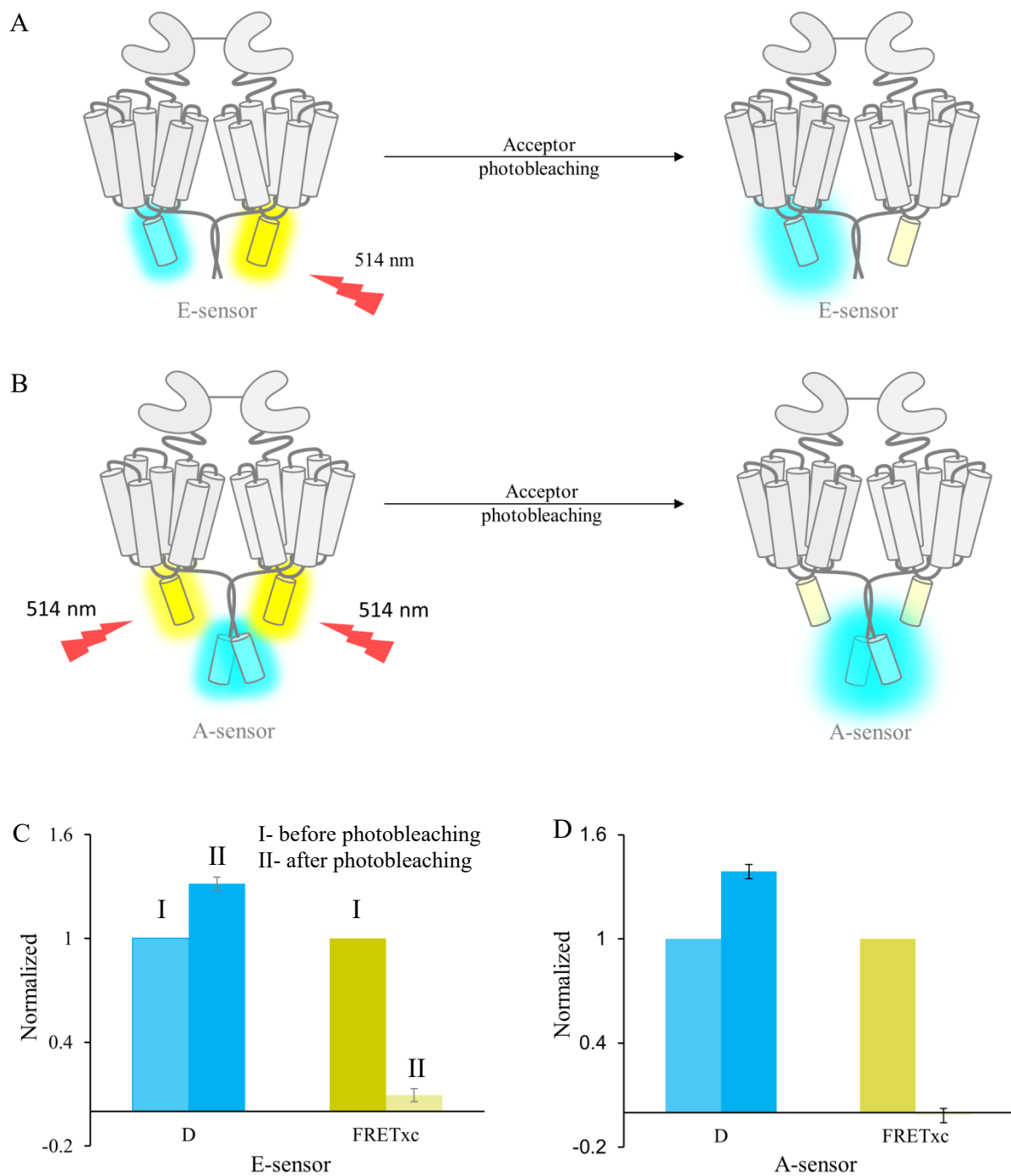


Figure 9: Dimerization of mGluR FRET sensors and their FRET efficiency. **A.** Scheme of acceptor photobleaching in the E-sensor and **B** in the A-sensor. **C.** Calculated FRET efficiency for the E-sensor: $23 \pm 2\%$ ($n=3$), and **D)** for the A-sensor $27 \pm 2\%$ ($n=7$).

4.4. Glutamate effect in mGluR1 FRET sensors

mGluR sensors are functional

Whole oocyte

Oocytes expressing mGluR1-CFP-C1 and mGluR1-YFP-C2 (E-sensor) were placed in a bath with KCl solution.

Images were acquired in the lambda mode of the LSM710 using the 10x objective. The region of interests (ROI) of the membrane was selected and averaged spectra inside the ROI were calculated before and after adding glutamate (1 mM). Glutamate was added to the bath solution to yield a final concentration of 1 mM. Spectral changes showed an increase of FRET upon glutamate addition (Fig. 10). This test was done to show that our constructs can be activated with glutamate, thus are functional in the membrane of *Xenopus laevis* oocytes.

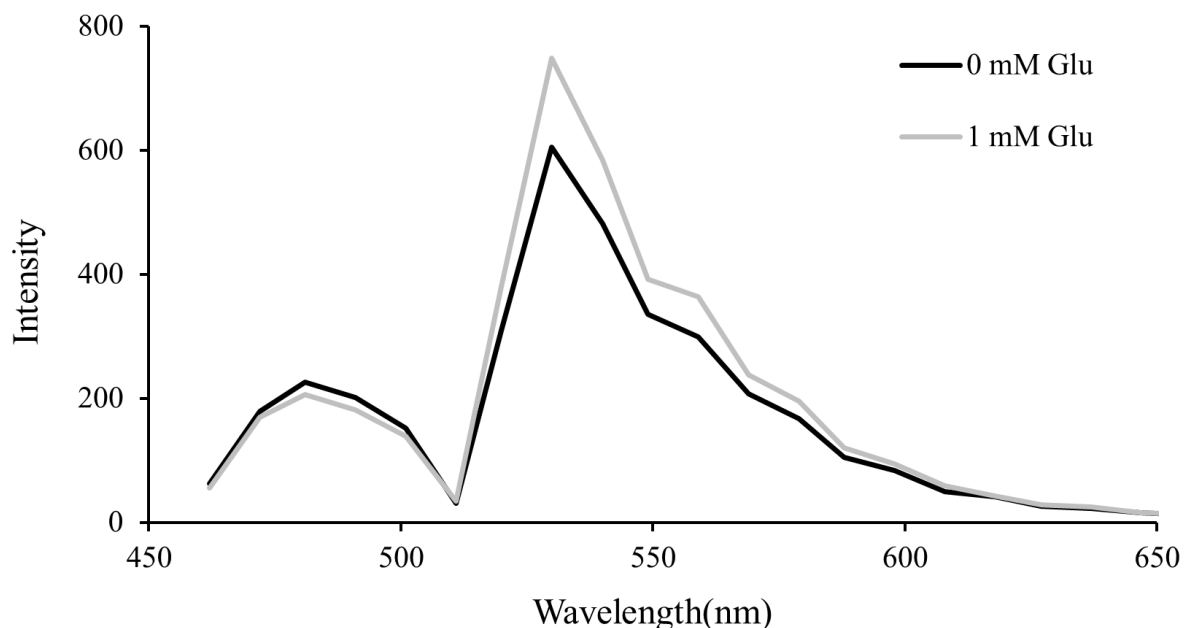
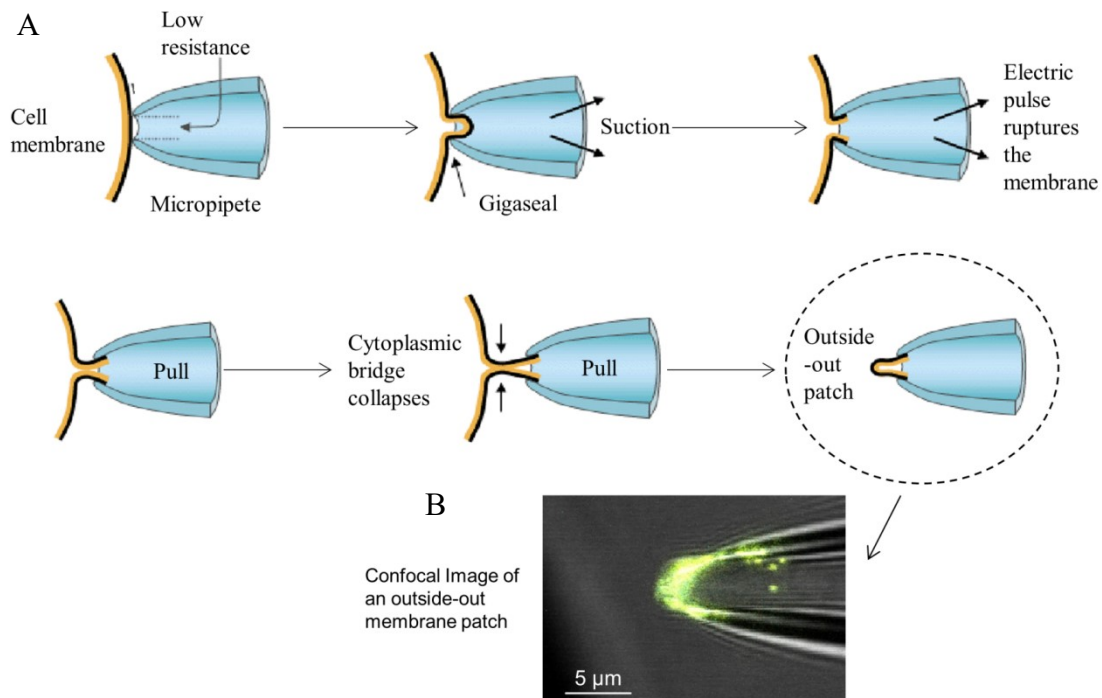


Figure 10: mGluR1 E-sensor causes a conformational change upon glutamate addition in the bath, recorded in a whole cell. Averaged spectra from a region of interest in the membrane, before (black) and after (grey) adding the glutamate are shown. The signal in the CFP region (~480 nm), decreases whereas the signal in YFP region (~515 nm) increases upon ligand addition, indicating increased FRET. Note that basal FRET is already present before the addition of glutamate.

Outside-out membrane patch

From oocytes expressing either E- or A-sensor, a piece of the membrane was excised in the outside-out configuration mode. Patching was realized using standard patch-clamp methods at room temperature. We generated outside-out membrane patches in order to have the extracellular site of the cell toward the application pipette. A scheme of generating outside-out-patches is described in the Scheme 2.



Scheme 2: Generation of an outside-out membrane patch. **A.** Schematic Illustration of all steps involved in making an outside-out membrane patch from a cell adapted from ‘Bioelectromagnetism’ Malmivuo J and Plonsey R. p154, 1995, Oxford University Press. **B.** Confocal image of an outside-out membrane patch expressing mGluR1 E-sensor.

Outside-out membrane patches containing the construct of interest were placed in the outflow of a double-barreled theta glass, containing either wash solution or solution containing glutamate towards the patch. Glutamate 1 mM was applied using a piezo-controlled jump. Fluorescent signals were recorded first when wash solution (KCl) was flowing to the patch, and after a time interval of 300 ms the outlet was stepped to the glutamate (1 mM) solution, staying in that position for 1 s, and was moved back to wash solution. One can easily see signal changes from CFP and YFP, which indicates an increase in FRET (increase in the distance between fluorophores in the case of E-sensor during activation, whereas the opposite

was observed for the A-sensor). The FRET changes in both sensors were reversible, allowing us to analyze also deactivation kinetics in addition to activation kinetics (Fig. 11). Kinetics measurements were performed in the LSM-channel mode to profit from the better signal to noise ratio than in the lambda mode.

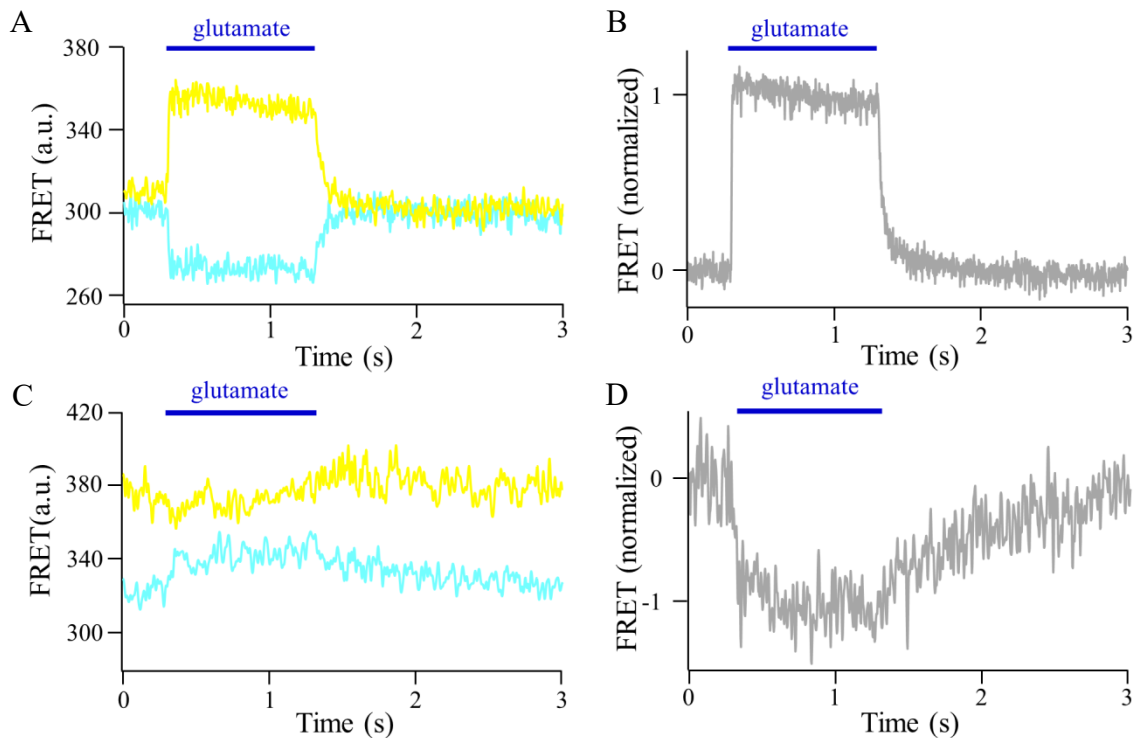


Figure 11: Activation of the mGluR1 E- and A-sensor in an outside-out membrane patch. **A.** E-sensor, crosstalk and photobleaching corrected signals from CFP and YFP, glutamate (1 mM) was added (indicated by blue line). The CFP signal decreased, whereas the YFP signal increased. **B.** Calculated relative FRET signal for the E-sensor. **C.** A-sensor. The CFP signal increased, whereas the YFP signal decreased when glutamate was applied. **D.** Calculated relative FRET signal for the A-sensor.

Furthermore, we investigated how the E-sensor behaves with other specific agonists for group I mGluRs. L-quisqualic acid is a potent mGluR agonist, and 3, 5-DHPG, a selective agonist for the group I metabotropic glutamate receptors (Fig. 12). Activation kinetics of the E-sensor with L-quisqualic acid yielded a time constant of 9 ± 2 ms, whereas deactivation kinetics yielded a time constant of 70 ± 4 ms ($n=3$). Kinetics for 3, 5-DHPG is a bit faster compared to L-quisqualic acid, where activation yielded a time constant of 7 ± 1 ms and deactivation of 29 ± 3 ms ($n=4$). With both agonists, the E-sensor activated as did natural agonist, glutamate. The FRET change was similar for glutamate and 3,5 DHPG, whereas it was a bit lower for L-quisqualic acid.

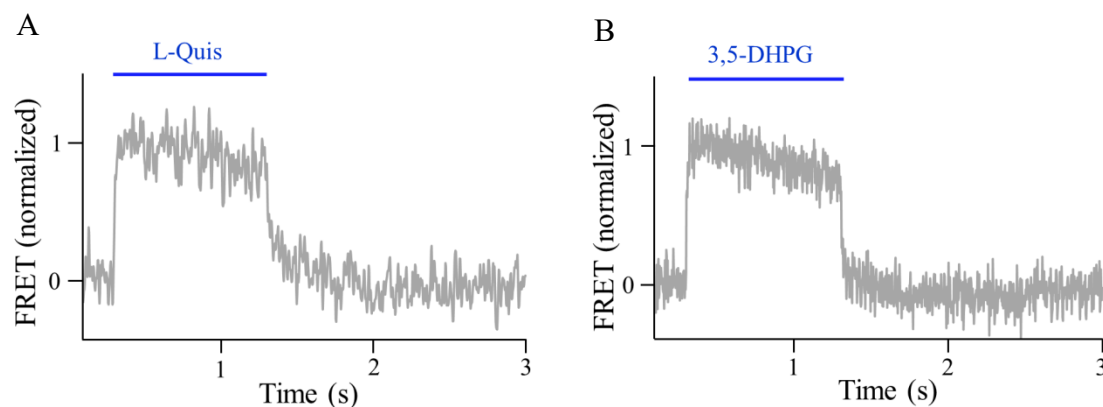


Figure 12: Activation of the mGluR1 E-sensor in an outside-out membrane patch using synthetic agonists. A. Calculated FRET change obtained from L-quisqualic acid ($50\ \mu\text{M}$), trace filtered using 66 Hz filter, $n=3$ and **B.** 3, 5-DHPG ($200\ \mu\text{M}$), $n=4$.

4.5. Kinetics

4.5.1. Activation and deactivation kinetics in the mGluR₁ E-sensor

Calculated FRET signals were normalized to unity, aligned to the concentration jumps and averaged. Activation and deactivation kinetics were analyzed by fitting with mono-exponential functions (Equation 4 and 6).

When analyzing activation kinetics from the data taken in confocal imaging mode (16x8 pixels) (Fig. 13A), the activation time constant was determined to 2.4 ± 0.1 ms (n=67). These results were very close to the limit of the time resolution in the confocal imaging mode (frame rate: 2.8 ms). Therefore, we chose to use the line scan mode (Fig. 13B) which has an enhanced time resolution (160 μ s), but records only a subset (one line) of the fluorophores in the patch, resulting in recording a lower number of photons and thus more noisy signals. In patches of well-expressing oocytes, we were still able to measure and resolve activation kinetics with τ_{on} of about 1 ms (1.2 ± 0.5 ms, n=5). The process is assumed to correspond to the movements of subunits towards each other. These data show faster activation kinetics for the E-sensor compared to that measured in the imaging mode, indicating that the previous studies were limited by the used methods (Marcaggi et al. 2009, Hlavackova et al. 2012).

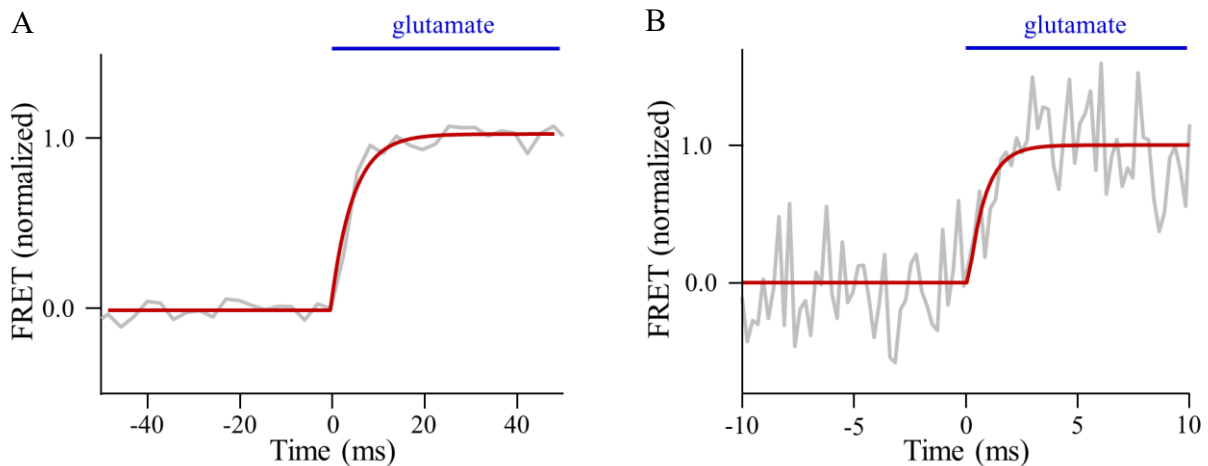


Figure 13: Activation kinetics of the mGluR1 E sensor: **A.** Averaged traces (grey), n=67 were fitted with monoexponential function (red line), yielding $\tau_{\text{on}}=2.4 \pm 0.1$ ms (n=67) which is limited by the recording method. **B.** Averaged traces measured at elevated time resolution with the line scan mode, yielding $\tau_{\text{on}}=1.2 \pm 0.5$ ms (n=5).

The line-scan mode provides the true activation kinetics

The first step in receptor activation, the ligand binding must be concentration-dependent at sufficiently low ligand concentration. However, when the concentration is sufficiently high a later transition can become rate limiting. To determine whether the 1.2 ms obtained with the line-scan mode reflect the binding itself or an evoked conformational change, we investigated the effect of glutamate at concentrations up to 10 mM (Fig. 14).

Data with concentrations below 1 mM were measured in the confocal imaging mode (data above the black dotted line in the Fig. 14, whereas data with concentrations above 1 mM we obtained from experiments with the line scan mode. Our data show that at concentrations above 1 mM and up to 10 mM, activation kinetics stays approximately the same. Therefore, we conclude that the activation kinetics in this concentration range is no longer limited by the concentration-dependent binding steps but corresponds to the speed of a rearrangement within the E-sensor.

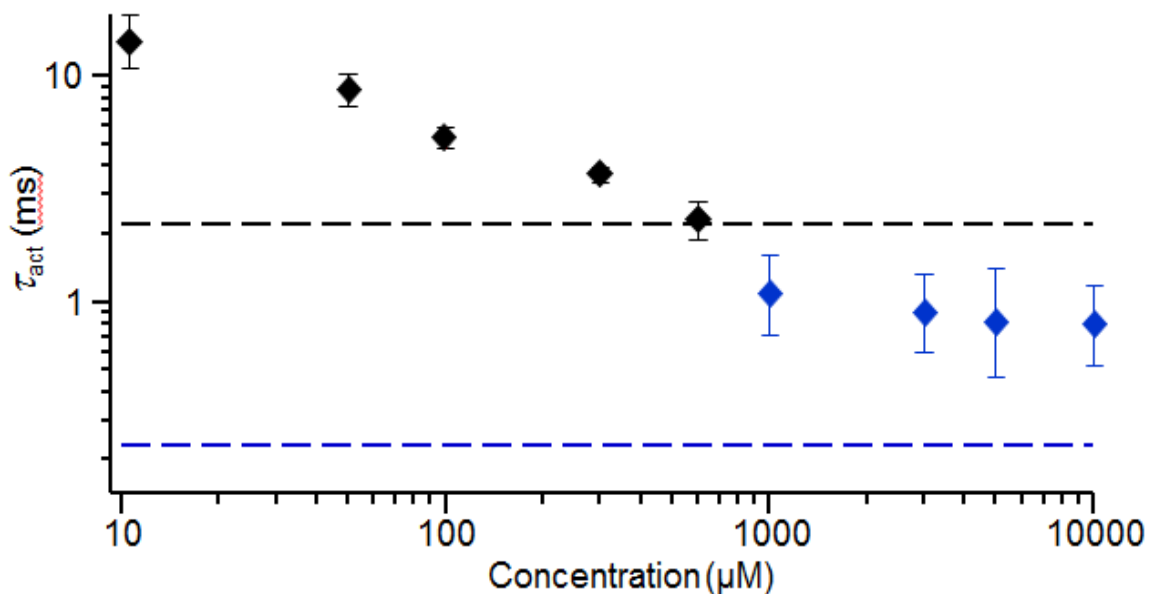


Figure 14: Concentration dependence of activation kinetics of the mGluR1 E sensor. Different concentrations of glutamate were applied to outside-out membrane patches expressing the E-sensor. Data obtained with concentrations at and above 1 mM were done using the line scan mode. Dashed lines indicate the time resolution of imaging (black) and line-scan mode (blue).

Deactivation kinetics in mGluR₁ E-sensor

Our piezo device allowed us also to remove the ligand by jumping back into the wash solution for studying both the activation and deactivation kinetics (Fig. 11). Deactivation was also fitted by using a mono exponential function (Equation 6). Deactivation kinetics turned out to be much slower compared to activation kinetics and is similar to the data published by Marcaggi et al. 2009. Deactivation kinetics was also analyzed using different concentrations (Figure 15 B); at low concentration, the absolute amplitude becomes rather low. Thus kinetic analyses become prone to systematic errors. The evaluable data suggest that deactivation kinetics is independent off the ligand concentration.

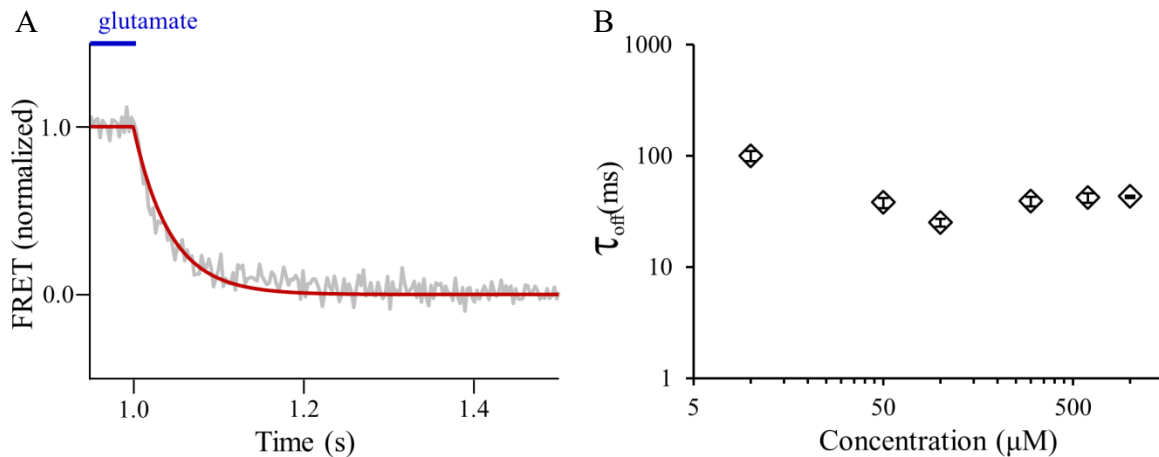


Figure 15: Deactivation kinetics of the mGluR1 E sensor in outside-out membrane patches. **A.** Deactivation kinetics of the E-sensor when jumping glutamate from 1 mM to wash solution. The process was fitted by a monoexponential function yielding $\tau_{\text{off}}=43 \pm 1$ ms (n=52). **B.** Deactivation kinetics is independent of the ligand concentration.

4.5.1.1. Further characterization of mGluR1 E-sensor

In the previous work from Mercaggi et al. 2009, using an mGluR1 FRET sensor similar to the sensor we use herein, it was shown that after long time exposure to glutamate mGluR1 becomes sensitized, contradicting desensitization reported for other GPCRs earlier (Kelly et al. 2008). To test for this phenomenon, we applied glutamate over four different time intervals (100 ms, 300 ms, 1 s and 3 s). The result was that we did not see sensitization or a difference in kinetics (Fig. 16). This phenomenon might be due to different experimental conditions that the other group used. Note that previous work was done in whole cells, and our experiments are done in excised membrane patches. Furthermore, we analyzed if different time exposure of glutamate would play a role in deactivation, but this was also not the case.

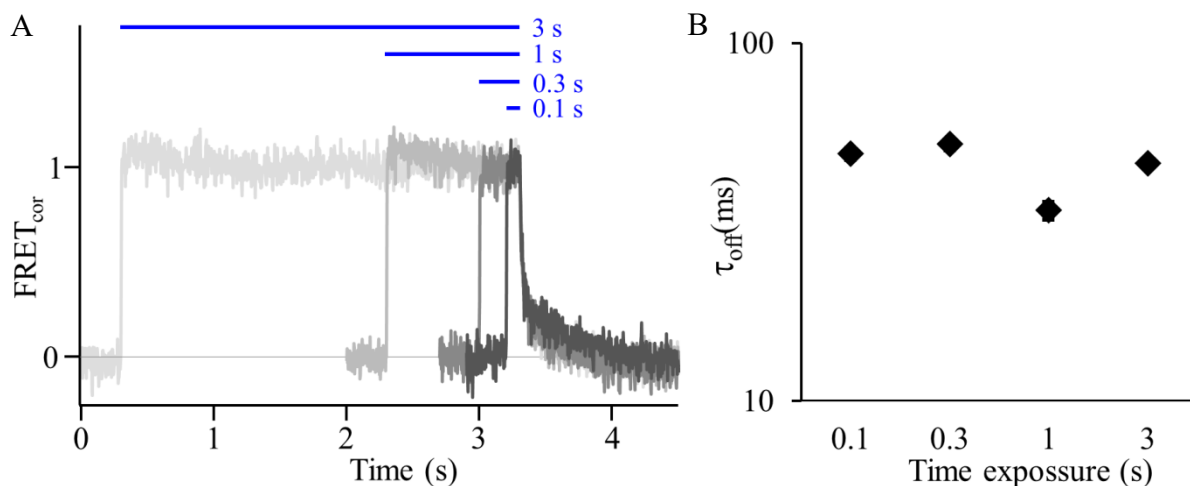


Figure 16: Different exposure time of glutamate in mGluR1 E-sensor. **A.** Normalized FRET traces are superimposed on each other. Glutamate (1mM) exposure time is indicated by blue lines above the traces. **B.** Deactivation kinetics remains in the same range despite different time exposure to glutamate.

4.5.1.2. The effect of one binding site in the kinetics of mGluR1 E-sensor

To test the contribution of the number of binding sites to the kinetics of the mGluR1 E-sensor, we introduced point mutations that disrupted the binding of glutamate to the orthosteric binding site. By introducing the well-established YADA mutations (Kniazeff et al. 2004), we generated constructs that are unable to bind glutamate and activate. We show that in dimers where both subunits bear the mutation (YADA: YADA), there was no signal change after 1 mM glutamate application (Fig. 17A). Dimers bearing one mutated binding site and one wild-type binding site (YADA: WT), a signal change was present, but it was lower compared to the wild type E-sensor (WT: WT). The kinetics was about six times slower, for both activation and deactivation (Fig. 17C, D). By this, we conclude that both binding sites are needed for the fast response in WT: WT receptors. However, when only one active binding site is present, the kinetics are slowed down.

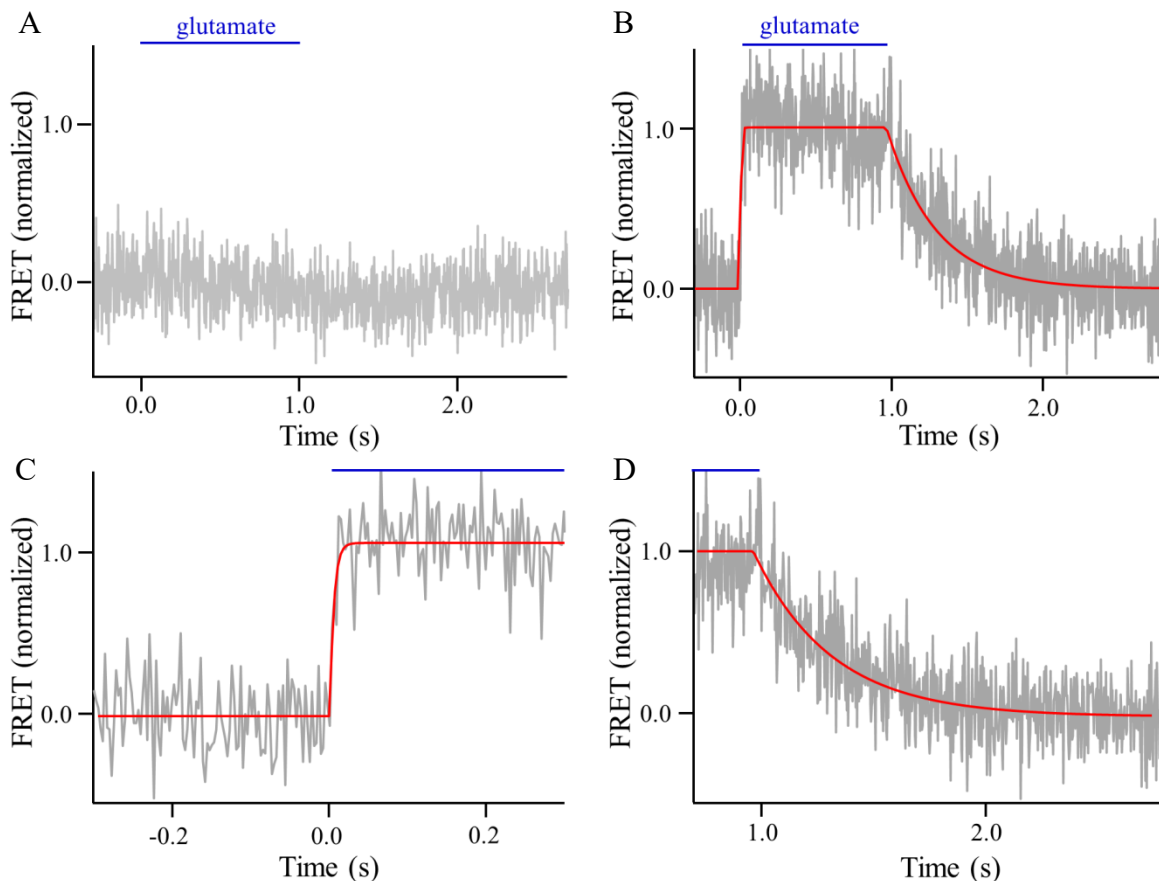


Figure 17: Activation and deactivation kinetics of the mGluR1 E sensor with mutated binding sites. **A.** Signal with both binding sites mutated. **B.** Signal with one binding site mutated with the YADA mutation. **C.** Monoexponential fit yields $\tau_{\text{on}}=7 \pm 2$ ms (n=6) and **D.** Deactivation kinetics of $\tau_{\text{off}}=295 \pm 6$ ms (n=6).

4.5.2. A-sensor

Activation of mGluR1 is believed to proceed in two subsequent steps (Hlavackova et al. 2012). The first step is associated with an intermolecular rearrangement that is followed by a conformational change within the monomers. For investigating the conformational changes of the second step, we used the A-sensor, with CFP fused in the C-terminus and YFP fused again in the intracellular loop 2. The signal change obtained by glutamate application was lower compared to the E-sensor. The FRET values were negative, meaning that the distance between CFP and YFP is increased at activation. Activation and deactivation kinetics were analyzed again by fitting monoexponential functions (Equations 4 and 6) yielding $\tau_{\text{on}}=25 \pm 7$ ms, and $\tau_{\text{off}}=900 \pm 60$ ms (Fig. 18). Hence, the kinetics of the A-sensor are slower compared to the E-sensor, for both, activation and deactivation.

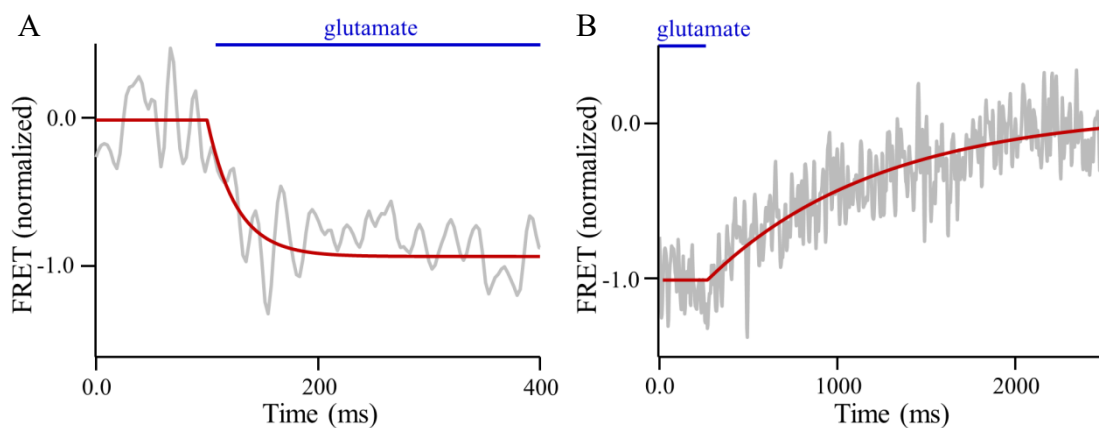


Figure 18: Activation and deactivation kinetics of the mGluR1 A-sensor. **A.** Activation kinetics fitted with monoexponential fit yielded $\tau_{\text{on}}=25 \pm 7$ ms ($n=7$) and **B.** $\tau_{\text{off}}=900 \pm 60$ ms ($n=6$).

4.6. Functional interaction of the subunits of all members in metabotropic glutamate receptors

We next studied the kinetics of all other metabotropic glutamate receptors (Fig. 19), in total eight homodimers and 28 possible heterodimers. It has been shown previously that mGluRs can form heterodimers within the family, as e.g. for mGluR2/3 by using a single-molecule approach (Levitz et al. 2016). Another example of heterodimerization has been reported between members of group II and III, mGluR2/7. This combination leads to a more efficient activation dimer than mGluR2 or mGluR7 as a homodimer (Habrian et al. 2019). Functionality has also been reported for mGluR2/4 (Moreno Delgado et al. 2017). Evidence was also shown for the presence of this heterodimer in native cells (Moreno Delgado et al. 2017). A comprehensive study including numerous mGluRs proved 11 out of 21 combinations to form heterodimers, but this study shows only the assembly of the monomers to dimers but not their functional interaction (Doumazane et al. 2011).

Herein we studied the kinetics of activation and deactivation in all homodimers, and all possible heteromeric combinations between all members using the same approach as described for mGluR1 above.

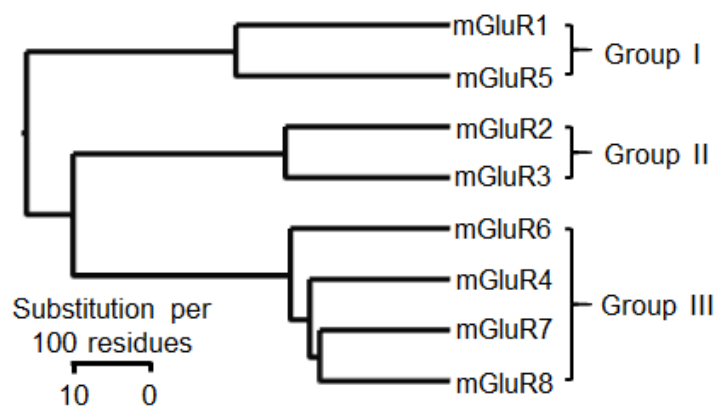


Figure 19: Classification of metabotropic glutamate receptors. Phylogenetic tree of the eight human mGluRs.

4.6.1. Dimer assembly studied by FRET efficiency

We studied the ability of the eight mGluR isoforms to assemble to homodimers or heterodimers. It turned out that the FRET efficiency suggests dimerization for all mGluRs except mGluR6, which has deficient expression. FRET efficiency values range from 18 % in mGluR7 to 30 % in mGluR3 (Fig. 20). Out of the 7 homodimers showing FRET efficiency, 5 were sensitive to glutamate jumps, except mGluR4 and mGluR7.

Regarding heterodimers, 16 out of 28 possible combinations formed heterodimers as shown by FRET efficiency. The FRET efficiency ranges from 13 % in mGluR4/8 to 35 % mGluR2/3 (Fig. 20). Notably, the values for FRET efficiency in the heterodimers are similar to the values in homodimers, suggesting that the distance between fluorophores in homo- and heterodimers are similar. 11 out of the 16 heterodimers were functional as judged by time courses following glutamate application.

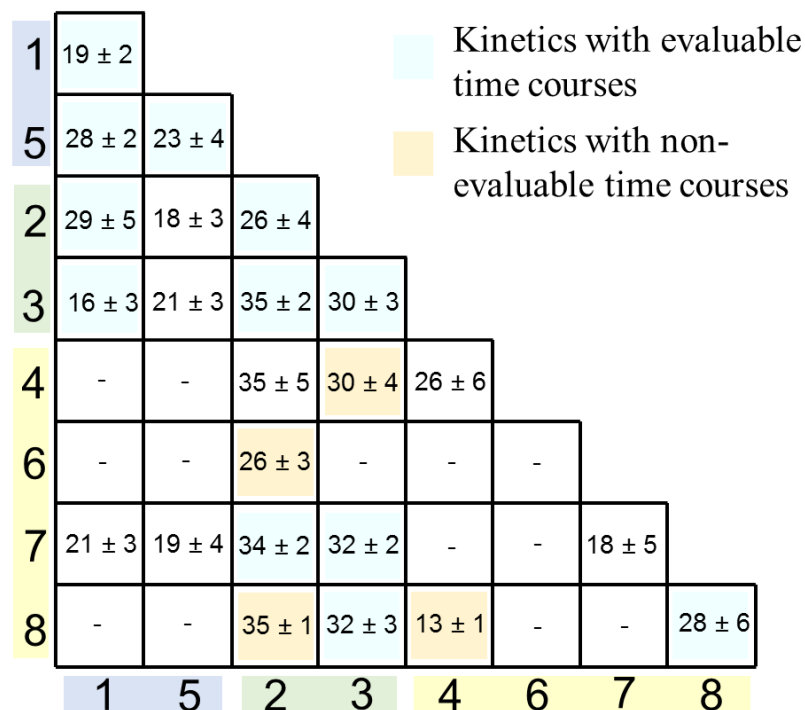


Figure 20: FRET efficiency in homo- and heterodimeric mGluRs. Matrix indicating the FRET efficiency by donor dequenching (in % ± SEM). The main diagonal represents the values of the homodimers. For better comparison combinations with evaluable and non-evaluable kinetics are indicated by colors. White fields containing numbers indicate dimers with no detectable dynamic responses. Fields with dashes indicate the absence of donor dequenching.

4.6.2. Kinetics in homodimers

4.6.2.1. Group I mGluRs

mGluR1 and mGluR5 E-sensors were expressed in *Xenopus laevis* oocytes, with mGluR1 expressing slightly better than mGluR5. Both sensors assembled to homodimers as confirmed by acceptor photobleaching. Activation and deactivation kinetics were fitted using monoexponential functions. Activation of the human mGluR1 E-sensor is likewise as rapid as that of rat mGluR1 (Hlavackova et al. 2012, Grushevskiy et al. 2019) while deactivation kinetics are slower compared to activation kinetics (Fig. 21).

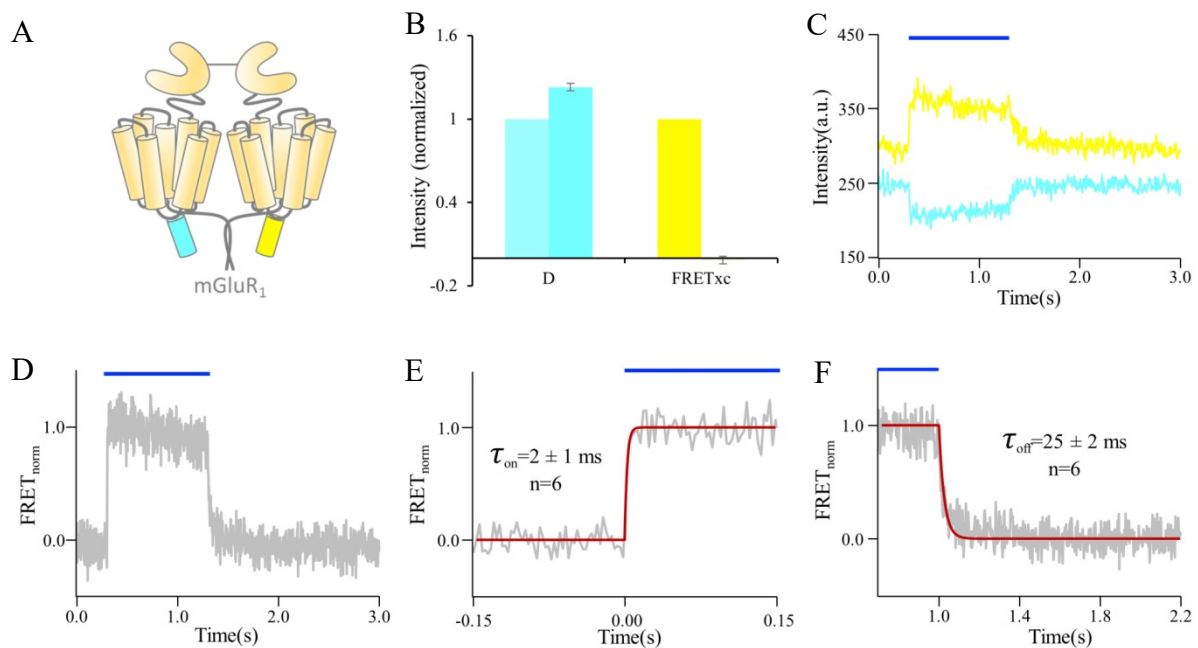


Figure 21: Kinetics for human mGluR1 E-sensor. **A.** Scheme of mGluR1 E-sensor. **B.** Calculated FRET efficiency after acceptor photo-bleaching, $\text{FRET}_{\text{ef}} = 18.6 \pm 2 \%$ (n=3). **C.** Signal changes of CFP (cyan) and YFP (yellow) upon fast glutamate application; crosstalk and photobleaching were corrected (blue). **D.** Calculated FRET from CFP and YFP signal. **E)** Activation and **F)** deactivation kinetics were fitted with a mono-exponential function (red) in averaged traces (grey). The time constants are indicated.

mGluR5 E-sensor activates with a similar speed as mGluR1, making both members of group I mGluRs fast activators. On the contrary, with mGluR1, deactivation is significantly slower, marking an essential difference between the two members of group I mGluRs. The complete kinetic profile for mGluR5 is summarized in Fig.22. Both activation and deactivation kinetics are fitted using monoexponential functions.

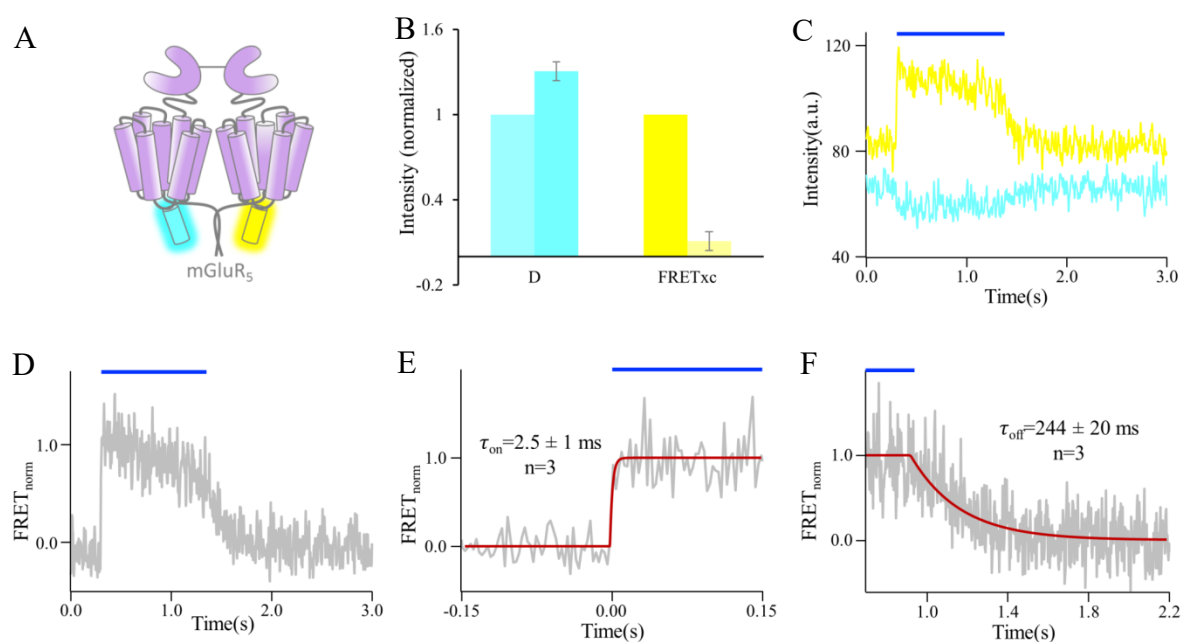


Figure 22: Kinetics for human mGluR5 E-sensor. **A.** Scheme of the mGluR5 E-sensor. **B.** Calculated FRET efficiency after acceptor photo-bleaching, $FRET_{ef} = 23 \pm 4$ ($n=5$). **C)** Signal changes of CFP (cyan) and YFP (yellow) upon fast glutamate application; crosstalk and photobleaching were corrected. **D.** Calculated FRET from CFP and YFP signal. **E.** Activation and, **F.** deactivation kinetics were fitted with a mono-exponential function (red) in averaged traces (grey). The time constants are indicated.

4.6.2.2. Group II mGluRs

Both group II mGluRs, mGluR2 and mGluR3, form functional dimers (Fig. 23 and 24). The expression level, however, was below that of group I mGluRs. mGluR2 activates very slow, it is the slowest dimer measured in comparison to all functional dimers analyzed in this study. The activation time constant is at about 30 ms. On the other hand, the deactivation kinetics are in the same range as activation or slightly faster, depicting a distinct feature of mGluR2.

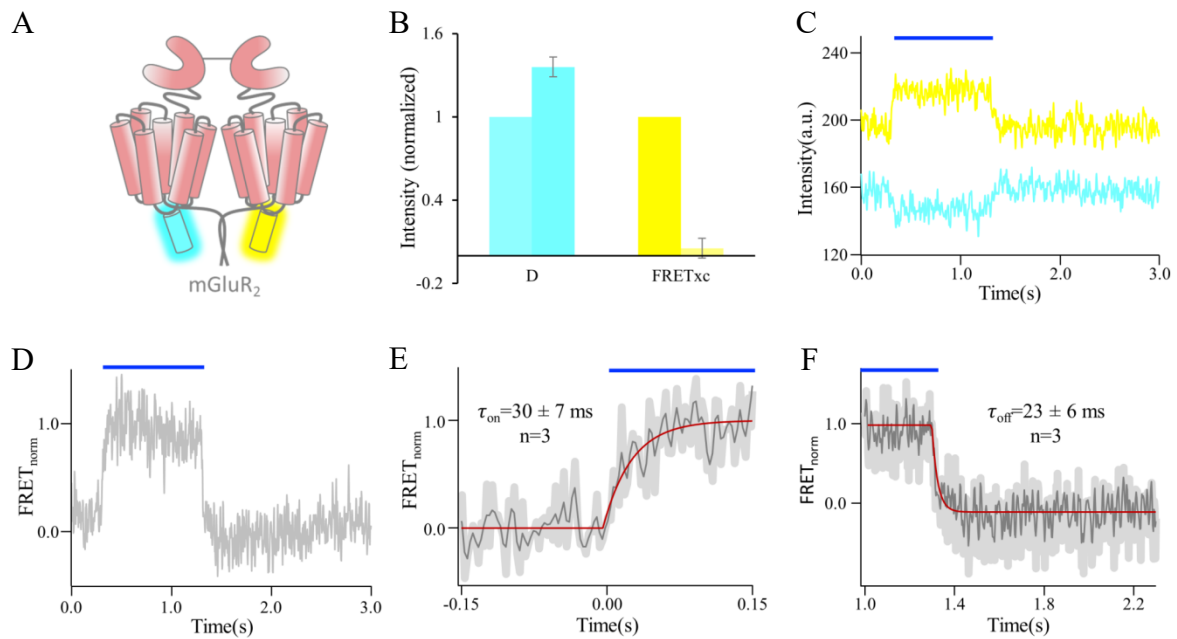


Figure 23: Kinetics for human mGluR2 E-sensor. **A.** Scheme of the mGluR2 E-sensor. **B.** Calculated FRET efficiency after acceptor photo-bleaching, $FRET_{ef} = 26 \pm 4$ (n=4). **C.** Signal changes of CFP (cyan) and YFP (yellow) upon fast glutamate application; crosstalk and photobleaching were corrected. **D.** Calculated FRET from CFP and YFP signal. **E.** Activation and, **F.** Deactivation kinetics were fitted with a mono-exponential function (red) in averaged traces (light grey) in raw data. Dark grey lines represent 66 Hz filter applied in raw data (light grey). The time constants are indicated.

mGluR3 displays a slightly faster activation kinetics ($\tau_{\text{on}}=13$ ms) in comparison with mGluR2, but is still significantly slower than both members of the group I (mGluR1 and mGluR5). Similar to the group I, where one of the members shows fast deactivation kinetics (mGluR1) and the other slow deactivation kinetics (mGluR5), also here mGluR3 exhibits slower deactivation kinetics compared to mGluR2.

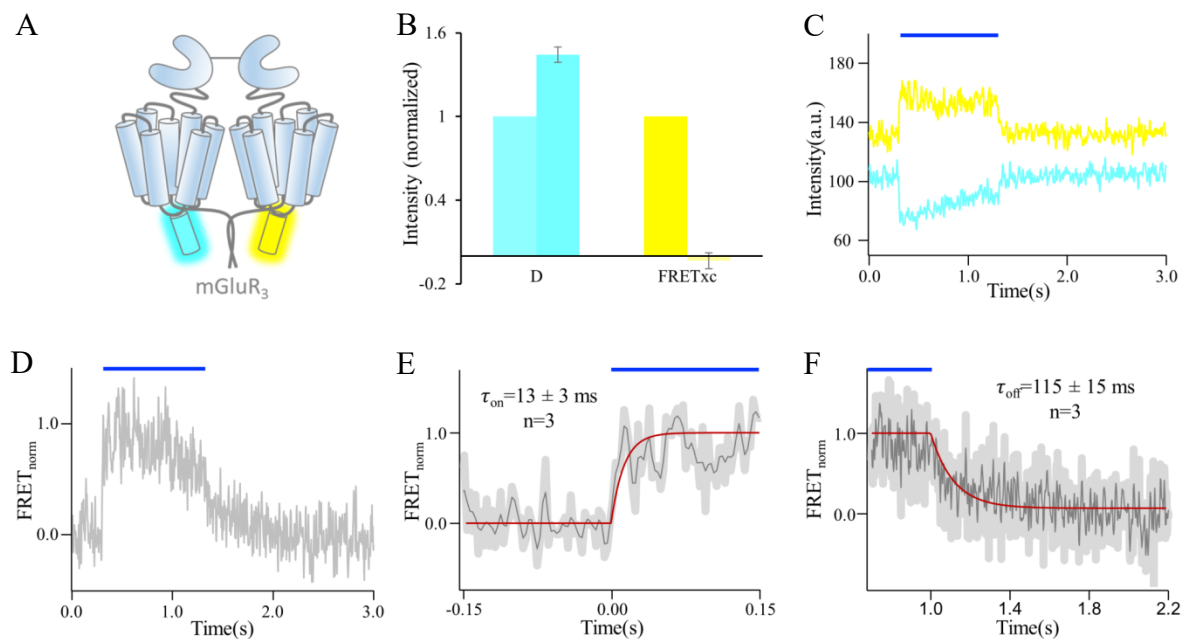


Figure 24: Kinetics for human mGluR3 E-sensor. **A.** Scheme of the mGluR3 E-sensor. **B.** Calculated FRET efficiency after acceptor photo-bleaching, $\text{FRET}_{\text{ef}}=30 \pm 3$ ($n=7$). **C.** Signal changes of CFP (cyan) and YFP (yellow) upon fast glutamate application; crosstalk and photobleaching were corrected. **D.** Calculated FRET from CFP and YFP signal. **E.** Activation and **F.** Deactivation kinetics were fitted with a mono-exponential function (red) in averaged traces (light grey) in raw data. Dark grey lines represent 66 Hz filter applied in raw data (light grey). The time constants are indicated.

4.6.2.3. Group III mGluRs

Members of group III exhibit similar or lower expression in comparison to the members of group II. Expression of mGluR6 was undetectable, precluding any analysis. For mGluR4 and mGluR7, the level of expression was better; nevertheless, both receptors were non-functional when applying 1 mM glutamate and the same negative results was obtained for mGluR7 when applying 10 mM glutamate. Kinetically only mGluR8 could be characterized (Fig. 25). Its activation kinetics were in the same range as for mGluR3 while deactivation kinetics remain in-between the values for mGluR2 and mGluR3.

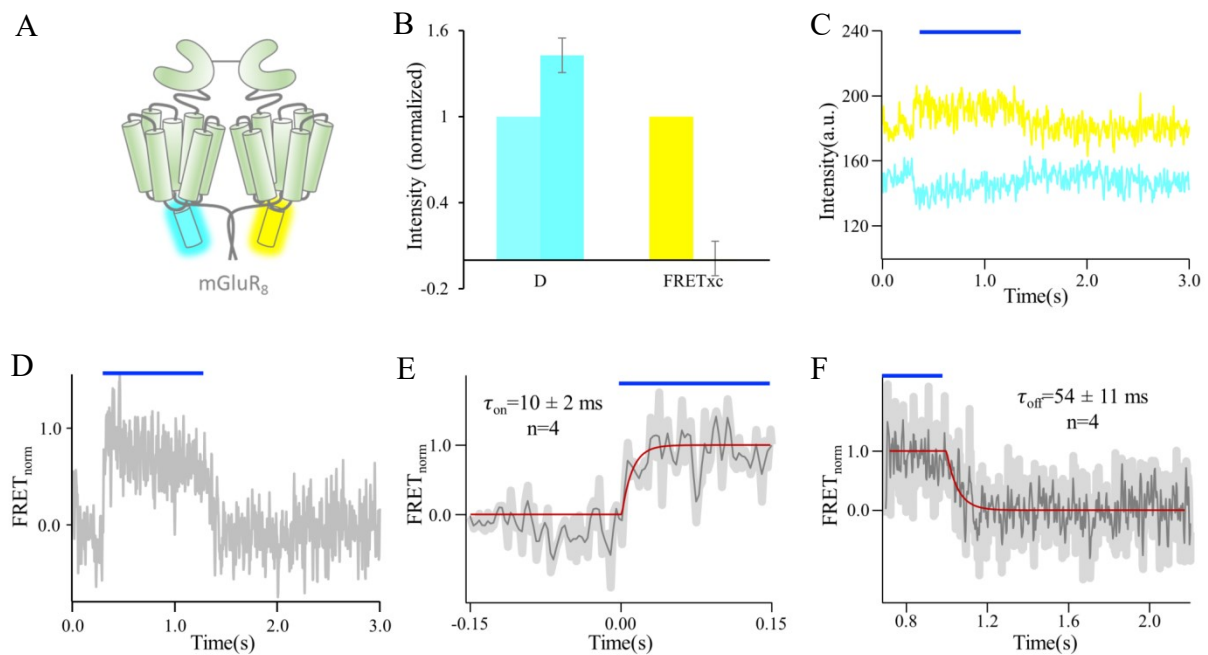


Figure 25: Kinetics for human mGluR8 E-sensor. **A.** Scheme of the mGluR8 E-sensor. **B.** Calculated FRET efficiency after acceptor photo-bleaching, $FRET_{ef} = 28 \pm 6$ ($n=5$). **C.** Signal changes of CFP (cyan) and YFP (yellow) upon fast glutamate application; crosstalk and photobleaching were corrected. **D.** Calculated FRET from CFP and YFP signal. **E.** Activation and **F.** Deactivation kinetics were fitted with a mono-exponential function (red) in averaged traces (light grey) in raw data. Dark grey lines represent 66 Hz filter applied in raw data (light grey). The time constants are indicated.

4.6.3. Kinetics of heterodimers

4.6.3.1. Heterodimerization within the same groups

Group I

mGluR1 forms functional heterodimer with mGluR5, shown in Fig. 26. Activation kinetic of mGluR1/5 heterodimer is very rapid, similar to the activation kinetics in mGluR1 and mGluR5 homodimers. Deactivation kinetics resembles that of mGluR5, i.e. mGluR5 slows down the kinetics of the mGluR1/5 heterodimer with respect to the mGluR1 homodimer. Deactivation kinetic of the mGluR1 subunit was decelerated about ten times.

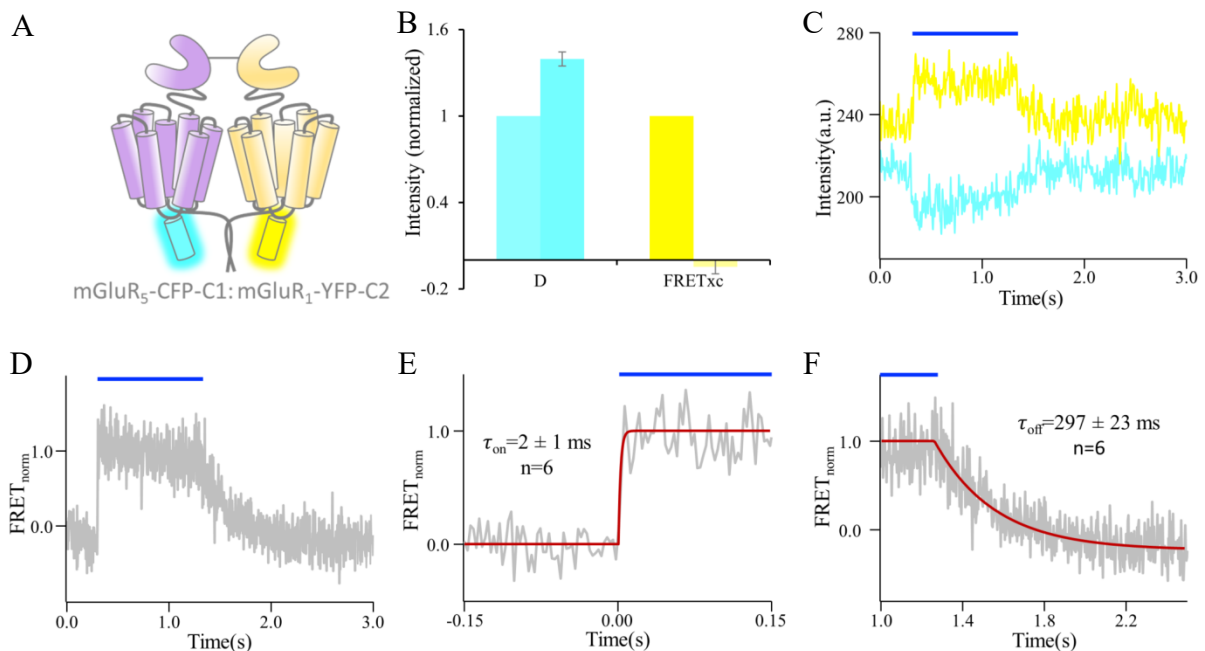


Figure 26: Kinetics for human mGluR5/1 E-sensor. A. Scheme of mGluR5/1 E-sensor. **B.** Calculated FRET efficiency after acceptor photobleaching, $FRET_{ef} = 28 \pm 2\%$ (n=5). **C.** Signal changes of CFP (cyan) and YFP (yellow) upon fast glutamate application (blue); crosstalk and photobleaching were corrected. **D.** Calculated FRET from CFP and YFP signal. **E.** Activation and, **F.** Deactivation kinetics were fitted with a mono-exponential function (red) in averaged traces (grey). Time constants are indicated.

Group II

A similar phenomenon of heterodimerization within a group is also detected for group II mGluRs. mGluR2 forms functional heterodimers with mGluR3 (Fig. 27). This dimer was also reported previously (Doumazane et al. 2011, Levitz et al. 2016). Activation kinetics of mGluR2/3 is significantly accelerated with respect to the mGluR2 homodimer, but it stays in a similar range to the mGluR3 homodimer. Deactivation kinetic is in-between the values reported for individual mGluR2 and mGluR3 homodimers.

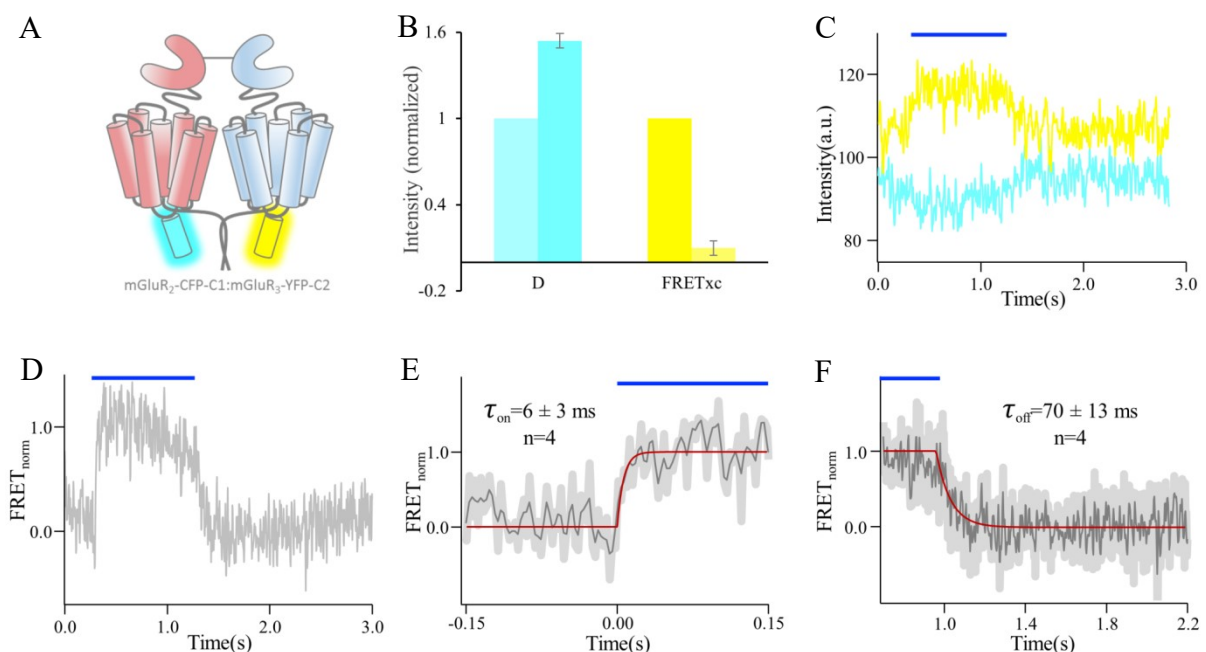


Figure 27: Kinetics for human mGluR2/3 E-sensor. **A.** Scheme of mGluR2/3 E-sensor. **B.** Calculated FRET efficiency after acceptor photo-bleaching, $FRET_{ef} = 35 \pm 2\%$ (n=4). **C.** Signal changes of CFP (cyan) and YFP (yellow) upon fast glutamate application (blue); crosstalk and photobleaching were corrected. **D.** Calculated FRET from CFP and YFP signal. **E.** Activation and, **F.** Deactivation kinetics were fitted with a mono-exponential function (red) in averaged traces (grey). Dark grey lines represent 66 Hz filter applied in raw data. Time constants are indicated.

4.6.3.2. Heterodimerization between groups

Group I and group II

Heterodimerization between group I and II was not reported before in literature and, particularly, in the work of Doumazane and coworkers (Doumazane et al. 2011), heterodimerization between these groups was not observed. Here we report functional heterodimerization for mGluR1, belonging to the group I, with both mGluR2 (Fig. 28) and mGluR3 (Fig. 29) of group II. In contrast, mGluR5 assembles to dimers with mGluR2 and mGluR3, as proved by FRET efficiency (Fig. 20), but does not form functional receptors generating a response upon glutamate jump.

τ_{on} of mGluR1/2 is about 16 ms. Hence, the mGluR2 subunit slows down activation kinetics of mGluR1 in heterodimeric composition. Deactivation kinetics of this combination is similar to the respective homodimers.

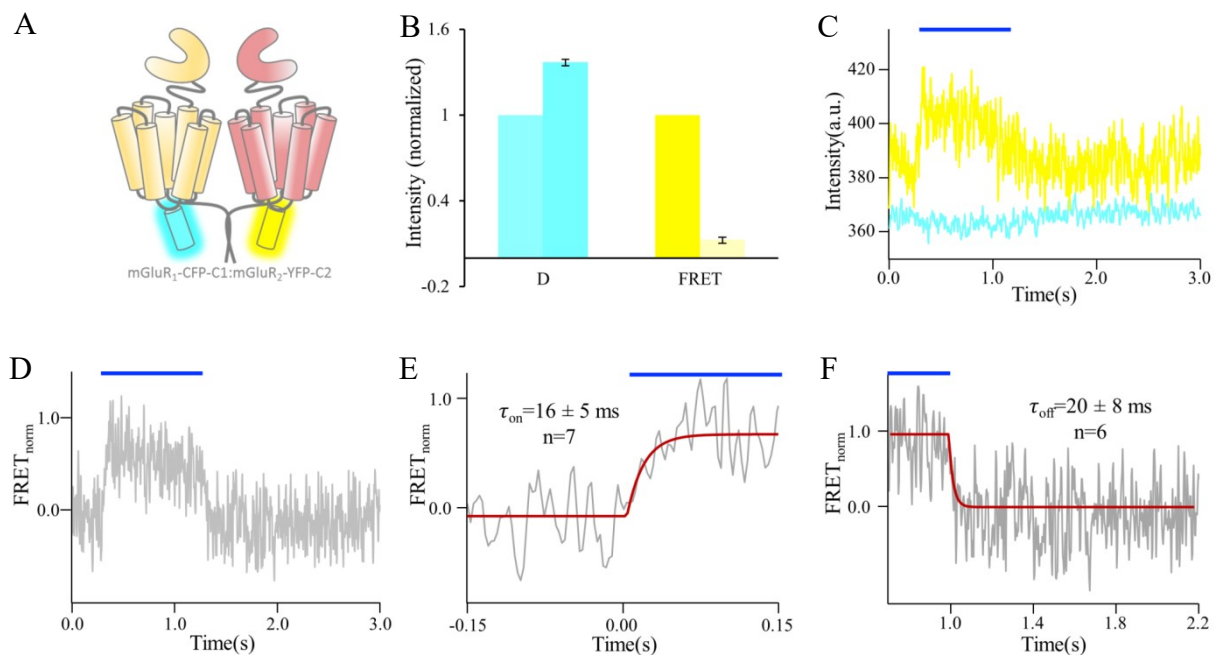


Figure 28: Kinetics for human mGluR1/2 E-sensor. **A.** Scheme of mGluR1/2 E-sensor. **B.** Calculated FRET efficiency after acceptor photo-bleaching, $\text{FRET}_{\text{eff}}=29\pm5\%$ ($n=10$). **C.** Signal changes of CFP (cyan) and YFP (yellow) upon fast glutamate application (blue); crosstalk and photobleaching were corrected. **D.** Calculated FRET from CFP and YFP signal. **E.** Activation and, **F.** deactivation kinetics were fitted with a mono-exponential function (red) in averaged traces (grey). Time constants are indicated.

The same pattern is present also in mGluR1/3 (Fig. 29); the slower subunit mGluR3 slows down the activation kinetics of the mGluR1 subunit in the heterodimer. As expected, deactivation is also affected by the slower subunit, slowing down deactivation kinetics in the mGluR1/3 heterodimer.

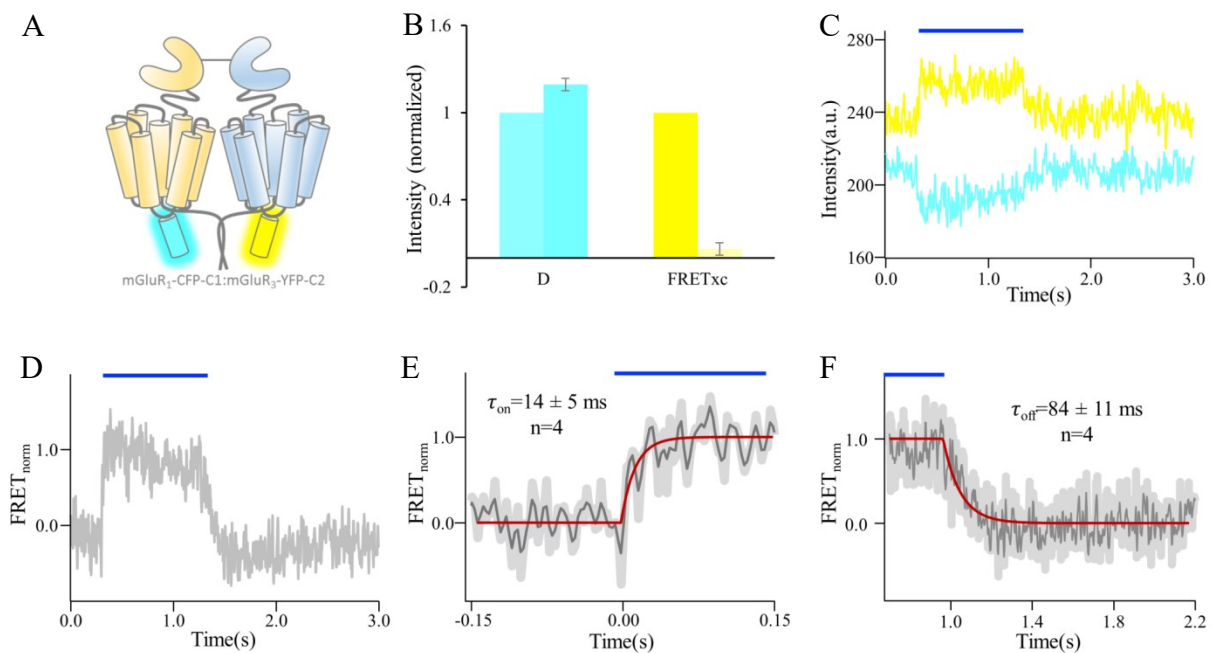


Figure 29: Kinetics for human mGluR1/3 E-sensor. **A.** Scheme of mGluR1/3 E-sensor. **B.** Calculated FRET efficiency after acceptor photo-bleaching, FRET_{eff}=16±3% (n=4). **C.** Signal changes of CFP (cyan) and YFP (yellow) upon fast glutamate application (blue); crosstalk and photobleaching were corrected. **D.** Calculated FRET from CFP and YFP signal. **E.** Activation and, **F.** deactivation kinetics were fitted with a mono-exponential function (red) in averaged traces (grey). Dark grey lines represent 66 Hz filter applied in raw data. Time constants are indicated.

Group II and group III

The highest number of heterodimers is observed between group II and group III. Three of these heterodimers could be fully analyzed kinetically, whereas in three others we identified a conformational change, which was however too small for quantification (Fig. 33). mGluR2 of group II forms functional heterodimers with mGluR7 of group III (Fig. 30); also mGluR3 of group II forms functional heterodimers with mGluR7 (Fig. 31) and mGluR8 of group III (Fig. 32).

Notably, in mGluR2/7 activation kinetics was strongly accelerated to the level of the members of group I. This is particularly remarkable because mGluR7 as homodimer is not sensitive at all at 1 mM glutamate.

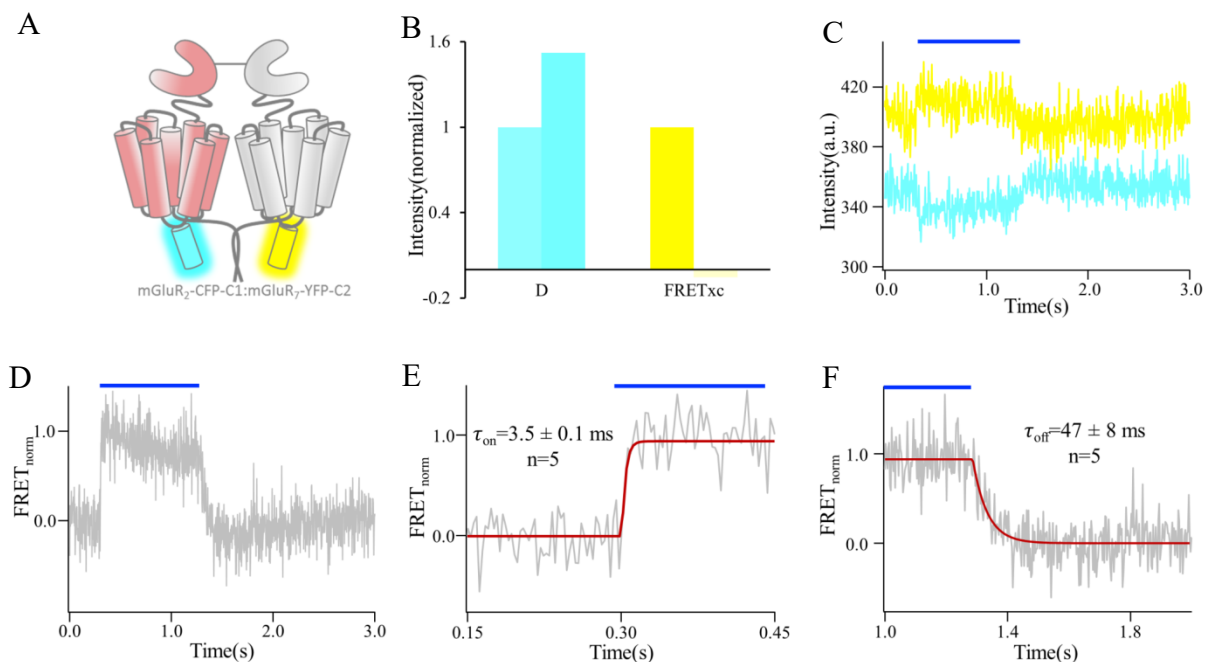


Figure 30: Kinetics for human mGluR2/7 E-sensor. A. Scheme of mGluR2/7 E-sensor. **B.** Calculated FRET efficiency after acceptor photo-bleaching, $FRET_{ef} = 34 \pm 2\%$ (n=4). **C.** Signal changes of CFP (cyan) and YFP (yellow) upon fast glutamate application (blue); crosstalk and photobleaching were corrected. **D.** Calculated FRET from CFP and YFP signal. **E.** Activation and, **F.** deactivation kinetics were fitted with a mono-exponential function (red) in averaged traces (grey). Time constants are indicated.

A similar accelerating effect of mGluR7 was observed for mGluR3/7: It strongly speeds up activation kinetics with respect to the mGluR3 homodimer. Whereas for the function of mGluR2/7 evidence has already presented (Habrian et al. 2019), heterodimerization of mGluR3/7 was not reported before. As in mGluR2/7, deactivation kinetic is decelerated compared to the mGluR3 homodimer.

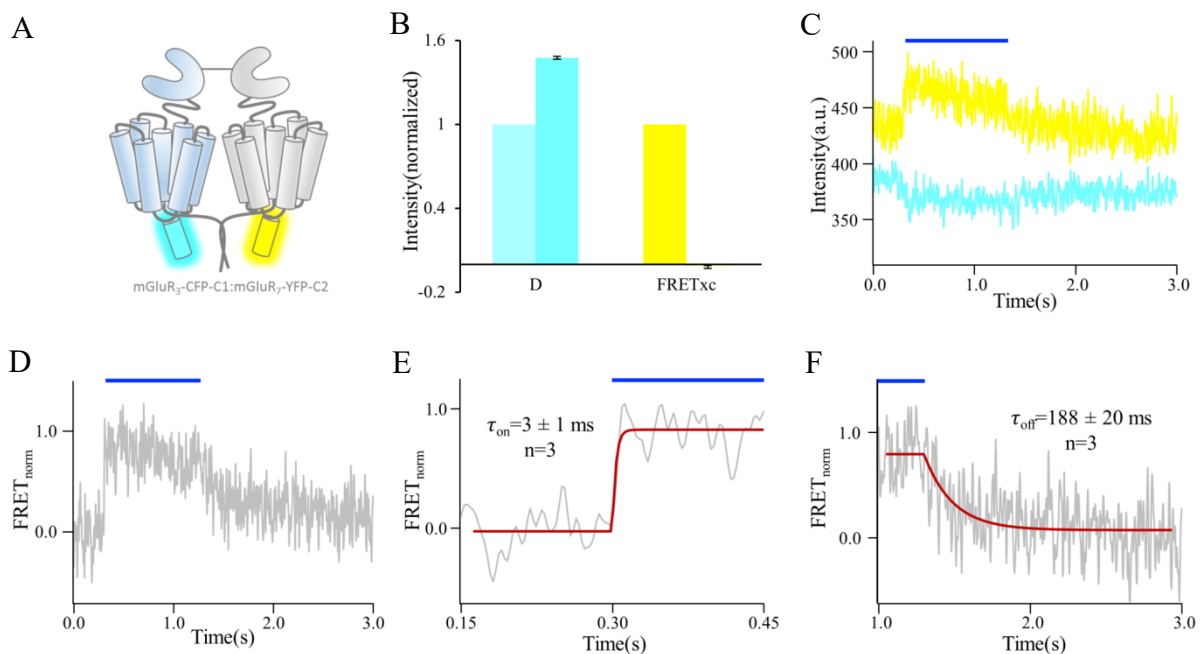


Figure 31: Kinetics for human mGluR3/7 E-sensor. **A.** Scheme of mGluR3/7 E-sensor. **B.** Calculated FRET efficiency after acceptor photo-bleaching, $FRET_{ef}=32\pm 2\%$ ($n=8$). **C.** Signal changes of CFP (cyan) and YFP (yellow) upon fast glutamate application (blue); crosstalk and photobleaching were corrected. **D.** Calculated FRET from CFP and YFP signal. **E.** Activation and, **F.** deactivation kinetics were fitted with a mono-exponential function (red) in averaged traces (grey). Time constants are indicated.

The third functional heterodimer between group II and III is formed by mGluR3 and mGluR8. Activation and deactivation kinetics of mGluR3 and mGluR8 homodimers are close by. When individual subunits combine in the mGluR3/8 heterodimer, none of the kinetic parameters change. Neither activation nor deactivation kinetics are changed. Hence, mGluR8 does not induce an accelerating effect on mGluR3, as observed for mGluR7 (Fig. 32).

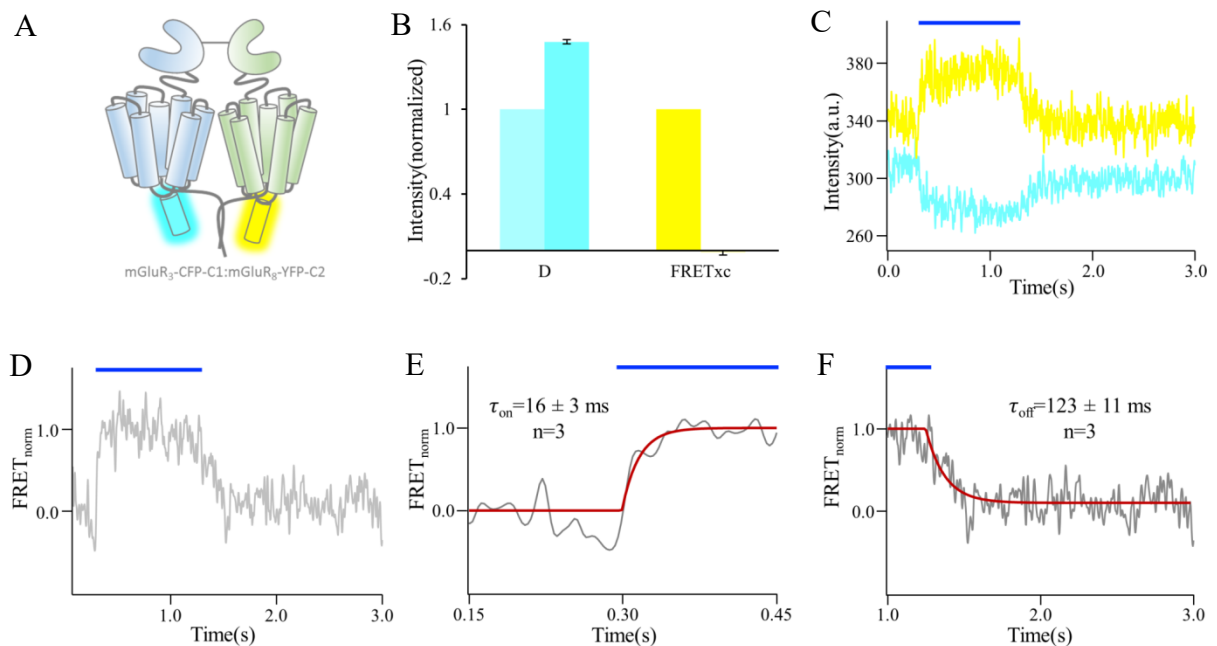


Figure 32: Kinetics for human mGluR3-8 E-sensor. A. Scheme of mGluR3/8 E-sensor. **B.** Calculated FRET efficiency after acceptor photo-bleaching, $FRET_{ef} = 32 \pm 3\%$ (n=5). **C.** Signal changes of CFP (cyan) and YFP (yellow) upon fast glutamate application (blue); crosstalk and photobleaching were corrected. **D.** Calculated FRET from CFP and YFP signal. **E.** Activation and, **F.** deactivation kinetics were fitted with a mono-exponential function (red) in averaged traces (grey). Time constants are indicated.

Besides the three functionally characterized heterodimers between group II and III, three others, mGluR3/4, mGluR2/6 and mGluR2/8 provide FRET signal changes, which were too small for quantification. A similar low resolution of the signals was also observed for mGluR4/8, which is a heterodimer within-group III. Despite the lower resolution of the signals from these four additional heterodimers, functionality is unambiguously there (Fig. 33).

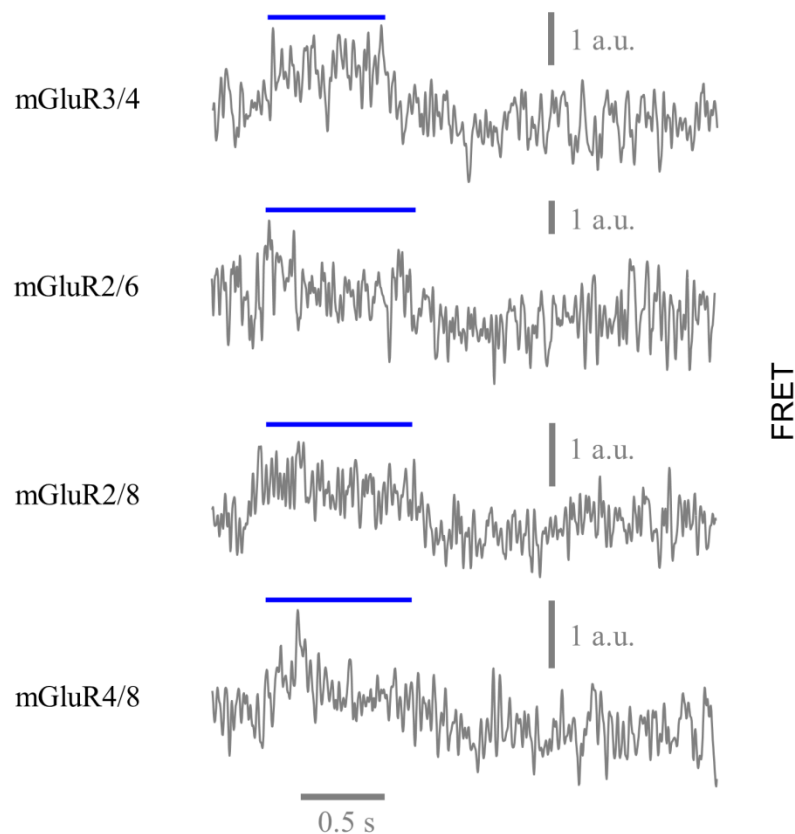


Figure 33: Heterodimers showing FRET changes too small for quantifying time courses. The four heterodimers mGluR3/4, mGluR2/6, mGluR2/8, and mGlu4/8, provided time-dependent responses too small to be subjected to kinetic analysis, proving, nevertheless, functionality of the heterodimers.

5. Discussion

Metabotropic glutamate receptors are members of family C G protein-coupled receptors, they are widely spread within the CNS, in both synaptic and extrasynaptic sites. They play a significant role in neuronal excitability and synaptic transmission by modulating ion channels and other signaling proteins (Niswender and Conn 2010).

The complete activation kinetics of G protein-coupled receptors is understood in detail only for one of their members, rhodopsin. Rhodopsin belongs to family A of G protein-coupled receptors, and it is known as the “light receptor” because it is activated by light. Activation of rhodopsin is associated with conformational changes in the seven-transmembrane domain, and the fully active state is the metarhodopsin-II state. This transition is the rate-limiting step in activation with a time constant of about 1 ms (Arshavsky et al. 2002). For other GPCRs literature suggests that activation requires 10 ms or much longer (Lohse et al. 2014, Marcaggi et al. 2009).

Recent studies in mGluR1, a member of class C G protein-coupled receptors, have shed somelight into the activation process of these dimeric receptors. mGluR1 is a homodimer, it is activated after glutamate binds to the ligand-binding domains. The first step of activation includes a movement of the monomers towards each other (Tateyama et al. 2004, Marcaggi et al. 2009, Hlavackova et al. 2012). It is followed by a second step that includes a conformational change within the monomer (Hlavackova et al. 2012). Kinetics of these processes were reported to be in tens of milliseconds, and the first step is shown to happen in ~10 ms (Marcaggi et al. 2009) or ~35 ms (Hlavackova et al. 2012). The second step was identified only by Hlavackova and coworkers (Hlavackova et al. 2012) and the time constants was ~50 ms. However, the observed activation kinetics were indistinguishable from the temporal resolution of their experiments. Furthermore, the activation kinetics was clearly concentration dependent up to the time resolution of their glutamate superfusion system (Marcaggi et al. 2009). The true activation kinetics is faster.

In this study, we measured the true activation kinetics of ~1 ms duration, which are presumably limited by intermolecular processes and not ligand binding. We further describe deactivation kinetics, and the contribution of the two binding sites in the kinetics. The study was extended to all homo- and heterodimeric mGluR receptors.

5.1. Fast solution exchange system in combination with cPCF

The patch-clamp technique is a standard method to study ion channels, including channels in excised patches. To investigate fast, ligand-dependent processes in ion channels, concentration jump techniques with a piezo device were combined with patch-clamp.

For nearly two decades patch clamp was also combined with fluorescent readouts in patches, as in patch-clamp fluorometry (PCF) (Zheng and Zagotta 2003) on labelled channels and cPCF with labelled ligands (Biskup et al. 2007, Kusch et al. 2011). The latter technique was used successfully to study fast binding processes and current responses (Nache et al. 2013) or fluorescence alone (Thon et al. 2013).

In the present study, we used the cPCF to measure kinetics outside-out patches containing metabotropic glutamate receptors (mGluRs). We optimized the speed of the solution exchange to about $\sim 200 \mu\text{s}$. Note, that this time resolution would be sufficient to resolve the rate-limiting step in Rhodopsin activation.

Having in hand such a fast solution exchange system, combined with the high resolution of the LSM line scan mode, allowed us to overcome technical limits in previous studies (Marcaggi et al. 2009, Hlavackova et al. 2012).

5.2. Characterization of mGluR1 FRET sensors in *Xenopus laevis* oocytes

Expression levels of mGluR FRET sensors in *Xenopus laevis* oocytes were robust as recorded by superimposed fluorescent signals of both, donor (CFP) and acceptor (YFP). Experimental conditions were optimized to avoid errors arising from crosstalk of the two fluorescent proteins.

In literature, it was shown that under some specific experimental conditions, YFP after bleaching could be converted into a species which give signals into the CFP region (Valentin et al. 2005). To exclude this phenomenon, we performed another control, bleaching YFP completely with the 514 nm argon laser while measuring the signal in both detection channels. During the bleaching of YFP, its signals dropped completely, whereas no signal appeared in the CFP detection channel, confirming that the phenomenon described in the paper cited above does not happen under our experimental conditions.

5.2.1. mGluR1 FRET sensors assemble as dimers in the cell membrane

Both E- and A-sensors were successfully expressed in *Xenopus laevis* oocytes. We quantified FRET efficiency (per donor) from acceptor photobleaching experiments by quantifying the donor dequenching for both sensors. FRET efficiency for the A- and E-sensor was determined to be $27 \pm 2 \%$ (n=7) and $23 \pm 2 \%$ (n=3), respectively. Lower FRET efficiency in the E-sensor might indicate a bigger distance between fluorophores in the receptor resting state or be related to fluorophore orientation.

With the intermolecular E-sensor, we detect between the two subunits of an mGluR1 as reported (Tateyama et al. 2004, Marcaggi et al. 2009, Hlavackova et al. 2012). To ensure the composition of the E-sensor that each CFP containing subunit is dimerized with a YFP containing subunit in the other, we used the “quality control system” from the GABA_B receptor (Margeta-Mitrovic et al. 2000, Pagano et al. 2001, Couve et al. 1998). This quality control system is located in the C-terminus of the GABA_B receptor. The C-terminal part of GABA_{B1} (one of the GABA_B subunits) possesses an endoplasmic retention signal. Transportation of a functional dimeric form of GABA_B is possible only when the ER retention signal from GABA_{B1} interacts with the C-terminal part present in the GABA_{B2} receptor (the second subunit of GABA_B) and masks it. C-terminal parts of GABA_B were transferred to the mGluR1 subunits, the one containing the retention signal to the subunit containing CFP and the other one to the subunits containing YFP. Application of this system was previously shown also in mGluRs (Hlavackova et al. 2012, Kniazeff et al. 2004).

5.2.2. mGluR1 FRET sensors are functional

mGluR1 FRET sensors expressed in *Xenopus laevis* oocytes were tested if they bind glutamate and activate. Both sensors respond to glutamate, tested in whole cells evaluating spectra and also in outside-out membrane patches evaluating signals.

In case of the E-sensor, FRET efficiency was increased upon activation, consistent with the idea that the distance between acceptor and donor placed in the intracellular loop 2 of each monomer decreases activation. This is consistent with literature data (Tateyama et al. 2004, Marcaggi et al. 2009, Hlavackova et al. 2012). It has been shown recently for mGluR5, that monomers are repositioned and moved towards each other upon activation (Koehl et al. 2019).

In contrast, with the A-sensor FRET decreased during activation, indicating that the distance between fluorophores placed in intracellular loop 2 and C-terminus within the monomer increase upon activation, similar as described previously (Hlavackova et al. 2012).

Combining both events during activation, we conclude that the activation step consists of two steps. There is an initial movement of the monomers towards each other, and then there is a conformational change within the monomers.

Interpretation of the FRET signals:

FRET amplitudes

FRET amplitudes are determined by the Förster radius, R_0 , and the distance between donor and acceptor, R . Thus, it is tempting to calculate distances from FRET efficiencies. However, the Förster radius R depends on the spectral overlap of the donor emission and acceptor excitation spectra and several other physical parameters, including the relative orientation between the transition dipole moment of donor and acceptor, parametrized as k^2 . Often, the orientation is assumed to be random ($k^2=2/3$). However, in our system, the fluorophores are fixed inside the CFP/YFP beta barrels, and the CFP/YFP are further fixed in orientation due to the position in the loop. Therefore, we cannot distinguish changes in distance from changes in relative orientation, thus, changes in R_0 . While techniques exist to gain orientation information (anisotropy and related techniques), there are not compatible with the high temporal resolution required in our experiments.

Kinetics of FRET changes

We assume that both E-sensor and A-sensor exist in two distinct FRET states, e.g. “resting” and “activated”, e.g. having performed an inter or intramolecular rearrangement respectively. The FRET kinetics observed are interpreted as chemical kinetics of the ensemble from one distribution over the states to another. In principal, more FRET states could exist. Consider this e.g. for the E-sensor: Such states could be resting, first subunit conformational shifted, second subunits conformational shifted, both shifted plus rearrangement within a subunit etc. Herein, we do not have indications of additional states, as would likely appear as additional exponential components in the activation and deactivation time courses. To resolve such details, other techniques as single-molecule FRET measurements or FLIM experiments are needed.

5.2.3. mGluR1 activates and deactivates nearly in a stepwise manner

Activation starts when glutamate binds to the binding site. This causes conformational changes within the ligand-binding domain, the closing of the flytrap. The speed of these rearrangements should happen on a sub-millisecond scale (Olofsson et al. 2014, Jingami et al. 2003). Conformational changes are then transmitted towards transmembrane domains, causing a movement of transmembrane domains, as shown for mGluR5 (Koehl et al. 2019).

Transmembrane domains during activation are repositioned and move towards each other, an event that we see with the E-sensor for mGluR1. This first step in activation is remarkably fast lasting only ~ 1 ms and, notably, much faster than previously reported (Marcaggi et al. 2009, Hlavackova et al. 2012).

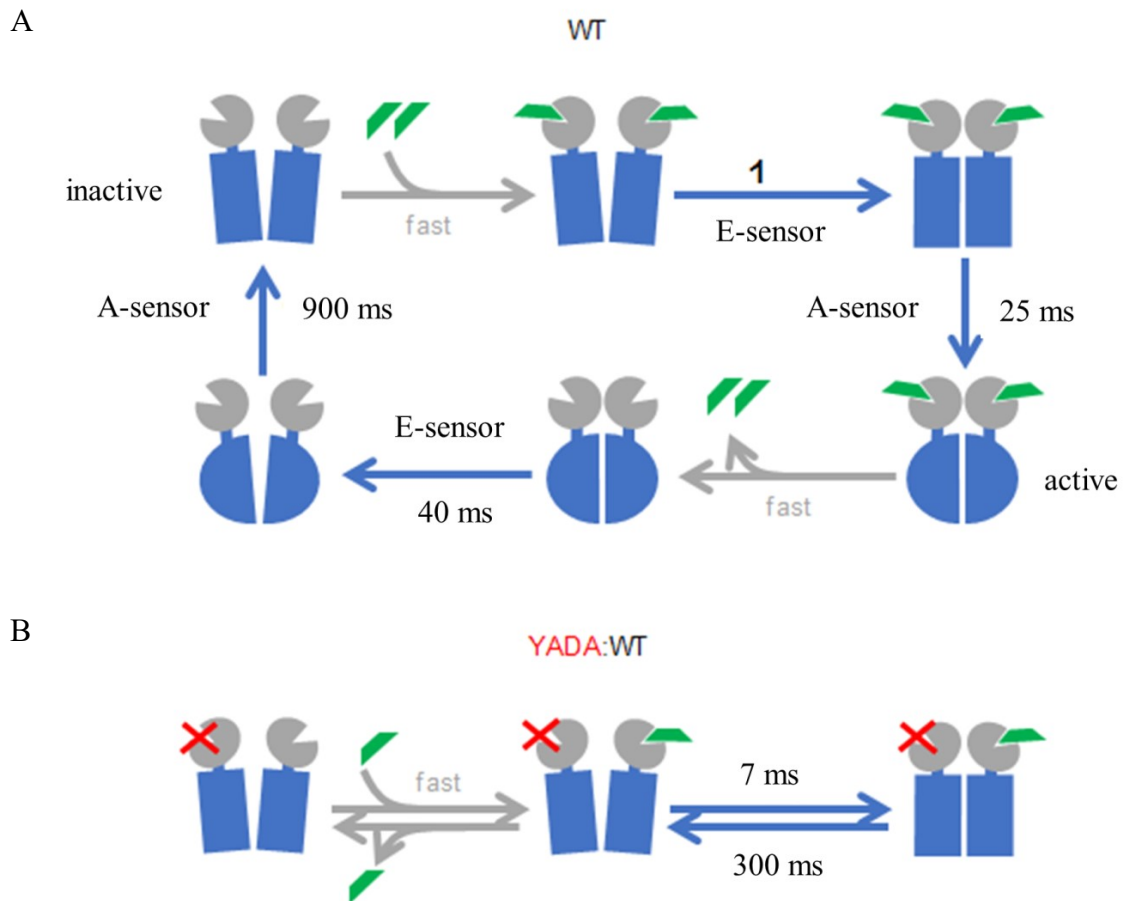
Furthermore, we studied the concentration dependence of the activation speed in the E-sensor, and we found out that glutamate concentrations 1 mM did not further increase the speed of activation. This shows that the first step of activation including the rearrangements of the two subunits is not limited by diffusion or binding dynamics of the ligand but is the real activation kinetics of the receptor.

In addition to the inter-subunit movement, there is a slower event in activation proceeding within the monomers. We studied this event using the A-sensor. These conformational changes within the transmembrane domain are associated with a negative FRET signal, indicating that the distance between loop 2 and C-terminal domain is increased. This step was notably slower compared to the first step, yielding τ_{on} of 25 ± 7 ms ($n=7$). As the fast step loses concentration dependence at ~ 1 mM, our measurements at 1 mM with the A-sensor can also be assumed to be limited by the molecular rearrangements in this case intramolecular arrangements. So there is an activation process that happens in two steps.

To test the contribution of both binding sites in activation and deactivation of mGluR1, we generated the YADA mutations (Kniazeff et al. 2004), which disrupts the binding of glutamate to the binding site. Previously, it was shown that mGluRs with one binding are still functional, but for a full effect, both binding sites are needed (Kniazeff et al. 2004). In E-sensors bearing the YADA mutations, we did not notice any glutamate effect in the FRET signal, while in sensors with one binding site free and one mutated, activation and deactivation kinetics were slowed down about six times. This shows that both binding sites are necessary for generating the fast kinetics.

Deactivation time courses are substantially slower and presumably also happen in a stepwise manner, the first step includes movement of monomers away from each other, a process that occurs in 43 ± 1 ms (n=52) and matches the findings from the literature (Marcaggi et al. 2009), followed by a slower movement within the transmembrane domain of 900 ± 60 ms (n=6). As expected, deactivation kinetics was not affected by changes in concentration.

Together, our data indicate that activation of mGluR1 begins with an intermolecular fast conformational change, lasting ~ 1 ms, that is followed by a slower conformational change within the transmembrane domains, lasting ~ 20 ms, to reach the fully active state. Deactivation also proceeds in a two-step manner, a first step between the dimers at last ~ 40 ms which is followed by a slower step within the transmembrane domain of ~ 900 ms. For full activation and deactivation speeds, both binding sites are needed, knocking out one of the binding sites considerably slows down both processes (Scheme 3).



Scheme 3: Cartoon illustration of the activation and deactivation kinetics in mGluR1. Glutamate is indicated in green. The specified times are the time constants determined by the fits. It is assumed that the ligand binding is not rate-limiting [i.e., the ligand concentration is sufficiently high, and that ligand binding and closure of the VFT domain occur at sub-millisecond speed (“fast”). **A.** WT receptor. **B.** YADA mutant in one subunit to eliminate ligand binding (red crosses).

5.3. Activation and deactivation kinetics of all other members of the human mGluR family

To study the kinetics of human metabotropic glutamate receptors, we generated the respective intermolecular FRET sensors. By placing either CFP or YFP in the intracellular loop 2 of each monomer, dimerization was controlled by putting in the C-terminus either the C1 or C2 C-terminal tails of the GABA_B receptor “quality control system” as described (Hlavackova et al. 2012, Grushevskiy et al. 2019). Using these sensors, we measured activation and deactivation kinetics in all eight homodimers. Furthermore, we tested the ability of each member to form dimers with all other mGluRs and determined activation and deactivation kinetics in the functional portion of the heterodimers.

First, we studied all homodimeric combinations in mGluR1-8. For seven out of the eight homodimers dimerization was observed. FRET efficiencies range from 18 % in mGluR7 to 30 % in mGluR3, confirming that the GABA_B system helps to distinguish donor-acceptor heterodimers from donor-donor or acceptor-acceptor homodimers. Only mGluR6 was so poorly expressed that it was not possible to investigate dimerization. Five out of seven expressing homodimers showed glutamate jump evoked FRET changes between CFP and YFP and were deemed functional.

16 out of 28 possible heterodimeric receptors gave FRET signals. The efficiencies ranged from 13 % for mGluR4/8 to 35 % for three heterodimers of mGluR2 (mGluR2/3, mGluR2/4 and mGluR2/8). The mean FRET efficiency of the heterodimers of $26.5 \pm 1.8\%$ does not significantly differ from that of the homodimers of 24.3 ± 1.7 (t-test, $p=0.46$). 11 out of 15 heterodimers were functional upon glutamate application. Activation and deactivation kinetics were analyzed by fitting with mono-exponential functions.

5.3.1. Kinetics within homodimeric mGluRs

Activation kinetics of both members in group II are significantly slower compared to members of group I (mGlu1 and mGluR5) as shown in Fig. 34A. mGluR2 is the slowest dimer measured, with an activation time constant of 30 ms. Deactivation kinetics of mGluR2 is faster than activation kinetics, whereas, deactivation kinetics of mGluR3 is 115 ms, significantly slower compared to mGluR2 (Fig. 34B).

In group III, kinetics could be measured only for mGluR8. The activation kinetics are in the same range as for the members of the group II (mGluR2 and mGluR3), but significantly slower than for both members of group I. Deactivation kinetics are 51 ms. To sum up, members of group I have activation kinetics significantly faster than members of group II and III, whereas deactivation kinetics are not consistent within the groups (Fig. 34).

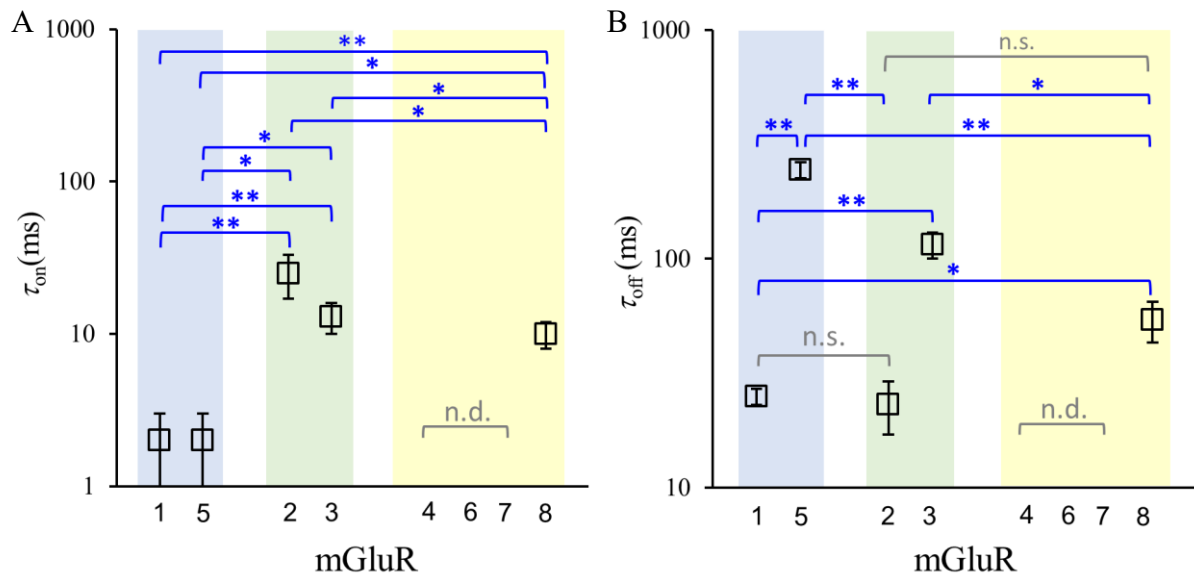


Figure 34: Comparison of the kinetics of all groups of homodimeric mGluRs. A. Activation and, **B.** Deactivation time constants for the mGluRs. Three mGluRs did not show evaluable time courses. n.d., not determinable. Significant differences are indicated (* $p < 0.05$, ** $p < 0.01$). n.s. indicates that the difference is ‘not significant’.

5.3.2. Kinetics in heterodimeric mGluRs

5.3.2.1. Heterodimeric mGluRs within the same group

Based on amino acid alignment and the degree of sequence homology which is from 61.8-75.0 % within the groups, heterodimerization of members of the same groups could be expected and was also reported previously (Doumazane et al. 2011). However, these authors

reported only information about the assembly of the two heterodimers without testing for function. They used the SNAP and CLIP technology and measured time-resolved FRET. Another study reported heterodimerization within members of group II (mGluR2/3) by using a single-molecule approach (Levitz et al. 2016). We confirmed previous findings, and furthermore, we show kinetic evidence of heterodimerization within groups for two combinations, one in group I, and the other in group II.

In group I, mGluR1 forms a functional heterodimer with mGluR5. Activation kinetics in this heterodimers are as quick as with the respective homodimers, mGluR1 and mGluR5. Deactivation kinetics, on the other hand, exhibits a major contrast with respect to the mGluR1 homodimer. Combination of mGluR1 with mGluR5 causes a deceleration in deactivation by roughly ten times compared to mGluR1 alone. Deactivation kinetics of mGluR1/5 heterodimer are similar to mGluR5 homodimer, suggesting that mGluR5 determines this step.

Furthermore, to test if swapping fluorophores and the GABA_B “quality control system” between the subunits of the mGluR1/5 combination affects kinetics, we replaced CFP and C1 in mGluR1 subunit with YFP and C2, whereas YFP and C2 in mGluR5 are replaced with CFP and C1. Both activation and deactivation kinetics were not affected by this swap (Fig. 35).

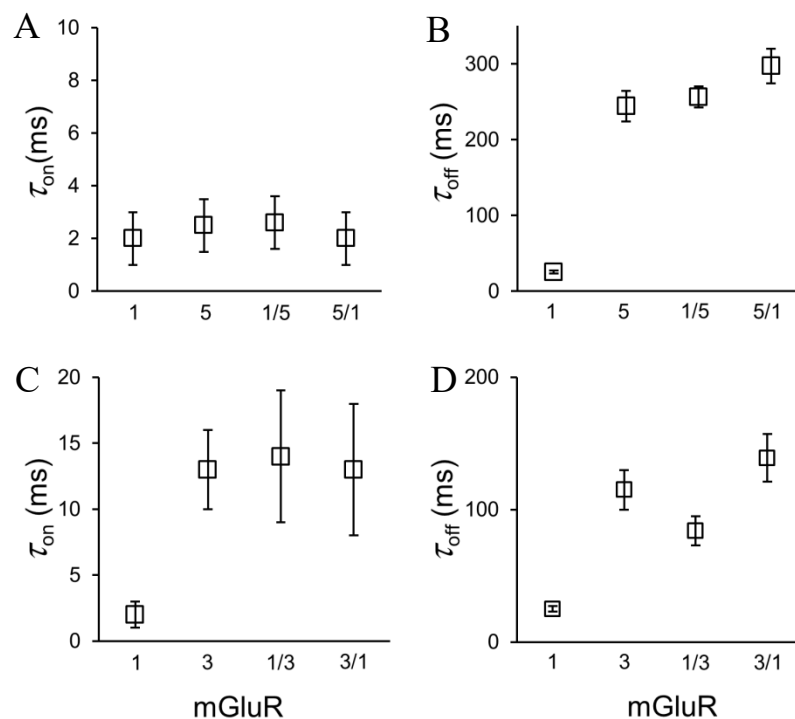


Figure 35: Activation and deactivation kinetics in heterodimers with swapped fluorophores and GABA_B “quality control system” between monomers . A). τ_{on} and B) τ_{off} for mGluR1, mGluR5, mGluR1/5 and mGluR5/1. C). τ_{on} and D) τ_{off} for mGluR1, mGluR3, mGluR1/3 and mGluR3/1.

Within group II we confirmed heterodimerization of mGluR2 and mGluR3. Combination of mGluR2 with mGluR3 significantly accelerates activation kinetics of the mGluR2 subunit. The opposite effect is seen in deactivation kinetics, mGluR3 significantly decelerates deactivation kinetics of the mGluR2 subunit. Both activation and deactivation kinetics of mGluR3 do not encounter a significant change as a result of the combination with mGluR2.

In both cases of heterodimerization within the group I and II, the slow subunit determines the kinetics of the heterodimer, except for mGluR2/3: Here activation kinetics was accelerated with respect to mGluR2.

A summary of the kinetics of heteromeric combinations within the group I and group II is shown in Fig. 36.

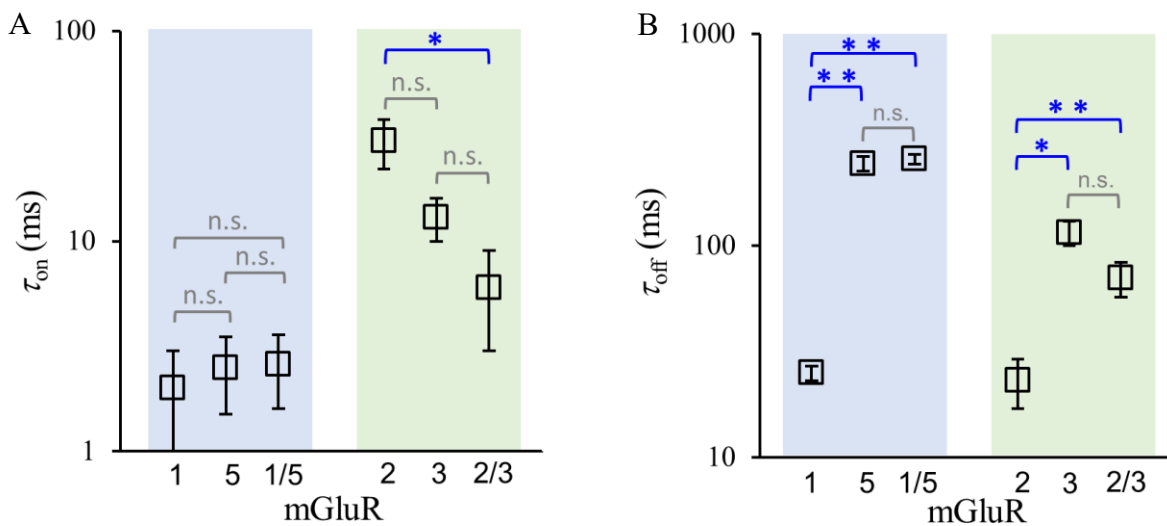


Figure 36: Activation and deactivation kinetics in heterodimers within groups. **A.** τ_{on} for two heterodimers in group I and II. **B.** τ_{off} for two heterodimers in group I and II. Significant differences are indicated (* $p < 0.05$, ** $p < 0.01$). n.s. indicates that the difference is ‘not significant’.

5.3.2.2. Heterodimeric mGluRs between different groups

For the first time, we show heterodimerization between members of group I and II, for two of the heterodimers we could also analyze the kinetics. As predicted from literature (Doumazane et al. 2011), heterodimerization between II and III was present in many cases. On the other hand, no functional heterodimers were noticed between the group I and III (Doumazane et al. 2011).

Two cases of heterodimerization were identified between group I and II, mGluR1 with either mGluR2 or mGluR3. Activation kinetics in mGluR1/2 and mGluR1/3 were dominated by the slower subunit mGluR2 or mGluR3 over mGluR1. Regarding deactivation kinetics, mGluR1/2 is not changed significantly because deactivation kinetics for mGluR1 and mGluR2 homodimers are similar. In case of mGluR1/3 slower mGluR3 subunit dominates the rate.

A striking feature was observed for mGluR7. Whereas homodimeric mGluR7 did not produce any evaluable kinetic response (tested with up to 10 mM glutamate), it accelerated activation in the heterodimer mGluR2/7 with respect to homodimeric mGluR2 by nearly an order of magnitude. A similar effect of mGluR7 was observed in mGluR3/7. This suggests an essential biological role of the mGluR7 as an accelerator for members of group II subunits (Fig. 37A).

Regarding deactivation kinetics, two out of the four heterodimers generating effects on activation kinetics also produced significantly changed deactivation kinetics: mGluR7, the strong accelerator of activation relative to mGluR2 and mGluR3, also slows deactivation in mGluR3/7 (Fig. 37B).

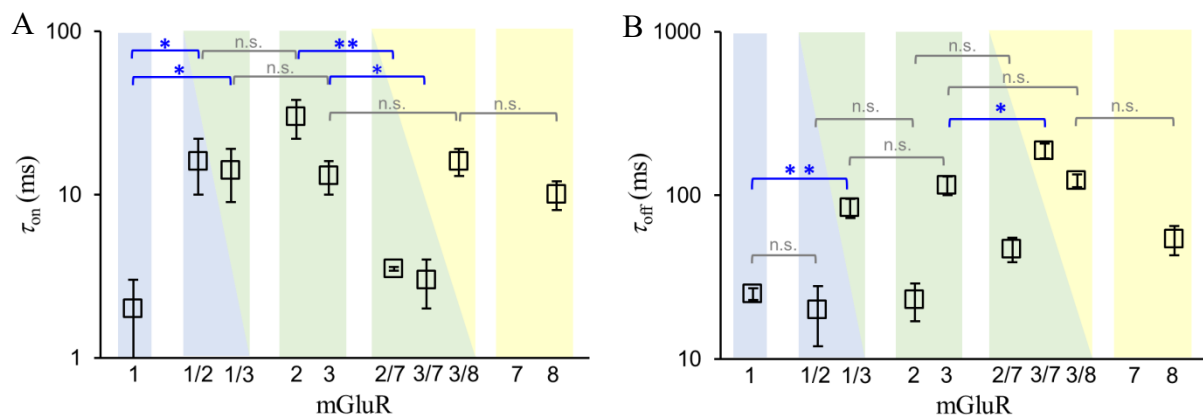


Figure 37: Kinetics in heterodimers involving group II and III. A. τ_{on} and, B. τ_{off} for two heterodimers between group I and II and three heterodimers between group II and III. Significant differences are indicated (* $p < 0.05$, ** $p < 0.01$). n.s. indicates that the difference is 'not significant'.

Since the interventions made by generating FRET sensors, as well as by introducing the GABA_B “quality control system” are located at the intracellular site of the constructs, and the primary dimer interface in mGluRs is in the extracellular ligand-binding domain (Levitz et al. 2016), we assume that the functional interactions identified in our study are representative also for the wild type receptors.

Helices B and C of the sequence (Fig. 37) in ligand binding-domain 1 have been shown to be essential for dimerization (Levitz et al. 2016). Notably, group I and II subunits share numerous identical positions in this region, whereas in group III at least one position is different. A similar pattern is noticed if comparing group II and III, then in group I at least one position is different. In contrast, there is only one identical position in comparison with group I and III, when in group II at least one position is different. This might provide an explanation for the experimental result that between group I and II and between group II and III, but not between group I and III, functional heterodimers were found. One may speculate that heterodimers containing one group II subunit and either one group I or one group III subunit, presumably play an essential role for multiple functions in neurons, both at the pre- and postsynaptic membrane.

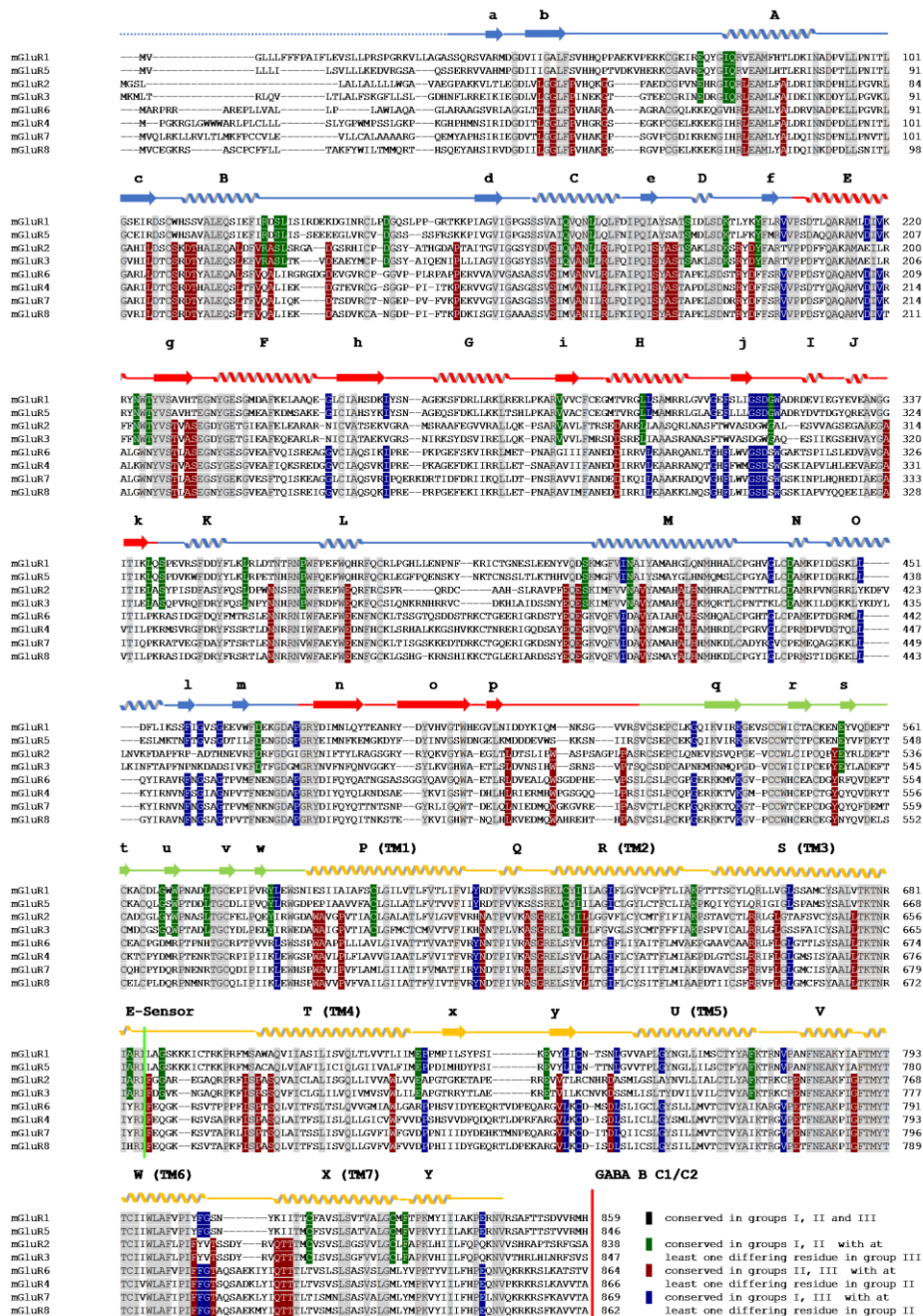


Figure 38: Full-length human mGluR1 to mGluR8 in the sequence given by the phylogenetic tree (Fig. 19). Secondary structures are represented by helices (α helices A-Y), arrows (β strands a-y), straight lines (loops, combining elements between secondary structures etc.), dotted lines (no information available). Symbols: blue - ligand binding domain 1, red - ligand binding domain 2, green - cysteine rich domain, orange - transmembrane domains, yellow box - amino acids involved in binding, bright green vertical line - position of the E-sensor, red vertical line - cutting sites for the constructs. Conserved residues are labelled according to the indicated color code. The following entries were used: mGluR1, Q14832; mGluR2, Q14416; mGluR3, Q14832; mGluR4, Q14833; mGluR5, P41594; mGluR6, Q15303; mGluR7, Q14831; mGluR8, O00222. (Figure prepared by Dr. Christian Sattler).

6. Conclusions

1. Speed of the solution exchange system at the tip of the patch pipette was measured to be in the range of 200 μ s. In combination with high-resolution LSM, we could measure any FRET change in the range of activation kinetics of rhodopsin.
2. Activation and deactivation kinetics in mGluR1 happen in a stepwise manner. The first step of activation includes subunit movement towards each other, and this step occurs in a notably fast speed, at about 1 ms, faster than data reported before for mGluR1 (Marcaggi et al. 2009), and was not limited by the technique. Activation continues with a slower step which consists of an intramolecular conformational change within subunits, and the speed is about 20 times slower compared to the first step.

In comparison with rhodopsin, a dimeric GPCR has a more complicated activation process, intermolecular movements between monomers happen in rhodopsin speed. However, the second step of activation in mGluRs, which is comparable with the conformational rearrangement occurring during activation of rhodopsin, is about 20 times slower.

Fast activation speed, which consists of inter-subunit movements, is not concentration-dependent. Even at concentrations up to 10 mM, the speed remains the same, indicating that the kinetics presented here represent the maximum speed.

Deactivation kinetics are slower than activation kinetics. The process also happens in two steps, inter-subunit movement away from each other requires about 40 ms, followed by a conformational change within the monomers of about 1 s.

3. We confirm that one binding site is enough to cause intermolecular movements in the mGluR1 E-sensor. However, the activation and deactivation kinetics are slowed down by factor six. It is still not clear, and remains to be clarified in the future, if one binding site is enough to cause movements of both transmembrane domains or one binding site causes a conformational change in only one transmembrane domain.
4. We were able to generate intermolecular FRET sensors for all eight members of metabotropic glutamate receptors by fusing CFP and YFP in each monomer, also adding the GABA_B “quality control system” as described before for mGluR1 rat

(Hlavackova et al. 2012). All mGluR members, except mGluR6, expressed on the membrane as homodimers as confirmed by acceptor photobleaching and donor dequenching. FRET efficiencies vary from 18 % for mGluR7 to 30 % for mGluR3. mGluR1 expresses at the highest levels in the membrane. Five out of seven mGluR sensors that form dimers in the membrane are functional when testing with glutamate jumps: mGluR1 and mGluR5 in group I, mGluR2 and mGluR3 in group II, and only mGluR8 in group III.

5. Both members of the group I (mGluR1 & mGluR5) activates very fast, thereby approximate the technical limitations, and are significantly different compared to activation kinetics of the members of group II (mGluR2 & mGluR3) and group III (mGluR8). Deactivation kinetics varies, mGluR1 has significantly faster deactivation kinetics compared to mGluR5. A similar pattern is noticed in group II, deactivation kinetics of mGluR2 is significantly slow compared to mGluR3. Whereas for mGluR8, deactivation kinetics has deactivation kinetics are between those of mGluR2 and mGluR3.
6. We could detect heterodimerization between members of each group, and also between members of different groups. Group I forms functional dimers with group II and group II forms dimers with group III. However, no functional heterodimerization was identified between group I and II. For mGluR1/2, mGluR1/3, mGluR1/5, mGluR2/3 and mGluR3/8 activation and deactivation kinetics are dominated by the slower subunit compared to the respective homodimers. A remarkable finding is that mGluR7 in combination with mGluR2 and mGluR3 causes acceleration in the activation kinetics of heterodimers in comparison with mGluR2 or mGluR3 homodimers.

7. References

- Aiba, A., Kano, M., Chen, C., Stanton, M. E., Fox, G. D., Herrup, K., Zwingman, T. A., & Tonegawa, S.** (1994). Deficient cerebellar long-term depression and impaired motor learning in mGluR1 mutant mice. *Cell*, **79**(2), 377–388.
- Arshavsky, V. Y., Lamb, T. D., & Pugh, E. N., Jr.** (2002). G proteins and phototransduction. *Annual review of physiology*, **64**, 153–187. doi:10.1146/annurev.physiol.64.082701.102229
- Baude, A., Nusser, Z., Roberts, J. D., Mulvihill, E., McIlhinney, R. A., & Somogyi, P.** (1993). The metabotropic glutamate receptor (mGluR1 alpha) is concentrated at perisynaptic membrane of neuronal subpopulations as detected by immunogold reaction. *Neuron*, **11**(4), 771–787. doi:10.1016/0896-6273(93)90086-7
- Bhattacharyya, S.** (2016). Inside story of Group I Metabotropic Glutamate Receptors (mGluRs). *The international journal of biochemistry & cell biology*, **77**(Pt B), 205–212. doi:10.1016/j.biocel.2016.03.003
- Bhave, G., Karim, F., Carlton, S. M., & Gereau, R. W.** (2001). Peripheral group I metabotropic glutamate receptors modulate nociception in mice. *Nature neuroscience*, **4**(4), 417–423. doi:10.1038/86075
- Biskup, C., Kusch, J., Schulz, E., Nache, V., Schwede, F., Lehmann, F., Hagen, V., & Benndorf, K.** (2007). Relating ligand binding to activation gating in CNGA2 channels. *Nature*, **446**(7134), 440–443. doi:10.1038/nature05596
- Blackshaw, L. A., Page, A. J., & Young, R. L.** (2011). Metabotropic glutamate receptors as novel therapeutic targets on visceral sensory pathways. *Frontiers in neuroscience*, **5**, 40. doi:10.3389/fnins.2011.00040
- Carlton, S. M., Zhou, S., Govea, R., & Du, J.** (2011). Group II/III metabotropic glutamate receptors exert endogenous activity-dependent modulation of TRPV1 receptors on peripheral nociceptors. *The Journal of neuroscience : the official journal of the Society for Neuroscience*, **31**(36), 12727–12737. doi:10.1523/JNEUROSCI.6558-10.2011
- Chachisvilis, M., Zhang, Y. L., & Frangos, J. A.** (2006). G protein-coupled receptors sense fluid shear stress in endothelial cells. *Proceedings of the National Academy of Sciences of the United States of America*, **103**(42), 15463–15468. doi:10.1073/pnas.0607224103
- Chalfie, M., Tu, Y., Euskirchen, G., Ward, W. W., & Prasher, D. C.** (1994). Green fluorescent protein as a marker for gene expression. *Science (New York, N.Y.)*, **263**(5148), 802–805. doi:10.1126/science.8303295

- Conn, P. J., & Pin, J. P.** (1997). Pharmacology and functions of metabotropic glutamate receptors. *Annual review of pharmacology and toxicology*, **37**, 205–237. doi:10.1146/annurev.pharmtox.37.1.205
- Conquet, F., Bashir, Z. I., Davies, C. H., Daniel, H., Ferraguti, F., Bordi, F., Franz-Bacon, K., Reggiani, A., Matarese, V., & Condé, F.** (1994). Motor deficit and impairment of synaptic plasticity in mice lacking mGluR1. *Nature*, **372(6503)**, 237–243. doi:10.1038/372237a0
- Couve, A., Filippov, A. K., Connolly, C. N., Bettler, B., Brown, D. A., & Moss, S. J.** (1998). Intracellular retention of recombinant GABAB receptors. *The Journal of biological chemistry*, **273(41)**, 26361–26367. doi:10.1074/jbc.273.41.26361
- Damian, M., Mary, S., Martin, A., Pin, J. P., & Banères, J. L.** (2008). G protein activation by the leukotriene B4 receptor dimer. Evidence for an absence of trans-activation. *The Journal of biological chemistry*, **283(30)**, 21084–21092. doi:10.1074/jbc.M710419200
- Davenport, D. & Nicol, J.A.C.** (1995). Luminiscence of hydromedusae. *Proc. R. Soc. Lond. B*, **144(916)**, 399–411. doi:10.1098/rspb.1955.0066
- Doumazane, E., Scholler, P., Zwier, J. M., Trinquet, E., Rondard, P., & Pin, J. P.** (2011). A new approach to analyze cell surface protein complexes reveals specific heterodimeric metabotropic glutamate receptors. *FASEB journal : official publication of the Federation of American Societies for Experimental Biology*, **25(1)**, 66–77. doi:10.1096/fj.10-163147
- Dumont, J. N.** (1972). Oogenesis in *Xenopus laevis* (Daudin). I. Stages of oocyte development in laboratory maintained animals. *Journal of morphology*, **136(2)**, 153–179. doi:10.1002/jmor.1051360203
- Duvoisin, R. M., Zhang, C., & Ramonell, K.** (1995). A novel metabotropic glutamate receptor expressed in the retina and olfactory bulb. *The Journal of neuroscience : the official journal of the Society for Neuroscience*, **15(4)**, 3075–3083. doi:10.1523/JNEUROSCI.15-04-03075.1995
- El Moustaine, D., Granier, S., Doumazane, E., Scholler, P., Rahmeh, R., Bron, P., Mouillac, B., Banères, J. L., Rondard, P., & Pin, J. P.** (2012). Distinct roles of metabotropic glutamate receptor dimerization in agonist activation and G-protein coupling. *Proceedings of the National Academy of Sciences of the United States of America*, **109(40)**, 16342–16347. doi:10.1073/pnas.1205838109
- Ernst, O. P., Bieri, C., Vogel, H., & Hofmann, K. P.** (2000). Intrinsic biophysical monitors of transducin activation: fluorescence, UV-visible spectroscopy, light scattering, and evanescent field techniques. *Methods in enzymology*, **315**, 471–489. doi:10.1016/s0076-6879(00)15862-8

- Farrens, D. L., Altenbach, C., Yang, K., Hubbell, W. L., & Khorana, H. G.** (1996). Requirement of rigid-body motion of transmembrane helices for light activation of rhodopsin. *Science (New York, N.Y.)*, **274**(5288), 768–770. doi:10.1126/science.274.5288.768
- Feng, Z., Ma, S., Hu, G., & Xie, X. Q.** (2015). Allosteric Binding Site and Activation Mechanism of Class C G-Protein Coupled Receptors: Metabotropic Glutamate Receptor Family. *The AAPS journal*, **17**(3), 737–753. doi:10.1208/s12248-015-9742-8
- Förster, T.** (1948). Intermolecular energy migration and fluorescence. *Ann. Phys.*, **2**, 55-75.
- Gether, U., Lin, S., & Kobilka, B. K.** (1995). Fluorescent labeling of purified beta 2 adrenergic receptor. Evidence for ligand-specific conformational changes. *The Journal of biological chemistry*, **270**(47), 28268–28275. doi:10.1074/jbc.270.47.28268
- Grushevskiy, E. O., Kukaj, T., Schmauder, R., Bock, A., Zabel, U., Schwabe, T., Benndorf, K., & Lohse, M. J.** (2019). Stepwise activation of a class C GPCR begins with millisecond dimer rearrangement. *Proceedings of the National Academy of Sciences of the United States of America*, **116**(20), 10150–10155. doi:10.1073/pnas.1900261116
- Habrian, C. H., Levitz, J., Vyklicky, V., Fu, Z., Hoagland, A., McCort-Tranchepain, I., Acher, F., & Isacoff, E. Y.** (2019). Conformational pathway provides unique sensitivity to a synaptic mGluR. *Nature communications*, **10**(1), 5572. doi:10.1038/s41467-019-13407-8
- Heck, M., Pulvermüller, A., & Hofmann, K. P.** (2000). Light scattering methods to monitor interactions between rhodopsin-containing membranes and soluble proteins. *Methods in enzymology*, **315**, 329–347. doi:10.1016/s0076-6879(00)15852-5
- Hlavackova, V., Prezeau L., Pin JP., Blahos, J.** (2017). Class C GPCRs: Metabotropic Glutamate Receptors. In K. M. Herrick-Davis, *The Receptors* (Vol. **33**, pp. **327-55**). Totowa, New Jersey: Humana Press. doi:10.1007/978-3-319-60174-8_13
- Hlavackova, V., Zabel, U., Frankova, D., Bätz, J., Hoffmann, C., Prezeau, L., Pin, J. P., Blahos, J., & Lohse, M. J.** (2012). Sequential inter- and intrasubunit rearrangements during activation of dimeric metabotropic glutamate receptor 1. *Science signaling*, **5**(237), ra59. doi:10.1126/scisignal.2002720
- Hoffmann, C., Gaietta, G., Bünemann, M., Adams, S. R., Oberdorff-Maass, S., Behr, B., Vilardaga, J. P., Tsien, R. Y., Ellisman, M. H., & Lohse, M. J.** (2005). A FAsH-based FRET approach to determine G protein-coupled receptor activation in living cells. *Nature methods*, **2**(3), 171–176. doi:10.1038/nmeth742
- Jia, H., Rustioni, A., & Valtschanoff, J. G.** (1999). Metabotropic glutamate receptors in superficial laminae of the rat dorsal horn. *The Journal of comparative neurology*, **410**(4), 627–642.

- Jingami, H., Nakanishi, S., & Morikawa, K.** (2003). Structure of the metabotropic glutamate receptor. *Current opinion in neurobiology*, **13(3)**, 271–278.
doi:10.1016/s0959-4388(03)00067-9
- Kammermeier, P. J.** (2012). Functional and pharmacological characteristics of metabotropic glutamate receptors 2/4 heterodimers. *Molecular pharmacology*, **82(3)**, 438–447.
doi:10.1124/mol.112.078501
- Kelly, E., Bailey, C. P., & Henderson, G.** (2008). Agonist-selective mechanisms of GPCR desensitization. *British journal of pharmacology*, **153 Suppl 1(Suppl 1)**, S379–S388.
doi:10.1038/sj.bjp.0707604
- Kim, C. H., Lee, J., Lee, J. Y., & Roche, K. W.** (2008). Metabotropic glutamate receptors: phosphorylation and receptor signaling. *Journal of neuroscience research*, **86(1)**, 1–10.
- Kniazeff, J., Bessis, A. S., Maurel, D., Ansanay, H., Prézeau, L., & Pin, J. P.** (2004). Closed state of both binding domains of homodimeric mGlu receptors is required for full activity. *Nature structural & molecular biology*, **11(8)**, 706–713.
doi:10.1038/nsmb794
- Antoine Koehl, Hongli Hu, Dan Feng, Bingfa Sun, Yan Zhang, Michael J Robertson, Matthew Chu, Tong Sun Kobilka, Toon Laeremans, Jan Steyaert, Jeffrey Tarrasch, Somnath Dutta, Rasmus Fonseca, William I Weis, Jesper M Mathiesen, Georgios Skiniotis, Brian K Kobilka** (2019). Structural insights into the activation of metabotropic glutamate receptors. *Nature*, **566(7742)**, 79-84. doi:10.1038/s41586-019-0881-4
- Kunishima, N., Shimada, Y., Tsuji, Y., Sato, T., Yamamoto, M., Kumasaka, T., Nakanishi, S., Jingami, H., & Morikawa, K.** (2000). Structural basis of glutamate recognition by a dimeric metabotropic glutamate receptor. *Nature*, **407(6807)**, 971–977. doi:10.1038/35039564
- Kusch, J., Thon, S., Schulz, E., Biskup, C., Nache, V., Zimmer, T., Seifert, R., Schwede, F., & Benndorf, K.** (2011). How subunits cooperate in cAMP-induced activation of homotetrameric HCN2 channels. *Nature chemical biology*, **8(2)**, 162–169.
doi:10.1038/nchembio.747
- Lee, J., Munguba, H., Gutzeit, V. A., Kristt, M., Dittman, J. S., & Levitz, J.** (2020). Defining the Homo- and Heterodimerization Propensities of Metabotropic Glutamate Receptors. *Cell reports*, **31(5)**, 107605. doi:10.1016/j.celrep.2020.107605
- Levitz, J., Habrian, C., Bharill, S., Fu, Z., Vafabakhsh, R., & Isacoff, E. Y.** (2016). Mechanism of Assembly and Cooperativity of Homomeric and Heteromeric Metabotropic Glutamate Receptors. *Neuron*, **92(1)**, 143–159.
doi:10.1016/j.neuron.2016.08.036

- Liman, E. R., Tytgat, J., & Hess, P.** (1992). Subunit stoichiometry of a mammalian K⁺ channel determined by construction of multimeric cDNAs. *Neuron*, **9(5)**, 861–871. doi:10.1016/0896-6273(92)90239-a
- Lohse, M. J., Hein, P., Hoffmann, C., Nikolaev, V. O., Vilardaga, J. P., & Bünemann, M.** (2008). Kinetics of G-protein-coupled receptor signals in intact cells. *British journal of pharmacology*, **153 Suppl 1(Suppl 1)**, S125–S132. doi:10.1038/sj.bjp.0707656
- Lohse, M. J., Maiellaro, I., & Calebiro, D.** (2014). Kinetics and mechanism of G protein-coupled receptor activation. *Current opinion in cell biology*, **27**, 87–93. doi:10.1016/j.ceb.2013.11.009
- Lourenço Neto, F., Schadrack, J., Berthele, A., Zieglgänsberger, W., Tölle, T. R., & Castro-Lopes, J. M.** (2000). Differential distribution of metabotropic glutamate receptor subtype mRNAs in the thalamus of the rat. *Brain research*, **854(1-2)**, 93–105. doi:10.1016/s0006-8993(99)02326-4
- Marcaggi, P., Mutoh, H., Dimitrov, D., Beato, M., & Knöpfel, T.** (2009). Optical measurement of mGluR1 conformational changes reveals fast activation, slow deactivation, and sensitization. *Proceedings of the National Academy of Sciences of the United States of America*, **106(27)**, 11388–11393. doi:10.1073/pnas.0901290106
- Margeta-Mitrovic, M., Jan, Y. N., & Jan, L. Y.** (2000). A trafficking checkpoint controls GABA(B) receptor heterodimerization. *Neuron*, **27(1)**, 97–106. doi:10.1016/s0896-6273(00)00012-x
- Marullo, S., & Bouvier, M.** (2007). Resonance energy transfer approaches in molecular pharmacology and beyond. *Trends in pharmacological sciences*, **28(8)**, 362–365. doi:10.1016/j.tips.2007.06.007
- Masu, M., Iwakabe, H., Tagawa, Y., Miyoshi, T., Yamashita, M., Fukuda, Y., Sasaki, H., Hiroi, K., Nakamura, Y., & Shigemoto, R.** (1995). Specific deficit of the ON response in visual transmission by targeted disruption of the mGluR6 gene. *Cell*, **80(5)**, 757–765. doi:10.1016/0092-8674(95)90354-2
- Matz, M. V., Lukyanov, K. A., & Lukyanov, S. A.** (2002). Family of the green fluorescent protein: journey to the end of the rainbow. *BioEssays : news and reviews in molecular, cellular and developmental biology*, **24(10)**, 953–959. doi:10.1002/bies.10154
- Miyata, M., Finch, E. A., Khiroug, L., Hashimoto, K., Hayasaka, S., Oda, S. I., Inouye, M., Takagishi, Y., Augustine, G. J., & Kano, M.** (2000). Local calcium release in dendritic spines required for long-term synaptic depression. *Neuron*, **28(1)**, 233–244. doi:10.1016/s0896-6273(00)00099-4

- Moreno Delgado, D., Møller, T. C., Ster, J., Giraldo, J., Maurel, D., Rovira, X., Scholler, P., Zwier, J. M., Perroy, J., Durroux, T., Trinquet, E., Prezeau, L., Rondard, P., & Pin, J. P.** (2017). Pharmacological evidence for a metabotropic glutamate receptor heterodimer in neuronal cells. *eLife*, **6**, e25233. doi:10.7554/eLife.25233
- Morise, H., Shimomura, O., Johnson, F. H., & Winant, J.** (1974). Intermolecular energy transfer in the bioluminescent system of *Aequorea*. *Biochemistry*, **13**(12), 2656–2662. doi:10.1021/bi00709a028
- Muto, T., Tsuchiya, D., Morikawa, K., & Jingami, H.** (2007). Structures of the extracellular regions of the group II/III metabotropic glutamate receptors. *Proceedings of the National Academy of Sciences of the United States of America*, **104**(10), 3759–3764. doi:10.1073/pnas.0611577104
- Nache, V., Eick, T., Schulz, E., Schmauder, R., & Benndorf, K.** (2013). Hysteresis of ligand binding in CNGA2 ion channels. *Nature communications*, **4**, 2866. doi:10.1038/ncomms3866
- Nakanishi, S.** (1994). Metabotropic glutamate receptors: synaptic transmission, modulation, and plasticity. *Neuron*, **13**(5), 1031–1037. doi:10.1016/0896-6273(94)90043-4
- Niswender, C. M., & Conn, P. J.** (2010). Metabotropic glutamate receptors: physiology, pharmacology, and disease. *Annual review of pharmacology and toxicology*, **50**, 295–322. doi:10.1146/annurev.pharmtox.011008.145533
- Okamoto, N., Hori, S., Akazawa, C., Hayashi, Y., Shigemoto, R., Mizuno, N., & Nakanishi, S.** (1994). Molecular characterization of a new metabotropic glutamate receptor mGluR7 coupled to inhibitory cyclic AMP signal transduction. *The Journal of biological chemistry*, **269**(2), 1231–1236.
- Olofsson, L., Felekyan, S., Doumazane, E., Scholler, P., Fabre, L., Zwier, J. M., Rondard, P., Seidel, C. A., Pin, J. P., & Margeat, E.** (2014). Fine tuning of sub-millisecond conformational dynamics controls metabotropic glutamate receptors agonist efficacy. *Nat Commun.*, **5**, 5206. doi:10.1038/ncomms6206
- Pagano, A., Rovelli, G., Mosbacher, J., Lohmann, T., Duthey, B., Stauffer, D., Ristig, D., Schuler, V., Meigel, I., Lampert, C., Stein, T., Prezeau, L., Blahos, J., Pin, J., Froestl, W., Kuhn, R., Heid, J., Kaupmann, K., & Bettler, B.** (2001). C-terminal interaction is essential for surface trafficking but not for heteromeric assembly of GABA(b) receptors. *The Journal of neuroscience : the official journal of the Society for Neuroscience*, **21**(4), 1189–1202. doi:10.1523/JNEUROSCI.21-04-01189.2001

- Pin, J. P., & Duvoisin, R.** (1995). The metabotropic glutamate receptors: structure and functions. *Neuropharmacology*, **34(1)**, 1–26.
doi:10.1016/0028-3908(94)00129-g
- Pin, J. P., & Acher, F.** (2002). The metabotropic glutamate receptors: structure, activation mechanism and pharmacology. *Current drug targets. CNS and neurological disorders*, **1(3)**, 297–317. doi:10.2174/1568007023339328
- Pin, J. P.** (2003). Evolution, structure, and activation mechanism of family 3/C G-protein-coupled receptors. *Pharmacology & therapeutics*, **98(3)**, 325–354.
doi:10.1016/s0163-7258(03)00038-x
- Prasher, D. C., Eckenrode, V. K., Ward, W. W., Prendergast, F. G., & Cormier, M. J.** (1992). Primary structure of the *Aequorea victoria* green-fluorescent protein. *Gene*, **111(2)**, 229–233.
doi:10.1016/0378-1119(92)90691-h
- Ridgway, E. B., & Ashley, C. C.** (1967). Calcium transients in single muscle fibers. *Biochemical and biophysical research communications*, **29(2)**, 229–234.
doi:10.1016/0006-291x(67)90592-x
- Robbins, M. J., Ciruela, F., Rhodes, A., & McIlhinney, R. A.** (1999). Characterization of the dimerization of metabotropic glutamate receptors using an N-terminal truncation of mGluR1alpha. *Journal of neurochemistry*, **72(6)**, 2539–2547.
doi:10.1046/j.1471-4159.1999.0722539.x
- Rochais, F., Vilardaga, J. P., Nikolaev, V. O., Bünemann, M., Lohse, M. J., & Engelhardt, S.** (2007). Real-time optical recording of beta1-adrenergic receptor activation reveals supersensitivity of the Arg389 variant to carvedilol. *The Journal of clinical investigation*, **117(1)**, 229–235.
doi:10.1172/JCI30012
- Romano, C., Yang, W. L., & O'Malley, K. L.** (1996). Metabotropic glutamate receptor 5 is a disulfide-linked dimer. *The Journal of biological chemistry*, **271(45)**, 28612–28616.
doi:10.1074/jbc.271.45.28612
- Rondard, P., Liu, J., Huang, S., Malhaire, F., Vol, C., Pinault, A., Labesse, G., Pin, J-P.** (2006). Coupling of agonist binding to effector domain activation in metabotropic glutamate-like receptors. *The Journal of biological chemistry*, **281(34)**, 24653–24661.
doi:10.1074/jbc.M602277200
- Saugstad, JA., Sagerson, TP., Westbrook, GL.** (1995). Modulation of ion channels and synaptic transmission by metabotropic glutamate receptors. In T. A. Wheal H, In: *Excitatory amino-acids and synaptic transmission*. New York: New York: Academic.
- Schoepp, D. D.** (2001). Unveiling the functions of presynaptic metabotropic glutamate receptors in the central nervous system. *The Journal of pharmacology and experimental therapeutics*, **299(1)**, 12–20.

- Sheikh, S. P., Zvyaga, T. A., Lichtarge, O., Sakmar, T. P., & Bourne, H. R.** (1996). Rhodopsin activation blocked by metal-ion-binding sites linking transmembrane helices C and F. *Nature*, **383(6598)**, 347–350.
doi:10.1038/383347a0
- Sheikh, S. P., Vilardarga, J. P., Baranski, T. J., Lichtarge, O., Iiri, T., Meng, E. C., Nissenson, R. A., & Bourne, H. R.** (1999). Similar structures and shared switch mechanisms of the beta2-adrenoceptor and the parathyroid hormone receptor. Zn(II) bridges between helices III and VI block activation. *The Journal of biological chemistry*, **274(24)**, 17033–17041.
doi:10.1074/jbc.274.24.17033
- Shimomura, O., Johnson, F. H., & Saiga, Y.** (1962). Extraction, purification and properties of aequorin, a bioluminescent protein from the luminous hydromedusan, *Aequorea*. *Journal of cellular and comparative physiology*, **59**, 223–239.
doi:10.1002/jcp.1030590302
- Swanson, C. J., & Schoepp, D. D.** (2002). The group II metabotropic glutamate receptor agonist (-)-2-oxa-4-aminobicyclo[3.1.0.]hexane-4,6-dicarboxylate (LY379268) and clozapine reverse phencyclidine-induced behaviors in monoamine-depleted rats. *The Journal of pharmacology and experimental therapeutics*, **303(3)**, 919–927.
doi:10.1124/jpet.102.038422
- Tanabe, Y., Masu, M., Ishii, T., Shigemoto, R., & Nakanishi, S.** (1992). A family of metabotropic glutamate receptors. *Neuron*, **8(1)**, 169–179.
doi:10.1016/0896-6273(92)90118-w
- Tateyama, M., Abe, H., Nakata, H., Saito, O., & Kubo, Y.** (2004). Ligand-induced rearrangement of the dimeric metabotropic glutamate receptor 1alpha. *Nature structural & molecular biology*, **11(7)**, 637–642.
doi:doi.org/10.1038/nsmb770
- Thon, S., Schmauder, R., & Benndorf, K.** (2013). Elementary functional properties of single HCN2 channels. *Biophysical journal*, **105(7)**, 1581–1589.
doi:10.1016/j.bpj.2013.08.027
- Tsien, R. Y.** (1998). The green fluorescent protein. *Annual review of biochemistry*, **67**, 509–544. doi:10.1146/annurev.biochem.67.1.509
- Tsuchiya, D., Kunishima, N., Kamiya, N., Jingami, H., & Morikawa, K.** (2002). Structural views of the ligand-binding cores of a metabotropic glutamate receptor complexed with an antagonist and both glutamate and Gd³⁺. *Proceedings of the National Academy of Sciences of the United States of America*, **99(5)**, 2660–2665.
doi:10.1073/pnas.052708599

- Valentin, G., Verheggen, C., Piolot, T., Neel, H., Coppey-Moisan, M., & Bertrand, E.** (2005). Photoconversion of YFP into a CFP-like species during acceptor photobleaching FRET experiments. *Nature methods*, **2**(11), 801. doi:10.1038/nmeth1105-801
- Vardi, N., Duvoisin, R., Wu, G., & Sterling, P.** (2000). Localization of mGluR6 to dendrites of ON bipolar cells in primate retina. *The Journal of comparative neurology*, **423**(3), 402–412. doi:10.1002/1096-9861(20000731)423:3<402::aid-cne4>3.0.co;2-e
- Verrier, S. E., & Söling, H. D.** (2006). Photobleaching of YFP does not produce a CFP-like species that affects FRET measurements. *Nature methods*, **3**(7), 491–493. doi:10.1038/nmeth0706-491b
- Villardaga, J. P., Bünemann, M., Krasel, C., Castro, M., & Lohse, M. J.** (2003). Measurement of the millisecond activation switch of G protein-coupled receptors in living cells. *Nature biotechnology*, **21**(7), 807–812. doi:10.1038/nbt838
- Vogel, S. S., Thaler, C., & Koushik, S. V.** (2006). Fanciful FRET. *Science's STKE : signal transduction knowledge environment*, **2006**(331), re2. doi:10.1126/stke.3312006re2
- Walker, K., Reeve, A., Bowes, M., Winter, J., Wotherspoon, G., Davis, A., Schmid, P., Gasparini, F., Kuhn, R., & Urban, L.** (2001). mGlu5 receptors and nociceptive function II. mGlu5 receptors functionally expressed on peripheral sensory neurones mediate inflammatory hyperalgesia. *Neuropharmacology*, **40**(1), 10–19. doi:10.1016/s0028-3908(00)00114-3
- Ward, S. D., Hamdan, F. F., Bloodworth, L. M., & Wess, J.** (2002). Conformational changes that occur during M3 muscarinic acetylcholine receptor activation probed by the use of an in situ disulfide cross-linking strategy. *The Journal of biological chemistry*, **277**(3), 2247–2257. doi:10.1074/jbc.M107647200
- Wieland, K., Zuurmond, H. M., Krasel, C., Ijzerman, A. P., & Lohse, M. J.** (1996). Involvement of Asn-293 in stereospecific agonist recognition and in activation of the beta 2-adrenergic receptor. *Proceedings of the National Academy of Sciences of the United States of America*, **93**(17), 9276–9281. doi:10.1073/pnas.93.17.9276
- Wu, H., Wang, C., Gregory, K. J., Han, G. W., Cho, H. P., Xia, Y., Niswender, C. M., Katritch, V., Meiler, J., Cherezov, V., Conn, P. J., & Stevens, R. C.** (2014). Structure of a class C GPCR metabotropic glutamate receptor 1 bound to an allosteric modulator. *Science (New York, N.Y.)*, **344**(6179), 58–64. doi:10.1126/science.1249489

Yanagawa, M., Yamashita, T., & Shichida, Y. (2011). Comparative fluorescence resonance energy transfer analysis of metabotropic glutamate receptors: implications about the dimeric arrangement and rearrangement upon ligand bindings. *The Journal of biological chemistry*, **286**(26), 22971–22981.
doi:10.1074/jbc.M110.206870

Zheng, J., & Zagotta, W. N. (2003). Patch-clamp fluorometry recording of conformational rearrangements of ion channels. *Science's STKE : signal transduction knowledge environment*, **2003**(176), PL7.
doi:10.1126/stke.2003.176.pl7

Declaration

I hereby declare that:

1. I am aware of the current course of examination for doctoral studies of the Faculty of Medicine at Friedrich Schiller University of Jena, Germany
2. I have researched and written the presented thesis myself, no passages of text have been taken from third parties or own exam papers without having been identified. All tools, personal notifications, and sources used by me have been indicated in the thesis.
3. My doctoral supervisor, Prof. Dr. Klaus Benndorf has supported me in selecting and analyzing the material and preparing the manuscripts for publication. Most of the presented thesis has already been published in a peer-reviewed scientific journal, *Proceedings of the National Academy of Sciences of the United States of America (PNAS)*.
4. The assistance of any doctoral consultant has not been utilized and no third parties have either directly or indirectly received monetary benefits from presented work or from related contents of the submitted thesis.
5. I have not submitted the thesis as an examination paper for state or other academic examinations.
6. I have not submitted the same, largely similar or any different treatises to another University as a dissertation.

Jena



Taulant Kukaj

[German translation]

Ehrenwörtliche Erklärung

Ich erkläre hiermit, dass:

1. mir die geltende Promotionsordnung der Medizinischen Fakultät der Friedrich-Schiller-Universität Jena, Deutschland bekannt ist.
2. ich die vorliegende Arbeit selbst angefertigt habe, keine Textabschnitte von Dritten oder eigene Prüfungsarbeiten übernommen habe ohne diese zu kennzeichnen. Alle von mir verwendeten Hilfsmittel, persönlichen Mitteilungen und Quellen wurden in der Arbeit angegeben.
3. mein Betreuer Prof. Dr. Klaus Benndorf, und Berater Dr. Ralf Schmauder haben mich bei der Auswahl und Analyse des Materials sowie bei der Erstellung des Manuskripts unterstützt hat. Der größte Teil der eingereichten Arbeit wurde bereits in einer von Experten begutachteten wissenschaftlichen Zeitschrift, *Proceedings of the National Academy of Sciences of the United States of America (PNAS)*
4. die Hilfe eines Promotionsberaters nicht in Anspruch genommen wurde und dass Dritte weder unmittelbar noch mittelbar geldwerte Leistungen von mir für Arbeiten erhalten haben, die im Zusammenhang mit dem Inhalt der vorgelegten Dissertation stehen.
5. ich die Dissertation noch nicht als Prüfungsarbeit für eine staatliche oder andere akademische Prüfung eingereicht habe.
6. ich die gleiche, eine in wesentlichen Teilen ähnliche oder eine andere Abhandlung bei einer anderen Hochschule als Dissertation nicht vorgelegt habe.

Jena



Taulant Kukaj

Acknowledgments

Firstly, I would like to express my acknowledgement to my supervisor Prof. Dr. Klaus Benndorf, for including me in this inspiring project. He was always available with suggestions on how to improve and push forward the project. During this period, I was always provided with limitless resources, with the opportunity to visit the best scientific conferences in the field, and the ability to have experience in the teaching of medical students. With one word, I had everything a young researcher needs to have a successful research.

Besides my supervisor, I wish to thank Dr. Ralf Schmauder for providing me with technical support and helping me to analyze and interpret the data.

Special thanks to Prof. Dr. Thomas Zimmer, Dr. Christian Sattler and Dr. Tina Schwabe for providing continues support related to molecular biology. Many thanks to Karin Schoknecht, Sandra Bernhardt and Claudia Ranke for technical support.

Furthermore, I like to thank Prof Regina Heller for organizing a summer school in molecular medicine and selecting me as a participant. Through this opportunity, I was able to come to Jena and follow my dream.

I want to thank all the former and present members of the Institute of Physiology II for offering a friendly working environment and support.

Last but not least. I want to thank and be grateful to my family, for giving me all the freedom and support in every decision affecting my future.

Curriculum Vitae and Publication List

Personal Details

Name: Taulant Kukaj

Place and date of birth: Glllogoc/Republic of Kosovo, 21.09.1988

Nationality: Kosovar

Address: 07743 Jena, Fischergasse 4

Email: taulant.kukaj@med.uni-jena.de
taulantkukaj@gmail.com

Telephone:

Education and Research Experience

From 07/2020 - Postdoctoral Researcher at Institute of Physiology II, Jena, Germany

11/2015-06/220 Doctoral student at Institute of Physiology II, Jena, Germany (Supervisor: Prof. Dr. Klaus Benndorf)

04/2014-10/2015 Pharmacist in Production at Gentipharm Pharmaceuticals, Prishtina, Kosovo

10/2012-08/2015 M.Sc. Organic Chemistry at Faculty of Natural Sciences and Mathematics, University of Prishtina, Prishtina, Kosovo

10/2007-08/2012 M.Pharm at Faculty of Medicine, University of Prishtina, Prishtina, Kosovo

Publications

Taulant Kukaj, Christian Sattler, Thomas Zimmer, Ralf Schmauder, and Klaus Benndorf (2020). **Kinetics fingerprinting reveals high and specific subunit promiscuity in human metabotropic glutamate receptors.** (*Under review*)

Florian Walther*, Dominic Feind*, Christian vom Dahl*, **Taulant Kukaj**, Christian Sattler, Georg Nagel, Shiqiang Gao, and Thomas Zimmer. (2020). **Action potentials in Xenopus oocytes triggered by blue light.** *JGP J Gen Physiol*, 152(5)

DOI: [10.1085/jgp.201912489](https://doi.org/10.1085/jgp.201912489)

Eugene O. Grushevskiy*, **Taulant Kukaj***, Ralf Schmauder*, Andreas Bock, Ulrike Zabel, Tina Schwabe, Klaus Benndorf, and Martin Lohse. (2019). **Stepwise activation of a class C GPCR begin with millisecond dimer rearrangement.** *Proc. Natl. Acad. Sci. USA*, 116(20), 10150–10155. DOI:[10.1073/pnas.1900261116](https://doi.org/10.1073/pnas.1900261116)

Posters:

1. **Taulant Kukaj**, Ralf Schmauder, Christian Sattler, Thomas Zimmer & Klaus Benndorf. **GPCR activation and deactivation kinetics by rapid solution exchange in excised membrane patches.** 64th BPS Meeting, San Diego, California, USA. Feb 15th – 19th, 2020.

2. **Taulant Kukaj**, Ralf Schmauder, Tina Schwabe, Ulrike Zabel, Martin Lohse & Klaus Benndorf. **Kinetics of Metabotropic Glutamate Receptor 1 investigated by piezo-controlled concentration jumps.** GRC Molecular Pharmacology. Ventura, California, USA. Feb 10th – 15th, 2019.

3. **Taulant Kukaj**, Ralf Schmauder, Tina Schwabe, Ulrike Zabel, Martin J. Lohse, Klaus Benndorf. **Activation and deactivation kinetics of class C GPCRs studied with confocal patch-clamp fluorometry.** 98th Meeting of the German Physiological Society/ Joint Meeting with the Austrian Physiological Society (APS) and Life Sciences Switzerland (LS2) Physiology. Ulm, Germany. Sep 30 – Oct 02.

4. **Taulant Kukaj***, Ralf Schmauder, Tina Schwabe, Ulrike Zabel, Martin Lohse & Klaus Benndorf. **Kinetics of Metabotropic Glutamate Receptor 1 investigated by piezo-controlled concentration jumps.** 7th Focused Meeting on Cells Signalling Nottingham, United Kingdom. Apr 16th – 18th, 2018

5. **Taulant Kukaj***, Ralf Schmauder, Tina Schwabe, Ulrike Zabel, Martin Lohse & Klaus Benndorf. **Kinetics of Metabotropic Glutamate Receptor 1 investigated by piezo-controlled concentration jumps.** 62nd BPS Meeting. San Francisco, California, USA. Feb 17th – 21th, 2018.

Scientific Talks

1. Taulant Kukaj, Ralf Schmauder, Ulrike Zabel, Martin J. Lohse, Klaus Benndorf. **Activation Kinetics of Metabotropic Glutamate Receptor 1 Investigated by Piezo-Controlled Concentration Jumps.** 6th Symposium of the Young Physiologists. Jena, Germany. Sep 28th-29th, 2018.

Jena, 02.07.2020



Taulant Kukaj